DISSERTATION

NATURAL FREQUENCIES OF TWISTED CABLES: A NUMERICAL AND EXPERIMENTAL STUDY

Submitted by

Mohammed K. Alkharisi

Department of Civil and Environmental Engineering

In partial fulfillment of the requirements

For the Degree of Doctor of Philosophy

Colorado State University

Fort Collins, Colorado

Summer 2021

Doctoral Committee:

Advisor: Paul Heyliger

John van de Lindt
Suren Chen
Lisa Stright

ABSTRACT

NATURAL FREQUENCIES OF TWISTED CABLES: A NUMERICAL AND EXPERIMENTAL STUDY

As the uses of cables have increased in different engineering applications, a better understating of their mechanical and dynamical behavior becomes more critical. Over the past several decades, many analytical, experimental, and finite element models have been developed to investigate vibrations of the cable structure. This attention explains the importance of such a structure, where it is more challenging than many ordinary structures because of the nonlinearity of the geometry and other combined effects. In addition, the twist along cable length leads to coupling behavior on the various kinematic variables of the cable system. This work is aimed at predicting and investigating the natural frequencies and the translations and rotations mode shapes occurring stimulatingly for both horizontal and inclined sagged cables, using both numerical and experimental methods

An efficient numerical procedure using elasticity-based finite elements is presented to generate the primary elastic stiffness coefficients of single-layered six-wire strands where the cables are subjected to axial and torsional loads in three-dimensional space. Cable models with lay angles varying from 5 to 30 degrees are then compared to eight different one-dimensional analytical models for the same range of angles. The finite element model gives stiffness coefficients that are in good agreement with the analytical models for angles below the maximum angle of the cable.

The free vibration behavior of untwisted and twisted cables is then analyzed using the derived stiffness and mass matrices. When discretized over the horizontal span, the sagged cable

is represented using transformed axial, coupling, and torsional characteristics where the resulting two-node cable element has three translational and three rotational degrees of freedom. A similar computational approach is used for inclined cables using inclination angles from 10 to 60 degrees. The natural frequencies and modal shapes are found to be in very good agreement in comparison with the results obtained using extensive experimental tests for identical cable geometries and materials. Where a harmonically time-varying support motion is employed, undergo different conditions. The acceleration and angular velocity time histories are then collected by sensors mounted on the mid and quarter span of the cables.

In addition to the experimental results, the frequency spectrum and the translational and rotational mode shapes are analyzed and compared with the limited analytical model available from the literature and the computer finite element software ABAQUS. Practical examples are used to demonstrate the validity and applicability of the finite element model for untwisted and twisted cables. Then, the influence of the principal and microstructural parameters variation on the dynamics of the cable is investigated.

This study shows that the elasticity, twist coupling, initial sag, inclination angle, and self-weight of the cable play a considerable role in the frequency and modal coupling behavior. It further suggests that some of the simple models available may not be adequate to fully understand the significant levels of modal coupling in the cable's dynamic behavior. The methods used in this study are finally extended to experimentally find the internal damping ratios and the reduction in the in-plane peak motions when a damper is used.

ACKNWLEDGMENTS

I would like to express my deep and sincere appreciation to all the people who helped me complete this research. My sincere gratitude to Prof. Paul Heyliger for allowing me to work with him; for his constant guidance, encouragement, and creative and comprehensive advice, without which this dissertation would not have been completed. It is a great honor to work under his supervision. And I could not have imagined having a better advisor and mentor for my Ph.D. studies. I would like to thank my committee, Prof. John van de Lindt, Prof. Suren Chen, and Dr. Lisa Stright for their assistance, suggestions, and advice.

It is a special and generous thanks to my father, my mother, and all my family members for their valuable prayers and continuous support. I am fully indebted to my beloved wife Hessah Alsaleem and my daughter Aljawhara for their love, patience, and encouragement. For all my friends who provided happy distractions to rest my mind outside of my research.

I extend my gratitude to thank the Saudi government and Qassim University for affording me the privilege of pursuing a Ph.D. in the Civil and Environmental Engineering Department at Colorado State University. And their financial support and cooperation.

TABLE OF CONTENTS

LIST OF TABLES

LIST OF FIGURES

CHAPTER 1: INTRODUCTION

1.1 Background

Cable structures have been widely used in a wide variety of tensile structures, for example, cable-supported bridges, large-span roof, marine, and offshore structures, guy lines for towers, and power supply lines as results of their capability of transmitting force, carrying payloads, and conducting signals, as well as their aesthetic appearance. A Cable is an old tool that humankind has used in the history of civilization; 700 B.C., as a structural element, after World War II, it was used as network systems in civil engineering architectures [1]. Recently, the interest in cables increased as their use, so the latter application required a more thorough and detailed investigation of the mechanics in cables.

The term cable is used to indicate a generic sense of a tension member that is a flexible metal. A cable can be in the form of a single line (untwisted) Fig. 1.1 or wrapping wires around a central line (twisted) Fig. 1.2 that may be a wire strand, a group of strands, rope, ropes, or a parallel wires that acts as a unit member. Besides, the wire strand can be defined as a group of wires that are wounded around a center straight wire (also called core wire) in one or more symmetrical layers. However, a wire rope has several strands that are twisted around a core; this core can be a solid wire or a wire made of metallic, polymeric, or natural materials.

Transmitting forces or singles is the main feature of cables. Cables are categorized as mechanical cable for guy wire and structural uses, electrical cable to transmit signals, or optical fiber cables. Mechanical wires can transmit forces between locations, while signal cables transmit signals, mechanical wires are subjected to much higher stress than signal wires; however, signal wires have greater requirements for minimal vibration [2].

Fig. 1.1 Untwisted cable

Fig. 1.2 Twisted cable

Cables can be subjected to axial forces, which result in tension, torsion, and lateral forces, which result in bending. So, it can be said that due to their construction, cables combine two functional properties that can be highly useful: high axial strength and flexibility in bending. These properties convert cables into indispensable transmission elements for many applications.

The mechanical behavior of cables, including static and dynamic, generally depends on their unique geometry, material properties, and lay configuration. This configuration is helping the cable to bind together [3]. A solid rod with the same cross-section area has a very close tensile strength of a cable. However, for flexural rigidity, it could be only 20% of solid beams; as result cables are particularly suitable for being used as a tension member [4]. A common property for such a structure is its ability to resist relatively large axial load in comparison to bending and torsion loads. Also, because of their high flexibility, they are subjected to high nonlinear behavior with large-amplitude vibration. Another essential characteristic is its damping capability. It is known that losses of energy in the cable are more significant than those caused by the material viscosity. This damping property attracts designers to use it as a flexible structure, and the reason for that is the self-damping feature, which is vital for dynamic stability. So, the analysis and the construction of such a structure are more challenging than ordinary structures.

Typically, the designer first starts with estimating the external load acting on a structural member. After that, the stresses are then calculated so the structure life is predicted by knowing the fatigue and correction data. The knowledge of stress would give an indication of the actual safety factor against the plastic or even the initial failure of a structure. That is done generally in the design process of structural members. However, for such a complex structure as cables and insufficient research on the topic has resulted in creating a complicated procedure for steel cables, for example [5]. Also, the inter-wire contact and coupling phenomena have even gotten little attention in all the published work for small and large cables.

Even though that cables were used a structural member for a long time, the theoretical and experimental work done to analyze and understand their behavior has fallen behind their applications when comparing with other studies on commonly used members such as rods, beams, and columns. Recently, the distinctive phenomena of the cable vibration attract researchers to understand better the behavior, of which certain are concerned by theoretical development and/or experimental validation of the relevant governing differential equations of motion, and others depend on the exact or approximate numerical approaches to find a proper solution. , Fig. 1.3 shows the number of publications in the past two decades.

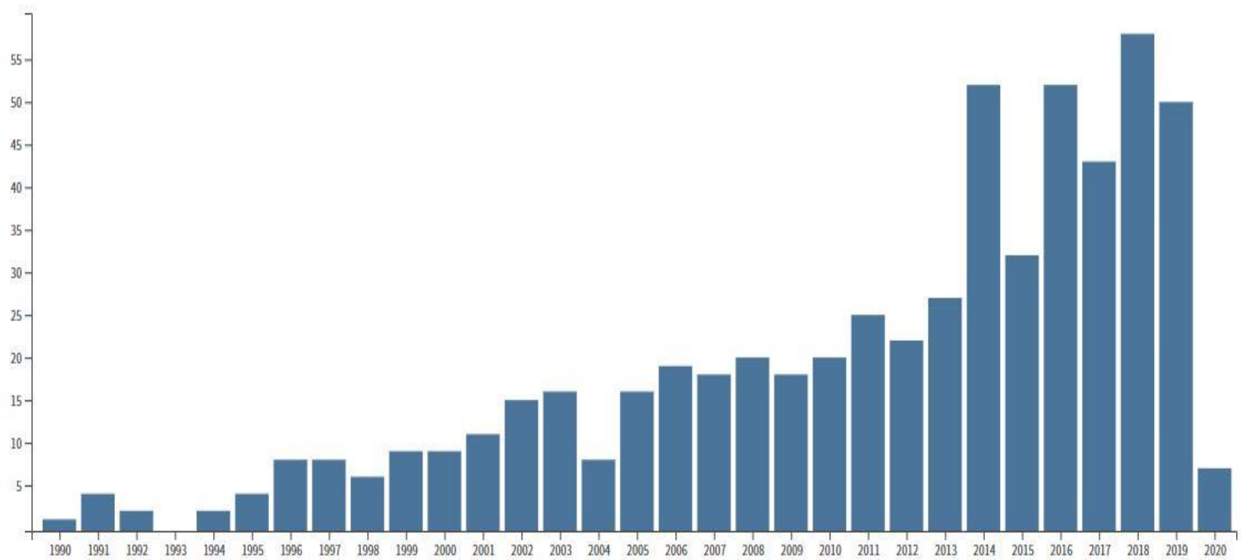

Fig. 1.3 Number of publications of cable vibration from 1990 to 2020 (image courtesy Web of Science)

The main goal of this dissertation is to study the dynamic behavior of cables. And since they have very complex geometry, the finite element method is used. This method was introduced in 1956, when Tuner et al. used pin-jointed bars and triangular plates to solve airplane structures [6]. It has the ability to describe the displacement field of a structure using differential equations for problems that are difficult to solve by analytical methods. The structure is discretized into a large number of small subdomains, which are called finite elements. This subdivision of the domain enables an accurate representation of the structure geometry, including material properties, a simple representation of the solution, and capturing all the local and global effects. In addition, since this method is based on numerical analysis, it has clear steps which lead to an accurate solution.

1.2 Problem Statement

The significant characteristic of twisted cables that their static response is coupled. This means that when a cable has a twist along its length, recent studies showed that, it exhibits coupled extensional-torsional behavior, when an axial load is in action it will undergoes simultaneous extensional and rotational displacements, similarly when torque load is subjected both rotational and extensional displacements exist in the longitudinal axis in case the cable is tight and horizontal. This behavior has a critical impact on the dynamic response of the cable; however, it has received little attention. In addition, the full effect of twist, sag, and cable weight on the coupling between extensional-torsional behavior on the longitudinal, vertical, and transverse axis and between each must be studied. When the mentioned loads undergo, six types of waves will propagate through the cable, three characterizing the extensional-compressive deformations and the others are describing the torsional deformations, the interaction, and superposition of these six waves will make the cable oscillation very complicated. The main objective herein is to investigate numerically and experimentally the ability to accurately predict and measure the dynamic motion and resonances considering the undamped and damped free vibrational analysis of the coupled extensional-torsional actions for untwisted and twisted cable, which is imperative to result in enhancing a safe design and reliable system for the cables as well as the structure associated with.

Vibration analysis of coupled behavior for cable is of considerable significance, and the reason for that is the practical nature of engineering applications of this structure member involved in. Failure to have an accurate estimating of the natural frequency and motion interaction may result in failure of the system under resonance. Therefore, the cable and, as a result, the structural element that associated, for example, towers in case of transmission lines, are subjected to higher dynamic stress, which may lead to mechanical failures, such as loosening, ejection or wear of bolts, ovalling of holes, and distortion of swivel. In addition, when all the mentioned failures happen, it will necessarily have a high average annual cost for repairing, as well as for control devices installation. This cost is additional to the loss of review during serving any application cables are employed in, and millions of dollars might be spent every ten years for that.

Designing tools for estimation the overall coupled elastic stiffness coefficients of twisted cable structure under different scenarios is a must for designers, where the coupled behavior of realistic helical strand is addressed. Simplified routines (using FORTRAN language) are presented in this work for obtaining the upper and lower bond to various strand stiffness using the elasticity method through a three-dimensional finite element model. Unlike several analytical models which some of them are replicated and presented here, this model includes the actual helical geometry, as well as the Poisson ratio, and the variation of the twist angle of the cable to have a realistic model, in addition to the influence of the principal cable parameters which are carefully studied. Numerical examples of twisted cables are shown to facilitate the use of the developed formulations.

The advantage of having these expressions will enable an accurate dynamic analysis of the considered horizontal and inclined cables first to construct the frequency spectrum and then the corresponding mode shapes resulting from the out-of-plane, symmetric in-plane, antisymmetric in-plane, axial, and torsional vibration. Then explore and analyze the complex waveform vibration that is repeated simultaneously resulting from considering the six degrees of freedom for the sagged cable system. This will be done throughout numerical data obtained through computer simulation of mathematical models obtained by the finite element model throughout FORTRAN and MATLAB codes. And procedure based on experimental work data by a campaign of dynamic tests. The validation of the numerical and experimental analysis proposed is done through confrontations of computational results of know analytical and ABAQUS model solution of the cable where the twist of the cable is usually ignored.

Cables are subjected to damping to some degree, and that resulted because of friction and other resistances. As a result of the cable's high flexibility, small weight, and long span, minimum vibrations can easily cause large amplitudes. To decrease the damages caused by that, many investigations into damping of the cable must undertake. Here the twisted and untwisted cables vibration mitigation feasibility is studied through an experimental tests campaign. The internal damping ratio is identified using multiple experimental tests. In addition, the in-plane vibration with and without damper on the support is investigated.

This work's challenge is the correlation between vibration data obtained numerically and experimentally introduces inherent difficulties in getting the same results. In addition, this is highly complex because of the cable's nonlinear geometry dependence and the twisted configuration, which cause interaction between the various vibration modes. These interactions are modeled using numerical time-marching in conjunction with the finite element procedure. Finite element models can have errors; incorrect modeling concepts, uncertainties in material properties, inaccurate modeling details, and applying wrong boundary conditions. When vibration experiments are conducted, many sources of errors can be present; mistakes in equipment calibration, noise, equipment damages, inaccurate interoperation data, and incorrect sensor positioning. For that, validating the numerical and experimental work proposed will be through a comparison with the analytical and ABAQUS model known results for uncoupled cables, as well as repeating the experimental tests multiple times.

1.3 Dissertation Organization

This dissertation has seven chapters. The first chapter is a general introduction that has two sections, (1) is an overview of cables, and (2) a problem statement where the overall mechanical and dynamic behavior of cables is described and the objectives of this work. Chapter 2 is a detailed and generalized literature review divided into 3 sections; the first is an overview, the second shows the cable stiffness previous work, and the third is about cable dynamics. In both sections, most of the previous analytical, experimental, and finite element models are reviewed. The third chapter is a study on the problem of motion interactions in untwisted cables and the effect of cable sag variation. This chapter is divided into 8 parts where a summary and introduction are given in (1) and (2), a very detailed explanation of the theory (3) where the finite element method is used, and the large-scale experimental model (4) and the available analytical solutions (5) used for validation for two types of cables (6). Results and discussion (7) and detailed conclusions (8) are also shown. Chapter 4 presents an experimental investigation of cable vibration damping, and this chapter consists of seven sections. A detailed explanation of the experimental setup is introduced (3), and a summary (1) and introduction (2) are given at the start. After that, the experimental procedure (4) and how the data were processed (5) are shown. This chapter shows the experimental results (6) and the drawn conclusions (7) for untwisted and twisted cable internal damping and studying the cable motions with and without using a damper on the support. Chapter 5 presents a study on twisted horizontal cables in seven sections, where the stiffness and the dynamic behavior are found. A summary (1) and an introduction (2) are first introduced, then the strand mechanics are explained in section (3), which then enable the free vibration analysis in section (4) where the finite element model, experimental, analytical, and ABAQUS model details are shown for cable application (5). The new findings are then discussed in results section (6) and listed in the conclusion (7). In chapter 6, the inclined twisted cables dynamic behavior is also presented. Similarly, a summary and an introduction are in sections (1) and (2). The twisted cables geometry and stiffness are discussed in section (3), then the vibration analysis using the same four approaches: finite element model, analytical model, ABAQUS model, and experimental model are described in section (4), and results and discussion and conclusions are illustrated in section (5) and (6). Chapter 7 is a general conclusion of this dissertation that has two sections, main concluding remarks, and research future work.

CHAPTER 2: LITERATURE

2.1 Overview

Cables are widely used as a structural member in many different engineering applications due to their advantages in carrying high tensile forces relative to small dead load and good electric conductively. As a results of its importance, in the last several decades, many mathematical models allow an analytical approach to the complex problem of calculating the global mechanical behavior of cable has been developed, despite the limitation due to simplification hypotheses regarding the practical cases which include ignoring friction between wires for example or small displacement and strain. The early theoretical work on the mechanical behavior of cable appeared in the 1950's. As a result of the complexity of the cable geometry, a great number of unknown variables are involved, for that different approximations and assumptions were made in order to access the difficult problem.

As introduced, cables term refer to strands or wire rope, where strands are made of helical wires that are twisted around a straight core, while wire ropes are obtained by helically twisting and grouping strands. More details about cables construction and typologies can be found in Feyrer [7] book, while insight into the geometry modeling of the helical assemblies was provided by Lee [3]. It should be noted that for simplicity the majority of the mathematical models have been applied on a single starlight strand, so the mechanical properties of the wire can be studied.

For describing cable behavior many researchers in the literature have been working on the analytical characterization of the mechanical response of helical structures to different loading scenarios. The analysis has been performed by modeling the cable as a perfectly flexible element, mostly reacting to only axial forces. Taking account of the bending and torsional stiffness contributions is necessary to overcome the entirely flexible structural model to represent the important features of cable mechanics. The analysis can be subdivided on the base of mechanical models in describing the wires inside the cable into: discrete and semi-homogenization formulations. Discrete models are based on the modeling the wires individually as curved beam or thin rod. Instead, semi-homogenization is based on replacing the layers of wires with and equivalent elastic continuum, which can be presented as an orthotropic thin layer in a three-dimensional cylinder or in plane stress state using orthotropic material.

To have a better understand of the cable behavior, a review on the most well-known models and the cable modeling evolution is presented in this chapter. The main objective here is to give a general overview of the basic classic models and exploration of new models as well as extension of previous models that find the stiffness (section 2) and present the classic and advanced model for finding cable vibration (section 3).

2.2 Cable Stiffness

Many analytical based models are available to predict the stiffness of isotropic cables that are subjected to axial loads, with the component geometry and material given. The first models were having the assumption of neglecting the bending and torsion effects on the stiffness of the wires and incorporates the effect of tension only. As Hruska [8,9] simple fiber model with clamping conditions, in his work friction and radial contraction were ignored. This model was extended and motived by Knapp [10] for the rigid central core wire, the same assumptions were applied. However, it should be emphasized that ignoring the bending and torsion effect was motived and the importance was explained extensively in later models. McConnell and Zemke [11] included the torsion stiffness effect on the external (outer) wires.

Further, more sophisticated analytical models are based on the assumptions of beam theory; individual wires are modeled using the equations' of Love [12] curved beam. Machida and Durelli [13] investigated the bending and torsion effect on the stiffness matrix of the outer wires, for each the bending and twisting moment were found, however, the stiffness matrix symmetry was lost. Knapp [14] introduced another stiffness matrix that are subjected to tension and torsion, the radius variation in the central wire also was studied, which comes from the pressure of the layers. In addition, the equations of equilibrium included the geometry non-linearity, and then it were linearized to give a linear stiffness matrix. Costello and Phillips [15] presented a nonlinear theory for a strand with one layer without a core or using soft core, in this model, the effect of lay angle and radius variation was considered (due to effect of Poisson's ratio); however, contact deformation and friction forced were ignored. Huang [16] investigated the condition of contact mode either radial or lateral for the straight simple strand, the Poisson ratio effect was included while contact deformation was neglected, it is stated that the radial contact is prevailing case even if there are no gaps between the wires in the layers [17]. Costello and Phillips [15] work was extended by Velinsky [18] and Phillips and Costello [19] to include internal wire rope. Velinsky [18] model included the effect of Poisson ratio, this model was used to study the multi-strand responses. Phillips and Costello [19] generalized Velinsky [18] work to be applied on any type of cable with an independent central core wire; the friction between wires was neglected in this model. Costello [20] presented a linear theory that included the curvature and twist variations effects (recently, Ghoreishi [21] gave a closed form matrix for this model, the symmetry in the matrix is lost). Kumar and Cochran [22] extended this theory to develop a linearized form, which results in a closed-form expression for the stiffness matrix terms, however, the stiffness matrix symmetry also is lost. Utting and Jones [23,24] continued Costello [20] work to include contact deformation (wire flattening) and friction effect, and the results showed that these phenomena have a small effect on calculating the global response of the cable. Clair and Costello [25] discussed the friction effect of bending load on strands. Jolicoeur and Cardou [26] compared the results of the mechanical response for the single straight rope which was predicated by Costello and Phillips [15] model with the simple model provided by Hruska [8,9], the comparison resulting in showing that the fiber model is not appropriate in case twisting moment and angle have to be taken into account and Costello and Phillips [15] model showed a good prediction with experimental results done by Utting and Jones [23,24] for cable stiffness. Labrosse [27] presented an analytical method that predicted the overall behavior of simple straight wire subjected to tension, bending, and torsion; this model excluded the Poisson's ratio and relatively included the motion between the core and the wires, in this theory wires were considered as curved beams. Kumar and Botsis [28] used Kumar and Cochran [22] model to find the expression of the maximum contact stress in multilayer strands.

Using discrete thin rod theory, Ramsey [29] introduce a mathematical approach based on differential geometry. He stated that more analysis should be done for twisted cable and for that he drive a constitutive equations using his theory. However, Ramsey [30] revised his previous work and that lead to have a non-zero distributed moment component specifically in the radial direction. Also, Sathikh et al. [31] derived a closed-form symmetric linear elastic model for cables with a rigid core, the tension, twist, and bending were taking into account, and the lack of symmetry was fixed in this model. In addition, after reviewing the discrete models mentioned above, it can be said that the neglecting of the helix radius of the outer wires will lead to overestimation of the elastic stiffness coefficients. As indicated when the Poisson effect is accounted for as well as the internal contact surfaces between the core wire and the outer wires will result in better estimation of the loads. A more recent discrete models are by: Argatov [32] where he has proposed a better formulation that considered the contraction between the outer wires and the core wire using the method of matched asymptotic expansions, and other using semi-analytical solutions by Meng et al. [33] and Chen et al. [34].

In addition, it is noted that whenever all the previous formulation take into account the change in the geometry internally which is obtained by stating the mechanical problem in non-linear geometric framing and then linearized it and when is done it result in non-symmetric stiffness matrix, which is known that violates Betti's reciprocal theorem. The base of elastic systems deepened on Betti's reciprocal theorem. Karathanasopoulos and Kress [35] found a symmetric matrix when proposed a mode to study helical rods response under axial-torsional loads and radial contraction was included. In this mode the formulation of the radial strain was considered as an external load (Poisson ratio and flattening effects not induced) which is different for the previous models. Karathanasopoulos et al. [36] used this model to study the effect of thermal loads on braided conductors. More recent, Foti & Martinelli [37] developed a model to evaluate the axial-torsional response of a single layered strand considering the deformability of the internal contact surfaces, and derived a symmetric the stiffness matrix.

A method called homogenization was used in introducing a semi-continuous model by Hobbs and Raoof [38] for multilayered cables where each layer is modeled as an equivalent orthotropic sheet. This methodology was extended by Raoof and his associates over two decades: Raoof [39], Raoof and Hobbs [40], Raoof [41], Raoof and Kraincanic [42], and Mohammed and Ivana [43]. This method was described more by Raoof [39]: this model replaced each layer with a thin cylindrical orthotropic layer; to be in a plane state of stress. Blouin and Cardou [44] also used the same homogenization to develop another semi-continuous model. Raoof and Kraincanic [42] stated after making a comparison between the semi-continuous models and the thin rod models analysis of cable that the thin rod theory was more reliable when the wire strand diameter is small or for one or few layers of external wires. However, the semi-continuous models would be advantageous when the cable is made with a large number of wires [45]. Jolicoeur [46] compared Raoof [39] and Blouin and Cardou [44] models and reported that the previous cylinder model is simple and preferred for axial or torsion loads; however, it will fail to capture the bending stiffness so the other model is perfect if bending will occur. This approach can be applied by replacing each layer with a cylinder of orthotropic, transversely isotropic material as in Claude and Alain [47], Crossley et al. [48], and Crossley et al. [49] work. Such an approach can be used when the number of wires in the layer is large [17]. Also, the use of semi-continuous models of wire ropes will shed light on aspects of the problem of bending and torsion behavior [32].

All the above-introduced models treat the single-helix wire strand only. In practice, wire ropes can have a more complex multi-strand cross-section, which may have a double-helix configuration. Lee [3] stated in his discussion of the geometrical property of single- helix and double-helix that there are differences between them. Stanova et al. [50] introduced a new mathematical model for both single-helix and double-helix in the form of parametric equations. This model showed high efficiency in building the finite element model of cable, and the results of a multi-layered strand under tension were given, and it agreed well with experimental data [45].

For cables with double-helix configuration; Elata et al. [51] were the first to fully consider this configuration. This new model simulated the wire rope behavior using independent wire core under axial loading. Rather than considering the effective response of wounded strands, this approach was used to consider the complete double-helix configuration of individual wires within the wound stand and relates the level of wire stress to the overall load applied. The individual wires bending and torsion stiffness are neglected, however, the lateral surface of the wires is subjected to loads, applied by adjacent wires. As a result, the accuracy increased in this model with the increase if the wires in the wire rope. It is emphasized that the main focus of Elata et al. [51] work was to analyze the double helix configuration effect; however, it did not lead to finding closed-form equations [17]. Another model was developed by Usabiaga [52] for double-helix cable, however, this model neglected the Poisson effect. Recently, Xiang et al. [45] developed a model where the focus was to predicted the global stiffness of the cable, and it found that the different friction stated between the wires can result in a different distribution of local deformation including bending and torsion in case of double-helix wire.

As for analyzing synthetic cable, many models are available. Leech et al. [53] intruded a quasi-static analysis of fiber ropes and included it in a software: Fiber Rope Modeller. Beltran et al. [54] developed another model and Beltran [55] and Beltran and Williamson [56] extended it. These models are similar to Leech et al. [53] model, however, they concentrated more on a damage model to take into account the degradation of cable properties as a function of loading history. The mentioned models are also implemented into a computer program. Ghoreishi et al. [57,58] developed two closed-form analytical models, that can be used in sequence to analyze synthetic cables.

As for using Finite Element Method, Carlson et al. [59] modeled the wire using bar elements as well as the connections between the wires. Cutchins et al. [60] modeled the wires using six node elements; the connections were simulated using springs. Chiang [61] modeled a small segment of the cable length to optimize the geometry and investigate the impact of factors like the radius of the core, the radius of wires, helical angle, and boundary conditions. These models used what is called volumic finite elements where the interwire mechanical behavior cannot be investigated, and as known, it is required to have larger elements number to have accurate analysis [62]. For the simple straight strand. Nawrocki [63] done an analysis using a one-dimensional curved beam element. It should be mentioned that some of the finite element method studies have investigated the local phenomena, as it was mentioned that the inclusion of the internal contact surface and Poisson effect increased the complexity of mechanical formulation which increased the need of using advanced numerical solutions such finite element method. For the simple straight strand Jiang et al. [64] presented a concise finite element using three-dimensional solid brick elements, the model took advantage of the cable loading symmetry and accounted for tension, shear, bending, torsion, contact, friction, as well as local plastic yielding under axial load. This model showed excellent agreement with Costello and Phillips [15] model and Utting and Jones [23,24] experiment work. For a three-layered straight strand Jiang et al. [65] extended the previous work; however, this model cannot work for the bending case or where very complex loading cases are assigned. These models showed that interwire pivoting and interwire sliding govern the global response for cable for axial and bending loads, respectively [17]. Nawrocki and Labrosse [66] used Nawrocki [63]'s element to investigate the motion between the core and wires. Wehking and Zieglen [67] devoted his work to compute the rope stress. Similarly, Messager and Cartraud [68] found a homogenization procedure, by applying the rigorous asymptotic development theory, a segment of the strand can be studied using the three-dimensional finite element model free of displacement assumption. For statically indeterminate contact problem when the wire is under axial load, Jiang et al. [69], investigated this problem and stated that the contact can occur at all possible contact points when wire is under tension and restrained against rotation. Since all this previous work is done under axial load Jiang [70] used the same extraction modal approach however under pure bending, as for global behavior of cable, bending moment verses bending curvature, the finite element results showed a good agreement with the analytical elastic cable of Costello [20], this modal also predicted the nonlinear plastic behavior.

For single helix configuration critical reviews of the models have been provided by Cardou and Jolicoeur [71], Xiang [45], and Liu et al. [72]. Using three-dimension finite element modeling Ghoreishi et al. [17] did excellent work in comparing the validity domain: Hruska [8,9], McConnell and Zemke [11], Machida and Durelli [13], Knapp [14], Kumar and Cochran [22], Ramsey [29,30], Sathikh et al. [31], Costello [20], and Labrosse [27] models. They have done that to address the problem that there are limited experimental results reported in the literature. This work was done on straight single layered stand subjected to axial load. The results for lay angles below 20 degrees showed that the finite element model gave a satisfactory estimating of the elastic stiffness constants. However, the study showed that the analytical models are limited due to different assumptions. Alkharisi and Heyliger [73] used the three dimensional elastic theory to exam the same range of twist angles from 0 degrees to 30 degrees of trapezoidal cable and twisted-pair cable that are subjected to pure deformation and pure twist to determine the stiffness coefficients which were used to describe the force-displacement relationship.

2.3 Cable Dynamics

Dynamics of cables has a long and very rich history which been documented in the classic paper of Irvine [74]. Starting from the first half of the eighteenth century, Taylor, D'Alembert, Euler, Bernoulli, and Lagrange presented the theory of vibration of a taut and sagged string that was fixed at both ends with concentrated masses, the transverse vibration was studied, with the development of the theory partial differential equations. In 1820, a huge contribution was made by Possion, where the general Cartesian partial differential equations of motion of cable element under a general force system action was derived. After that, Rohrs [75] introduced the symmetric vertical vibration of a uniform suspended cable with small ratio of sag to span, he arrived to an approximate solution using a form of the equations introduced by Possion. Similarly, Routh [76] found a closed form solution for the symmetric vertical vibrations as well as the longitudinal motion of the uniform cable. After that, for a long period of time this topic was set aside, in the middle of the twentieth century; there was a renewal of the interest for the dynamics of cable topic which is after the collapse of the Tacoma Narrow Bridge late in1940. Pugsley [77] solved the first three in-plane modes of a uniform suspended cable using a semi-empirical theory, different range of sag to span ratio from 1:10 to 1:4 was used. Saxon and Cahn [78] derived the fourth order differential equation which govern the small amplitude, then they got the results which effectively reduced the inextensible cables with small sag to span ratio model, asymptotic solution gave very good results for large ratio to span. It should be noted that Pugsley [77] and Saxon and Cahn [78] solutions failed to reproduce the classical spectrum for the taut string when the sag value is zero. Until 1970s there was neither theoretical nor experimental work done to deal with the remarkable discrepancy between the theories known by then: when reducing the sag to zero the frequencies and the symmetric in plane mode of cable have inextensible sag do not equal the result of the corresponding natural frequency of a taut string [79].

Irvine and Caughey [80] did a remarkable work developing a novel linear theory for the free vibration of a uniform suspended untwisted (uncoupling) cable with ratio of sag to span about 1:8, or less assuming a parabolic profile. In addition, they used a basic and simple assumption which was that the dynamic cable tension is a function of time alone, meaning that the elastic deformation is set to be quasistatic [79]. This work, considered both out-of-plane and in-plane motion, and the analysis results showed that the symmetric in-plane modes depend on only a parameter allowing for the effect of cable geometry and elasticity, and showed its importance in the solutions. They studied the equations that account for the modal crossover phenomenon in the frequency. The frequency of the symmetric in-plane modes showed that it vary with the introduced parameter which resulted to the existent of the cross over points when the frequencies of the symmetric in-plane modes are equal to those of neighbor antisymmetric in-plane modes [81]. They also conducted experiments, and reported the validly of the theory using the results of a simple taut horizontal chord cable which was exited to demonstrate the modal crossover phenomena. Irvine and Griffin [82] done more work on cable response analysis due to dynamic loading as it occurs in case of support acceleration. It can be seen that these early models were limited due to difficulty in using the mathematical tools to find solutions [83].

Irvine [84] extend the work and applied the introduced linear theory of horizontal cable on inclined cables, where the supports are not at same level. The addition was simply using a coordinate transformation to the cable chord. However, in this work he ignored the weight component which is parallel to the cable chord. More work into finding solution for the free vibration of an inclined extensile sagged cable was by Triantafyllou [85], in his work weight component and spatial variability of dynamic tension were taking into account. In addition, he showed that the inclined cables differ than the horizontal cables regarding properties, stating that it cannot be obtained by simply extending the horizontal cable results. Nevertheless, the Irvine's theory was validate by confirming for a range of parameters. In addition, the weight component from other point of views was studied by many scholars; Triantafyllou and Grinfogel [86] where they extended Triantafullou's work and drive a simple approximate formulas for the inclined cables. Burgess and Triantafyllou [87] used an asymptotic solution to explore the properties details of the out-of-plane modes for horizontal and inclined cables of small sag. Zhou et al. [81] stated that all the models dealt with inclined cable showed that the natural frequencies did not cross over because of the inclination the modes become hybrid modes, a mix of symmetric and antisymmetric shapes, with an effect on the dynamic tension, and this phenomenon is accompanied by the variation of the curvature along the catenary profile in the static state when the cable is inclined which would not occur is the parabolic assumption is adopted.

For the study of the interaction between transversal, vertical, and torsional motions for untwisted sagged cable, it started with the focus on investigation of the cable galloping phenomena. Galloping is a low frequency, high amplitude vibration that occur on iced cables in a steady-side wind [88]. For that, many simplified theories are introduced, Nigol and Power [89] and Desai et al. [90] described the coupling between vertical and torsion, Jones [91] studied the coupled vertical and horizontal motion, Yu et al. [92,93] proposed an analysis for the horizontal, vertical, and torsional coupling. Yu et al. stated that the previous investigations on that resolved to be not satisfactorily, and the reason for this shortcoming is that there is no simple model available that capture the coupling between the cable motions. In addition, it is noted that the problem in the proposed theories may be simplified because it did not account for nonlinearity of the geometry and accommodate the various of interactions between the motions [94]. The dynamic interaction between other system elements and cables require studying the boundary induce cable vibrations. Davenport and Steels [95] have investigated this problem. More work have been done on that by Veletsos and Darbre [96], Starossek [97,98] have completed a linear theory of damped cable of boundary induced vibration.

As a result, the use of finite element method or finite difference will easily enable embedding these effect in the cable model. For finite element modeling, a range of different elements types were used, from simple two-nodes to a higher order element to analysis the dynamic response. Among which have been reviewed in Desai et al. [99], where they developed a three-node isoperimetric cable element to perform a geometric nonlinear, static analysis of single cable structure experiencing only translational deformations. Desai et al. [94] enhanced the three-node element model to include the torsion and analyze the galloping of a multi-span transmission line.

As it has been long recognized that due to the twist in the cable, in another words the helical geometry, an axial load not only produces an extension but also rotation and a torque load produces a torsion along with extension. There are number of failure mechanisms associated with the extensional-torsional characteristics of which are hocking, kinking, and birdcaging [100]. When including the bending stiffness effect, the bending and torsional angels can be used to describe the cable motion, this formulation is referred to as the Kirchhoff-Love rod theory by Love [12]. Most of these models introduced previously studied the axial loading with ignoring the torsional associated when solving the dynamic of taut lines. Samras et al. [101] initiated the investigating and emphasis on the importance of taking the couple extensional-torsional behavior into account of cable under dynamic loading. Samras et al. studied the couple extensional torsional problem on a straight twisted cable stretching for ocean floor to the surface with one end subjected to sinusoidal forcing function to represent the oceanic wave and found the equations of motion and derived a closed form solutions to solve the frequency under four different boundary conditions while ignoring the internal and external damping. The frequency results were compared with the result in the case if only extensional deformation is considered. It showed that the results of the coupled frequencies have lower results that the one with extensional theory, and they stated that the torsional behavior of the cable needs more exploring, considering the importance of cable structures.

Samras et al. [101] also examine the coupling coefficients and stated that the axial-torsional stiffness coefficient is approximately equal to the torsional-axial stiffness coefficient [102]. In another related paper, Skop and Samras [103] analyzed two different types of cables one torque balanced and the other is not, although the previous classic theories viewpoint treated only the extensional vibration which gave a similar results for both cable construction, inclusion of coupled extensional-torsional vibration showed a significant different between their responses [100]. On both papers for their dynamic analysis, they found the stiffness matrix of steel cables experimentally. In addition, the experiment found that the axial-torsional stiffness coefficient is approximately equal to the torsional-axial stiffness coefficient. Jiang et al. [104] pointed that helical springs under same loading exhibits similar axial-torsional coupling effect, and that has considerable amount of attention in the literature. So, for springs system Jiang et al. [104] derived a closed form analytical solution of the coupled behavior where the system is under dynamic load and that was a continuation of their previous work, Jiang et al. [105], the presented results was only for helical spring which have finite length. Their method could be applied on cables under similar type of forces.

Raoof et al. [106] work showed the relation of spiral strand which is under impact loading, and developed a closed-form solution that predict the extensional wave speed and displacement for spiral strand loaded axially and experiencing specific forms of impact loading at one end while the other end is fixed. Furthermore, there are many studies that studied the response of a coupled behavior cable under specific forms of impact loading. Phillips and Cosfello [107] preformed a preliminary investigation on the response of a single layer strand with no core cable to impact loading with negligent the friction in the model. Leech and Overington [108] extended the work done by Phillips and Cosfello [107] however a different method was used to solve the derived basic equations, they also conducted experiments on the single layer cable and supported their theory.

Apart from the explicit analytical approaches, the finite element analysis is widely used to solved the static and dynamic problems of cables structure, which is based on approximate interpolation function, because the accordingly and versatility amount of work devoted to develop the finite cable elements. Many researchers; Kwan [109], Mitsugi [110], Stefanou et al. [111], Vilnay & Rogers [112]; developed straight linear elements where these elements resulted in a proper response when having a small sag with high pretension. The multi-node elements which have higher order interpellation polynomials also were used to model cable with large sages, it is seen that finite element analysis has the ability to solve such a problem with no limitation. However, the main problem of using finite element analysis is that it is difficult to determine the accurate coordinates of the internal nodes of the cable corresponding to the cable catenary configuration when having large sag, to overcome this problem, a family of isogeometric analysis have been introduced by Hughes et al. [113] as an efficient approach in the engineering and science disciplines, the main idea of it to bridge the gap between the computer-aided design and finite element analysis [83]. Thai et al. [83] used this method to determine the natural frequencies and exact geometries of mode shapes for cable structures. Hashemi and Roach [114] derived a dynamic finite element for the coupled extension-torsional vibration analysis of a uniform cable and found the coupled frequencies. Alkharisi and Heyliger [73] found the effective mass and stiffness component for coupled cables using constants that are driven from three-dimensional model. Moreover, using that the vibration behavior of a typical cable segment was studied using these properties with both analytical and finite element models, that was applied and discussed for homogenous and composite cable geometries for three representative types of cables.

Other studies focused more into the nonlinear interaction which increase in the finite-amplitude dynamic of elastic suspended cable such in Henghold et al. [115] where they did a three-dimensional analysis for the free vibration of a single span cable by employing a nonlinear finite element technique. Many other researchers have been working on the matter if nonlinear free and forced vibration of cables to formulate theories and analyze the behavior. And, recently, by Rega [116,117] discuss the main features and problems associated with the nonlinear vibration analysis of suspended cables as well as other researchers as Perkins [118], Srinil and Rega [119], Wang and Zhao [120], Lacarbonara and Pacitti [121], and Lacarbonara [122]. Lacarbonara and Pacitti [123] and Arena et al. [123] studied the nonlinear response of cables that are elastic including the flexural stiffness or flexural-torsional stiffness. These studies are essential to understand the large amplitude mechanism in the cables vibration analysis. Thai and Kim [124] solved the nonlinear dynamic problems of cable structure using the catenary cable element for the Newton-Raphson and Newmark direct integration methods. It stated that the cable with the cure configuration is model using a single two-node catenary element without adding internal nodes, by applying this approach less number of degree of freedom is required, however as a result, it is not easy to obtain a realistic vibrational mode of shapes of cable because the lack of the internal nodes, in addition, it is impossible to model the prefect vertical cable because of the mathematical error occurring when the projected lengths of catenary cable is used [83]. In addition, Lepidi and Gattulli [125] studied the effect of the temperature on the static as well as the dynamic behavior of suspended inclined cable using continuous mono-dimensional model which considers the nonlinearly in the geometry, a closed-form solution was presented including the properties featuring the dynamics, however they were narrowed to the isolated shallow parabolic cables with low frequency range.

CHAPTER 3: FREQUENCY ORDER AND MODAL SHIFTS IN SAGGED CABLES

3.1 Summary

The free vibration of uniform isotropic cables has wide application in various engineering fields. In this study, the natural frequencies and modes shapes of vibration of sagged cables fixed at the same level are investigated using both numerical models and experimental results. The axial and torsional characteristics of the cable element are fully considered and a generalized cable finite element with six degrees of freedom model is formulated to describe the dynamic motion of cable line in which longitudinal, vertical, and transverse translations and rotations included. The finite element model is applied to two cables that are replicated by experimental work. Results from the proposed finite element model are compared to the analytical solution of Irvine and Caughey [80]. Special focus is given to the influence of the non-dimensional parameter λ^2, which defines the combination of geometric and material properties that influences frequency order. Excellent agreement found with experimental results that indicate significant levels of modal coupling that do not appear in analytical solutions.

3.2 Introduction

The use of cables as structural elements has increased since they are capable of taking large axial loads and have a relatively high strength to weight ratio. Their mechanical and dynamical behavior heavily depends on their geometry, material properties, and other combined effects. Much of the recent literature on cables focuses primarily on static linear behavior. However, the emphasis here is on the dynamic response of sagged cables whose endpoints are supported at the same level where the cable cross-section is assumed to be circular and isotropic. The special focus of this study is to examine how the frequencies change order and study how the modal displacements in the out-of-plane, in-plane, axial, and torsional directions interact.

The dynamics of uniform cables has a long and rich history starting from the first half of the eighteenth century. Taylor, D'Alembert, Euler, Bernoulli, and Lagrange (see [76]) presented the theory of vibration of a taut and sagged string that was fixed at each end with concentrated masses. Rohrs [75] later developed an approximate solution for the symmetric vertical vibration of a uniform suspended cable with small ratio of sag to span. After this development, interest in this topic waned until the collapse of the Tacoma Narrow's Bridge late in 1940. A significant advance was documented in the classic paper of Irvine and Caughey [80]. In their comprehensive work, they developed a novel linear theory for the free vibration of a uniformly suspended untwisted cable, with both out-of-plane and in-plane motion considered. Their results showed that the symmetric in-plane modes depended on a single parameter that incorporated the combined effects of cable geometry and elasticity. They also conducted experiments and reported the validity of the theory using a simple taut horizontal cable that was excited to demonstrate the modal cross-over phenomena, which occurred between the symmetric and anti-symmetric in-plane frequencies and mode shapes.

The study of the interaction between transverse (out-of-plane) and vertical (in-plane) translations, and longitudinal rotation motions for sagged cables began with the investigation of the cable galloping phenomena. For this type of problem, many simplified theories have been introduced such as that of the Nigol and Power [89] model to describe the coupling between vertical translation and longitudinal rotations. With an increase in the complexity of cable geometry, a great number of unknown variables were involved that required differing approximations and assumptions to consider an extremely challenging problem. Apart from explicit analytical approaches, the finite element method has been widely used to solve both the static and dynamic problems of cable structures. Many researchers including Vilnay and Rogers

[112], Stefanou et al. [111], Mitsugi [110], and Kwan [109] have developed straight linear elements resulting in an accurate response when the cable possesses small sag with a high pretension.

A range of different finite element cable models have been used, from simple two-node approximations to a higher order element, to analyze static and dynamic cable response. Desai et al. [99] developed a three-node isoparametric cable element to perform a geometric nonlinear static analysis of single cable structure experiencing only translational deformations. For the dynamic problem, Desai et al. [90] described coupling between vertical translation and longitudinal rotations. Starossek [98] studied the vertical vibration behavior of sagged cables using a dynamic stiffness matrix where the viscous damping due to external fluid was considered where only motion within the vertical cable plane was considered. Jones [91] studied the coupled vertical and longitudinal translation motion of cables, while Yu et al. [92,93] proposed methods to study the longitudinal and vertical translations and longitudinal rotation coupling, where they stated that previous investigations on galloping had not yet been resolved. The primary reason for this shortcoming was that there was no simple model available that captured all of the coupling that can exist as the cable displaces. Desai et al. [94] enhanced the three-node element model to include the longitudinal rotation with the longitudinal, vertical, transverse translation motion (4 degrees of freedom) and analyzed the galloping of a multi-span transmission line.

Other recent studies focused more on the nonlinear interactions that can occur in the finite-amplitude dynamics of elastic cables. Rega [116,117] discussed the main features and problems associated with this behavior. Multi-node elements that possess higher order interpolation polynomials were also used to model cables with large sag. The main problem of using finite element analysis for this class of problem is that it is difficult to determine the accurate coordinates of the internal nodes of the cable corresponding to the cable catenary configuration when having large sag. To overcome this problem, a family of isogeometric analyses were introduced by Hughes and co-worders [113] and Thai and co-workers [19]. Thai and Kim [124] solved the nonlinear problem of cable structure using the catenary cable element subjected to static and dynamic loading. The incremental iteration solution which are based on the Newton-Raphson and Newmark direct integration methods were used for solving the nonlinear equations. Thai [83] continued using this method to determine the in-plane natural frequencies and exact geometries of mode shapes for cable structures. However, modal coupling was not discussed.

Many previous studies of cable vibration have somewhat limited application because of the restrictive geometries and boundary conditions used. In addition, many commercial finite element programs cannot be readily used when modeling and analyzing cable structures since they frequently lack the cable elements that are able to model actual displacements that include coupling and torsional stiffness [126]. In this paper, a three-dimensional finite element model is used to study the free vibration characteristics of the three-dimensional cable after a geometrically nonlinear deformation from the cable weight, taking advantage of this method to deal with the sagged cables and effectively show the influence of various parameters of the cable system. Axial and torsion coupling terms resulting from a twisted in the cable is not included in this study. The results of two examples are compared and assessed against a series of cable vibration experiments and the well-established analytical model from the literature. Several conclusions are drawn from the comparisons and some important new results are discussed.

3.3 Theory

The numerical method used here is based on representing the sagged cable line as a series of one-dimensional finite elements that have isotropic and linear elastic properties and are assumed to have n nodal points; each node has six degrees of freedom along the directions of the three axes. The element's stiffnesses and mass matrices and the nodal translations and rotations are given in terms of the global coordinate system. The equation of motion is derived and is based on small dynamic perturbations about the deformed equilibrium state caused by the cable weight. The static configuration prior to vibration includes the initial sag of the cable and the appropriate boundary conditions. The equation of motion takes the usual form

$$[M]\{\ddot{q}\}+[K_t]\{q\}=\{F\} \qquad (3.1)$$

Here $[M]$ and $[K_t]$ are the $N \times N$ global mass and stiffness matrices of the cable structure, respectively, and formed after employing the regular assembly procedure over all the discretized elements, where N is the total number of degrees of freedom. The $\{q\}$ vector contains the global translations and rotations and $\{F\}$ is the external dynamic load specified to be zero to study the free vibration. The dot superscript denotes differentiation with respect to time t. In the parametric study presented in this paper, Eq. (3.1) is used to find the natural frequencies and corresponding mode shapes, which are obtained by solving the standard eigenvalue problem, obtained after imposing the assumption of harmonic motion. This appears in the usual form:

$$[K_t]\{q\}=\omega^2[M]\{q\} \quad (3.2)$$

Damping effects, though very important, are not included in this study. The elastic, geometric, and mass matrices and the load vector are derived for a cable element in the following subsections. Details of material, span, and supports are also given for the two examples. In this work, the frequency order for the out-of-plane, symmetric in-plane, anti-symmetric in-plane, axial, and torsional modes are studied for a range of different sag values, and the nature of these modes are thoroughly discussed.

3.3.1 The Two-Node Cable Element

The static configuration of the cable line is subjected initially to its gravity load. The initial vertical position of the cable is given by the parabola using [82]

$$Y = 4d\left\{\frac{X}{L} - \left(\frac{X}{L}\right)^2\right\} \qquad (3.3)$$

Here L is the span and d is the sag value of the cable structure.

Several approaches to analyze the static behavior of sagged cable structures have been reviewed by Desai et al. [99]. Some are based on the discretization of the equilibrium expressions followed by an iterative solution of the resulting non-linear algebraic equation. This method has been largely used and applied here using straight-line elements that possess all nodal translations and rotations based on the primary axial and torsional stiffnesses possessed by the cable. All other stiffness contributions, such as those related to bending, are assumed to be small relative to these primary stiffness contributions and can be neglected.

The cable line is first discretized over its length using two-node isoparametric elements. Each element is referred to the global X, Y, Z axes and the initial intrinsic coordinate S. The three translations are denoted as U, which is the longitudinal in-plane motion (parallel to the X axis), V, which is the vertical in-plane motion (parallel to the Y axis), and W as the transverse out-of-plane motion (parallel to Z axis). The rotations are denoted as $\theta_X, \theta_Y, \theta_Z$, in the X, Y, Z

directions, respectively. A schematic of these parameters is shown in Fig. 3.1. The nodal displacement vector for each element is therefore defined as

$$\left\{q^e\right\} = \left[U_1 \quad V_1 \quad W_1 \quad \theta_{X1} \quad \theta_{Y1} \quad \theta_{Z1} \quad U_2 \quad V_2 \quad W_2 \quad \theta_{X2} \quad \theta_{Y2} \quad \theta_{Z2}\right]^T \quad (3.4)$$

Here the T superscript denotes the transpose and the numbers 1 and 2 refer to the left and right endpoints. For all problems studied, a pin-pin conditions is applied at the endpoints where all three translations are specified to be zero and the rotations are unrestrained.

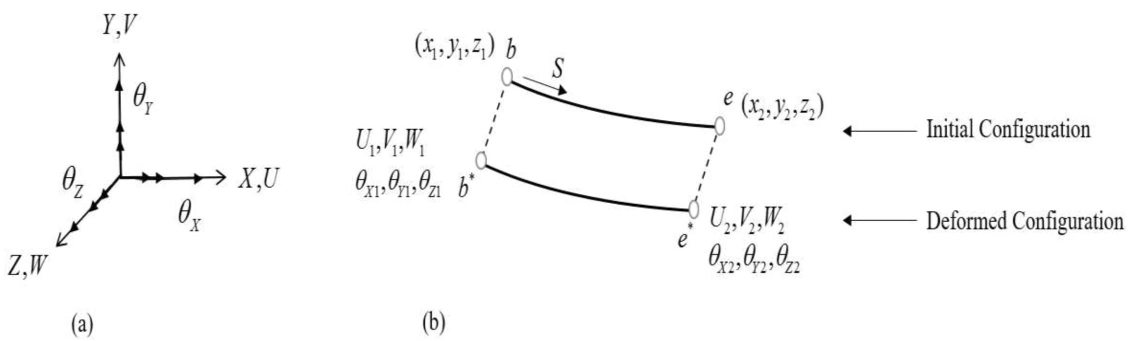

Fig. 3.1 Characteristics of the cable element: (a) global coordinate system and displacements (b) the two nodes cable elements in two-dimensions

3.3.2 Stiffness Matrix of Cable Element

The total element stiffness matrix is derived in the global coordinate system directly and is defined as

$$\left[K_t\right] = \left[K^e\right] + \left[K^g\right] \qquad (3.5)$$

Here $\left[K^e\right]$ is the elastic stiffness matrix and $\left[K^g\right]$ is the geometric stiffness matrix. The elastic stiffness is merely the modified form of the conventional symmetric spatial truss stiffness matrix, along with torsion about the longitudinal axis that is included with the extension of the cable. The local elastic stiffness expressed as

$$
\left[k^e\right]=\begin{bmatrix}
\frac{EA}{h} & 0 & 0 & 0 & 0 & 0 & -\frac{EA}{h} & 0 & 0 & 0 & 0 & 0 \\
0 & 0 & 0 & 0 & 0 & 0 & 0 & 0 & 0 & 0 & 0 & 0 \\
0 & 0 & 0 & 0 & 0 & 0 & 0 & 0 & 0 & 0 & 0 & 0 \\
0 & 0 & 0 & \frac{GJ}{h} & 0 & 0 & 0 & 0 & 0 & -\frac{GJ}{h} & 0 & 0 \\
0 & 0 & 0 & 0 & 0 & 0 & 0 & 0 & 0 & 0 & 0 & 0 \\
0 & 0 & 0 & 0 & 0 & 0 & 0 & 0 & 0 & 0 & 0 & 0 \\
-\frac{EA}{h} & 0 & 0 & 0 & 0 & 0 & \frac{EA}{h} & 0 & 0 & 0 & 0 & 0 \\
0 & 0 & 0 & 0 & 0 & 0 & 0 & 0 & 0 & 0 & 0 & 0 \\
0 & 0 & 0 & 0 & 0 & 0 & 0 & 0 & 0 & 0 & 0 & 0 \\
0 & 0 & 0 & -\frac{GJ}{h} & 0 & 0 & 0 & 0 & 0 & \frac{GJ}{h} & 0 & 0 \\
0 & 0 & 0 & 0 & 0 & 0 & 0 & 0 & 0 & 0 & 0 & 0 \\
0 & 0 & 0 & 0 & 0 & 0 & 0 & 0 & 0 & 0 & 0 & 0
\end{bmatrix} \quad (3.6)
$$

Here E is the modulus of elasticity, A is the cross-sectional area, G is the shear modulus, J is the polar moment of inertia, and h is the element length which can be found using

$$
h=\sqrt{(X_e-X_b)^2+(Y_e-Y_b)^2+(Z_e-Z_b)^2} \qquad (3.7)
$$

The locations X_e, Y_e ,and Z_e, and X_b, Y_b, and Z_b donate the global coordinate of the nodes to which element ends b and e, respectively.

The geometric stiffness matrix is associated with the forces employed by the stressed element due to the direction changes of the element when displaced. This matrix can be described in the local coordinate system as

$$\left[k^g\right] = \frac{F_a}{h}\begin{bmatrix} I & O & -I & O \\ O & O & O & O \\ -I & O & I & O \\ O & O & O & O \end{bmatrix} \quad (3.8)$$

Where F_a is the axial force at the beginning of each incremental step and I is a 3×3 identity matrix.

3.3.3 *Mass Matrix of the Cable Element*

The kinetic energy terms represented in the mass matrix for predicting the axial and torsional behavior can be easily determined by pre-integrating the mass using

$$m_{uu} = \int_V \rho dV \qquad (3.9)$$

$$m_{\theta_x\theta_x} = \int_V \rho r^2 dV \qquad (3.10)$$

These terms depend on the pointwise mass density ρ, r is the distance from the polar origin to any arbitrary location in the cable cross-section, and V is the total volume. The consistent mass in matrix form is then given as

$$[m] = \frac{h}{6}\begin{bmatrix} 2m_{uu}I & O & m_{uu}I & O \\ O & 2m_{\theta_x\theta_x}I & O & m_{\theta_x\theta_x}I \\ m_{uu}I & O & 2m_{uu}I & O \\ O & m_{\theta_x\theta_x}I & O & 2m_{\theta_x\theta_x}I \end{bmatrix} (11)$$

Here O is a 3×3 null matrix.

3.3.4 *Finite Element Solution*

To solve the vibration problem for the cable system, the matrices introduced previously need to be transformed from the local to global coordinate system. The transformation matrix T for a cable element can be derived using similar procedures for other structural members and is not repeated here. The three-dimensional cable element orientation is defined by the angles between the local coordinate system axes and the global coordinate system axes. Considering the end forces from global to the local coordinate system at b and e (Fig. 3.1(b)), the cable elements local forces are equal to the sum of the components of the forces in the global system in the direction of local axes. Similarly, the local moments at both ends are expressed in terms of global counterparts. The transformation relationship can be found between the cable local end forces and global end force vectors in compact form as

$$[T]=\begin{bmatrix} c & O & O & O \\ O & c & O & O \\ O & O & c & O \\ O & O & O & c \end{bmatrix} \qquad (3.12)$$

Here c is the cable element rotation matrix and is given as

$$[c]=\begin{bmatrix} c_{xX} & c_{xY} & c_{xZ} \\ -c_{xY} & c_{xX} & c_{xZ} \\ -c_{xZ} & -c_{xY} & c_{xX} \end{bmatrix} \qquad (3.13)$$

The direction cosines contained in this matrix are given as

$$c_{xX} = \cos\theta_{xX}$$

$$c_{xY} = \cos\theta_{xY}$$

$$c_{xZ} = \cos\theta_{xZ} \qquad (3.14)$$

The transformation matrix plays a crucial role in the three-dimensional analysis of cable structures by representing all element translations and rotations in a single coordinate system. It will enable identifying the finite member's orientation in a convenient method.

The shape associated with the original sag of the cable is idealized. In practice, the cable is arranged according to its parabolic shape without any loading applied. The difficult issue is that the final equilibrium position of the cable cannot be determined before the self-weight of the cable has been applied. Hence after beginning the analysis with the cable in ideal parabolic form, the uniform load is then applied from the self-weight of the cable (applied as a concentrated point load at each node). The load was then applied incrementally and the geometry and forces were updated iteratively. The initial sag value was specified as $d = 17.13\ \text{cm}$. This distance increased because of the cable weight and axial stretching as shown in Fig 3.2. This step is usually ignored in the previous classic analysis because the finite element model needs to generate the internal axial force as a function of total cable stretch and applied load. After the equilibrium position of the stretched cable has been obtained, the eigenvalue problem was then solved to find the frequencies and corresponding mode shapes.

In all cases, convergence of the frequencies were tested using meshes of 4, 8, 16, 32, and 64 elements. There was little difference between 32 and 64 element results, indicating that 32 elements were sufficient for most of the analyses considered.

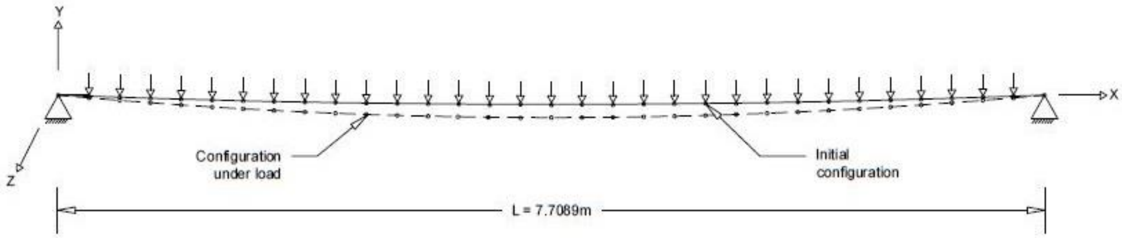

Fig. 3.2 Cable configuration before and after applying load

3.4 Experimental Model

An experimental study investigating the frequency spectrum of two uniform cables undergoing forced support motion was conducted to buttress results from the numerical models. The cable length was chosen based on the facility capacity as $L = 7.7089\ \text{m}$. A MTS's 243.20 hydraulic actuator [127] was used to excite a single end of the cable under harmonic support motion. The focus was on the out-of-plane, symmetric in-plane, and anti-symmetric in-plane vibrational modes. The experimental setup overview is shown in Fig 3.3, where the sagged cables are hanging fixed from both supports at the same vertical level.

The experiments were used to investigate the behavior of an extensible sagged cable ($d = 17.13\ \text{cm}$). Each test was repeated 20 times for each frequency. The protocol was to subject one end of the cable to a harmonically time-varying support motion in the vertical direction using the actuator driven via a power control unit (MTS's 407 controller [128]). MetaTracker sensors [129] were used to obtain the vibration data for the cables. These sensors include an accelerometer that gives the acceleration records in all three directions, including acceleration time history signal for $\ddot{W}$ which is the transverse out-of-plane motion , $\ddot{V}$ as the vertical in-plane motion, and $\ddot{U}$ as the longitudinal in-plane motion. Two trackers were used for the first and second application points on the cables at one quarter and one half distances of the cable span.

For each cable configuration, a series of tests were carried out by varying the frequency at the support to force the cable to vibrate at the excitation frequency. If the exciting frequency coincides with the natural frequency of the cable, resonance is encountered, and the oscillation results are collected. The acquisition duration for each reading ranged from 15 to 30 seconds, and the sampling frequency for the measured accelerations was 12.5 Hz. For each in-plane and out-of-plane vibrational mode and each cable configuration, a total of six data sets were collected. The natural frequencies of the two cables considered in this paper were obtained by recording the frequency when a response peak was observed being driven by support motion of the cable.

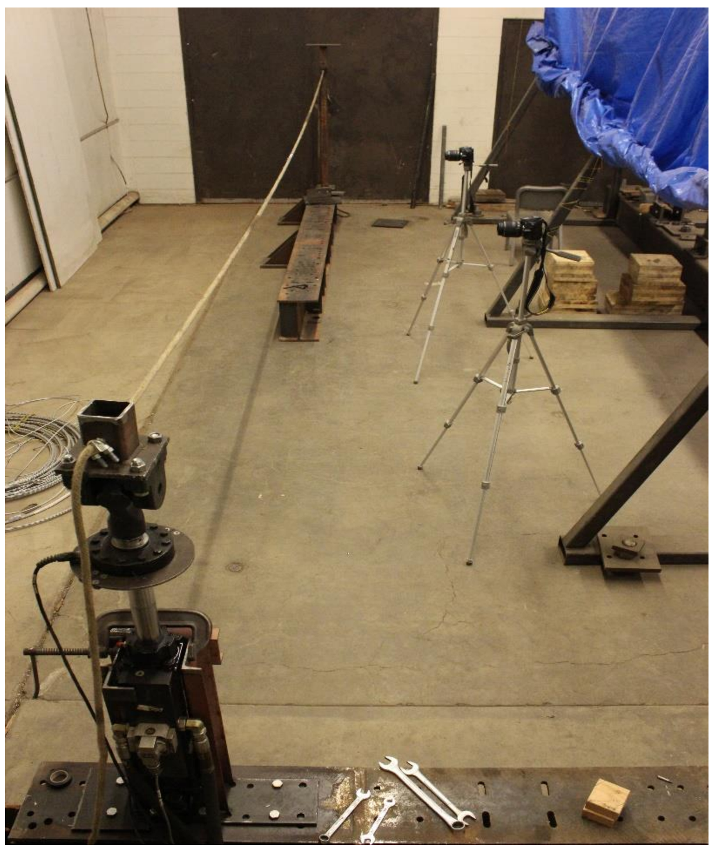

Fig. 3.3 Experimental setup for the sagged cables study with the actuator at one end and a fixed support at the far end

3.5 Analytical Solutions

The finite element model generates predictions of the natural frequencies and mode shapes of the out-of-plane, symmetric in-plane, and anti-symmetric in-plane modes that can be compared with the experimental results and the analytical solution Irvine and Caughey [80]. These latter frequencies are given by

$$f_o = \frac{i}{2\pi}\sqrt{\frac{H}{m}} \qquad (3.15)$$

$$f_{anti} = \frac{2i}{2\pi}\sqrt{\frac{H}{m}} \qquad (3.16)$$

$$f_s = \sqrt{\frac{\beta_i^{\,2} H}{m}} \qquad (3.17)$$

Here f_o, f_{anti}, and f_s are the corresponding out-of-plane, anti-symmetric in-plane, and symmetric in-plane frequencies where the second out-of-plane frequency is equal to the first anti-symmetric frequency. The parameter H is the horizontal component of the cable tension specified by Irvine and Caughey [80] as

$$H = \frac{mgL^2}{8d} \qquad (3.18)$$

And it is the determination of this value and its relationship with the sag *d* that requires additional effort in the finite element model. Here m is the mass per unit length of the cable and g is the acceleration of gravity. The $\beta_i l$ value follows from the transcendental equation

$$\tan\left(\frac{1}{2}\beta L\right) = \left(\frac{1}{2}\beta L\right) - \left(\frac{4}{\lambda^2}\right)\left(\frac{1}{2}\beta L\right)^3 \qquad (3.19)$$

Where

$$\lambda^2 = \left(\frac{8d}{L}\right)\frac{L}{\left(HL_e / EA\right)} \qquad (3.21)$$

The non-dimensional parameter λ^2 accounts for the geometric and elastic properties of the cable and its value allows for significant insight into the behavior of the vibrational modes of the cable. Irvine and Caughey [80] extensively studied a cross-over phenomena that occurred between the symmetric and the anti-symmetric frequencies and mode shapes. They found that when $\lambda^2 > 4\pi^2$, the first symmetric in-plane frequency is greater than the first anti-symmetric in-plane frequency. In addition, the first symmetric in-plane mode has two internal nodes along the span. In contrast, when $\lambda^2 < 4\pi^2$, the first symmetric in-plane frequency is lower than the first anti-symmetric in-plane frequency, and the mode shape has no internal node. When $\lambda^2 = 4\pi^2$ the two frequencies are equal and the mode shape takes the static profile of the cable shape with no internal node. These cases are all explored in this study.

The axial and torsional frequencies and mode shapes were not considered by Irvine and Caughey [80] since they were outside the bounds of the frequencies of interest. However, these are still of interest and the analytical solution for the axial and twisting modes of a straight bar provide values for these frequencies given by [130]

$$f_a = \frac{i}{2L}\sqrt{\frac{E}{\rho}} \qquad (3.21)$$

$$f_t = \frac{i}{2L}\sqrt{\frac{G}{\rho}} \qquad (3.22)$$

3.6 Application

To verify the applicability and performance of the finite element model, the solutions were compared with the results obtained from the experimental model and those obtained using the analytical models available in the literature and replicated here.

Unless stated otherwise, the cables under investigation here have the following material and physical parameters. Cable 1 is an Aluminum Conductor Steel Reinforced cable (ACSR) with mass density $m = 0.35\ \mathrm{kg/m}$, a modulus of elasticity of $E = 74.2\ \mathrm{GPa}$, shear modulus $G = 37.1\ \mathrm{GPa}$, and cross-section area of $A = 91.3\ \mathrm{mm}^2$. Cable 2, is a circular plastic tube with a mass density of $m = 0.2\ \mathrm{kg/m}$, a modulus of elasticity of $E = 8.27\ \mathrm{GPa}$, shear modulus $G = 4.135\ \mathrm{GPa}$, and cross-section area $A = 0.576\ \mathrm{mm}^2$. For both specimens a cable length of $L = 7.7089\ \mathrm{m}$ value was used. The configuration of the cables varied from a relatively small amount of sag ($d = 2\ \mathrm{cm}$) to relatively large sag ($d = 20\ \mathrm{cm}$). The values of the non-dimensional parameter λ^2 changed both with the sag value d, and the static cable tension component H.

3.7 Results and Dissection

The natural frequencies and mode shapes for the two representative uniform sagged cables are presented in this section. The finite element results are compared to the experimental and analytical results. The results include the interactions observed between the longitudinal transversal and vertical translations and rotations, which occur in the out-of-plane, symmetric in-plane, anti-symmetric in-plane, axial, and torsional frequencies. The effect of sag variation on the cable dynamics is also considered.

A convergence study for the finite element model for Cable 1 is presented in Table 3.1. The results show excellent convergence when there are more than eight elements used to model the cable with a relatively large value of sag ($d = 17.13\ \text{cm}$).The results show that all frequencies resulting from 64 elements have less than 0.1% error from the analytical solutions. This indicates that the present finite element approximation with 64 elements used is sufficient in calculating the modal frequencies of the uniform sagged cable.

Table 3.1 Convergence of natural frequencies for Cable 1 (d=17.137 cm)

	Frequency $f\,(\text{Hz})$						
	Irvine	Circular Bar	Finite Element Model Elements in Selected Span				
			4	8	16	32	64
Out-of-Plane	1.329	-	1.363	1.337	1.331	1.329	1.329
In-plane symmetric	3.791	-	4.624	4.020	3.852	3.811	3.801
In-plane anti-symmetric	2.658	-	2.929	2.726	2.675	2.662	2.659
Axial	-	280.051	287.221	281.809	280.471	280.144	280.067
Torsional	-	198.026	203.322	199.390	198.412	198.169	198.108

The frequency spectrum for both cables was then found experimentally. At two points on the cable span (mid and quarter span), the trackers captured the acceleration values with each signal processed using the Fast Fourier Transform algorithm function. The primary focus of these experiment was to confirm the values of the out-of-plane, symmetric in-plane, and anti-symmetric in-plane frequencies but also determine the appearance and level of coupling between the types of vibrational modes. Table 3.2 summarizes the frequency results for both cables. The experimental frequencies are in excellent agreement with those obtained using the finite element model. For both cables, the finite element model yields frequencies that are larger by 0.55%, 0.63%, and 1.23% for the out-of-plane, symmetric in-plane, and anti-symmetric in-plane frequencies, respectively.

Table 3.2 Finite element and experimental natural frequencies results (d=17.13 cm)

	Frequency $f\,(\mathrm{Hz})$			
	Cable 1		Cable 2	
	Experiment (Median)	Present Finite Element Model	Experiment (Median)	Present Finite Element Model
Out-of-Plane	1.329	1.329	0.830	0.835
In-plane symmetric	3.825	3.801	1.500	1.503
In-plane anti-symmetric	2.662	2.659	1.612	1.639

The non-dimensional parameter λ^2 was then studied numerically for both cables using a total of 11 different sag values, starting from *d*=0 (no-sag) until *d*=20 cm. Fig. 3.4 shows the relationship between these parameters, with the vertical line indicating that the value of $\lambda^2 = 4\pi^2$ is reached when the sag value is approximately 4 cm. Hence it is expected that Cable 1 will change its behavior (as indicated by the cross-over of modal shapes) at this value of sag. For Cable 2, the parameter λ^2 is always less than $4\pi^2$ and hence the lowest in-plane symmetric mode is always less than the lowest anti-symmetric frequency.

Using the finite element model developed in this work, the frequencies and the corresponding mode shapes were found for all sag values studied for the two cables. The frequencies are listed in Tables 3.3 and 3.4 for Cable 1 and 2, respectively. The present model successfully replicates the cross-over phenomena on the frequency spectrum studied by Irvine and

Caughey [80] analytically and experimentally and other researchers, and also gives the axial and torsional frequencies for different values of sag.

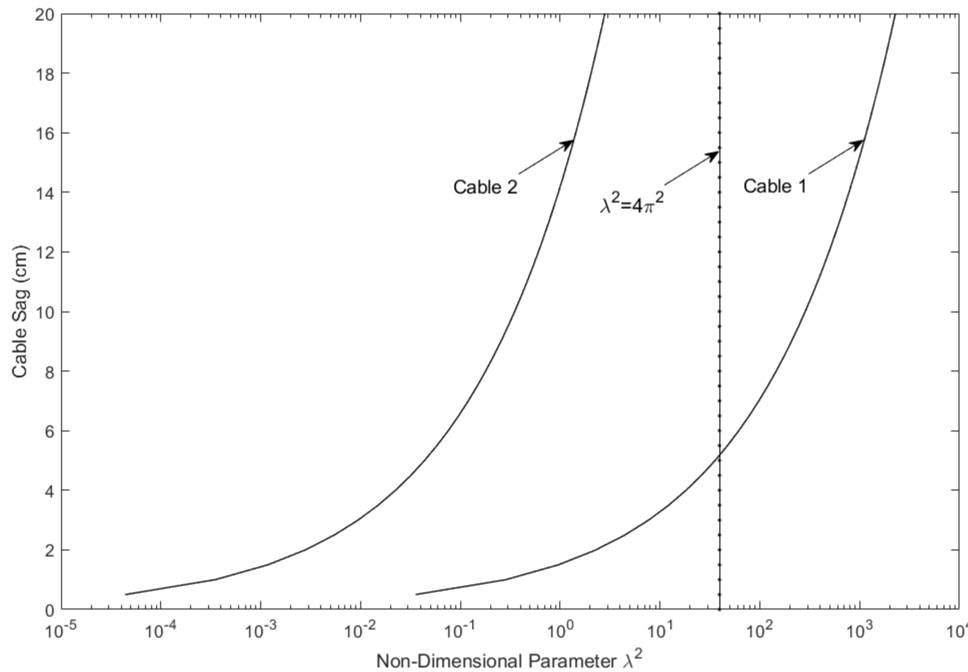

Fig. 3.4 Non-dimensional parameter versus sag value for Cables 1 and 2

For Cable 1, it can be seen from Table 3.3 that the out-of-plane frequencies decrease to 53% of their d=0 value when reaching the maximum sag value (20cm). Starting from $\lambda^2 > 4\pi^2$ the symmetric in-plane frequency becomes larger than the anti-symmetric in-plane frequency. This is consistent with the Irvine and Caughey [80] theory (the eigenvalue here is strongly non-linear with respect to this parameter for higher modes). The axial frequencies only slightly decrease and then increase when $\lambda^2 > 4\pi^2$. But this frequency changes only 0.02% for the case with no sag to the maximum sag. Similarly, the torsional frequency decreases only by 0.03%. Hence the axial and torsional modes are only negligibly impacted by sag and are far higher than other frequencies of vibration. This is in part why these frequencies have seen little discussion in the literature when the cables are isotropic and do not possess axial-torsional coupling.

Since $\lambda^2 < 4\pi^2$ for Cable 2 for all values of sag, the frequencies are consistently increasing or decreasing as shown in Table 3.4. The out-of-plane frequencies decrease about 4% from no sag to the maximum value of sag. The symmetric in-plane frequencies are always less than the anti-symmetric in-plane frequencies, and then increase by 3.4% from no sag to d=20 cm. The same percentage decrease is found for the anti-symmetric in-plane frequencies. For the axial and torsional frequencies, the same percentages of decrease were calculated for Cable 1 that were also found for Cable 2.

Table 3.3 The natural frequencies for Cable 1 using different sag values

	Frequency f (Hz)										
Sag Value (cm)	**No Sag**	**2**	**4**	**6**	**8**	**10**	**12**	**14**	**16**	**18**	**20**
Out-of-Plane	2.629	2.544	2.336	2.097	1.886	1.714	1.577	1.466	1.374	1.297	1.231
In-plane symmetric	4.473	4.608	**5.012**	5.379	5.204	4.831	4.479	4.180	3.927	3.712	3.527
In-plane anti-symmetric	5.260	5.090	**4.674**	4.196	3.773	3.430	3.156	2.934	2.750	2.596	2.464
Axial	280.029	280.027	280.024	280.023	280.024	280.029	280.037	280.047	280.059	280.073	280.089
Torsional	198.067	198.066	198.066	198.066	198.069	198.074	198.081	198.090	198.101	198.113	198.127

Table 3.4 The natural frequencies for Cable 2 using different sag values

	Frequency f (Hz)										
Sag Value (cm)	**No Sag**	**2**	**4**	**6**	**8**	**10**	**12**	**14**	**16**	**18**	**20**
Out-of-Plane	0.860	0.859	0.858	0.856	0.854	0.851	0.847	0.843	0.838	0.833	0.827
In-plane symmetric	1.466	1.466	1.468	1.470	1.474	1.478	1.484	1.491	1.498	1.507	1.517
In-plane anti-symmetric	1.691	1.690	1.688	1.684	1.679	1.672	1.665	1.655	1.645	1.634	1.621
Axial	10.141	10.141	10.141	10.140	10.139	10.138	10.136	10.134	10.131	10.12	10.123
Torsional	7.087	7.085	7.076	7.062	7.043	7.018	6.988	6.953	6.913	6.870	6.822

The corresponding mode shapes for Cable 1 and 2 were also studied numerically and experimentally specifically to show the interaction between modes. This subject has received relatively little attention in prior studies and is of significant interest. The objective here was to also explore the sag variation effect (where the cross-over phenomena was observed for this specific cable). The means of obtaining all experimental values for this part of the work was to take the obtained acceleration data from the experimental tests and integrate the peak quantities to obtain the three translation displacements at their peak. For example, the *U* displacement can be found using

$$U = -\frac{\ddot{U}_{data}}{\omega^2}\sin(\omega t) \qquad (3.23)$$

Similarity for the displacement components V and W, the peak displacement motions from both sensor locations on the cable (mid and quarter span) can also be obtained.

Figure 3.5 shows the displacements for the lowest out-of-plane mode in the X, Y, and Z directions for Cable 1. The displacements are normalized with respect to the peak transverse translation W (the displacement out-of-plane). There are simultaneous translation displacements in the other two directions when the cable undergoes primarily transversal motion. The out-of-plane mode consists of a well-known symmetric transverse component that is the dominant modal displacement but also contains a symmetric longitudinal and vertical component that was captured both in the experimental and finite element results. The results from finite element model show that the maximum amplitude (at mid span) increases 120% and 78.72% in U and V as the sag value increases from 0 to 20 cm. Even when the initial sag is zero, there are small but non-zero displacements in Y and Z directions because of the small sag resulting from the static analysis where the cable weight was considered. The experimental results show generally a good agreement with the finite element results and are given in all Figures as single data points at the ¼ and ½ span length locations. For the primary motion (W), the experimental results were 4.10% higher at the ¼ span sensor location, and lower by 25% for U and higher by 35.3% for V at the mid-span location. The maximum amplitude magnitudes in these two directions are very small (0.0009 and 0.057) compared to the peak value at mid-span. Nevertheless, these values are non-zero and are consistent in both magnitude and modal behavior between finite element and experimental evidence.

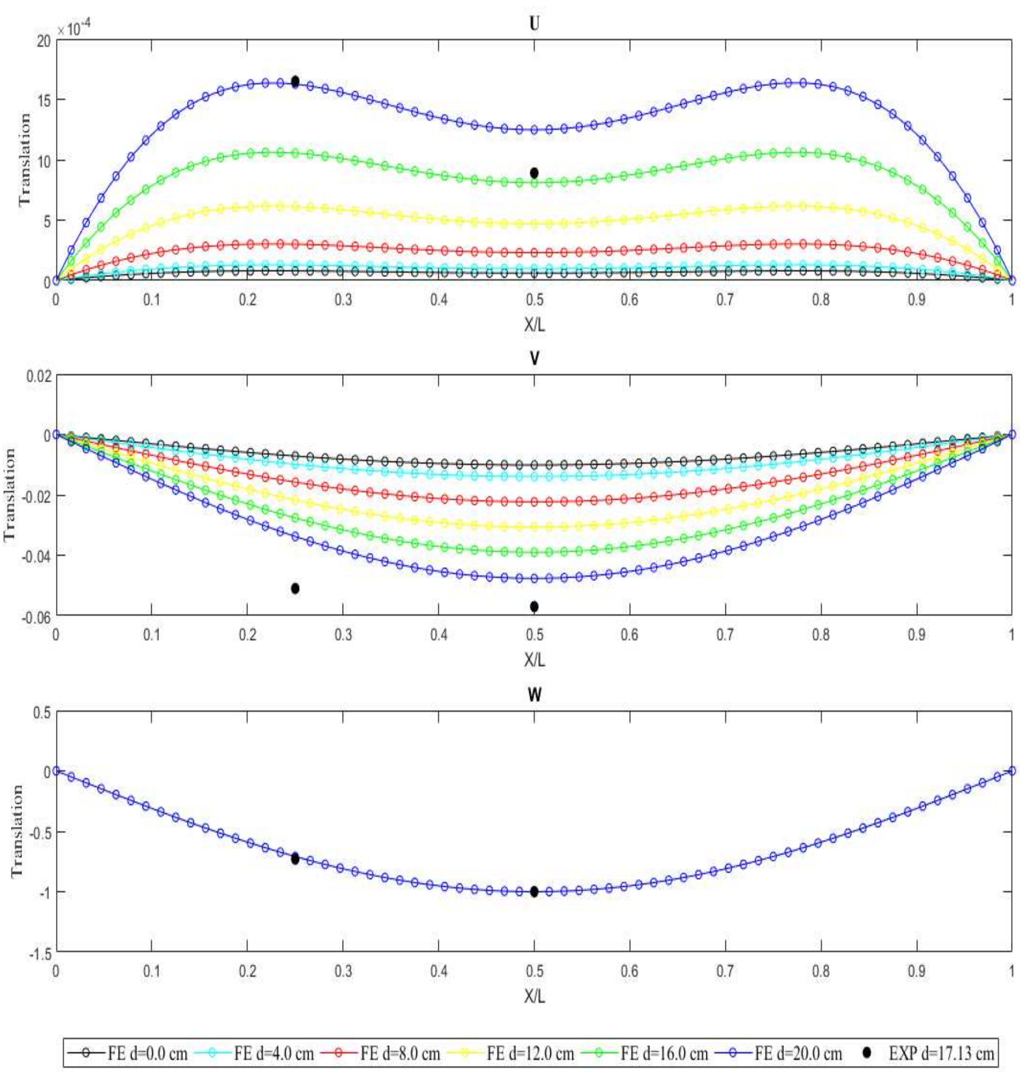

Fig. 3.5 The out-of-plane modal shapes displacements for Cable 1 versus sag values

The effect of sag is significant for the symmetric in-plane modes and it is shown in Fig. 3.6 and Fig. 3.7 for Cable 1 and Cable 2, respectively. When λ^2 is less than, almost equal to, and larger than $4\pi^2$, the cable changes its modal shape as shown in Fig. 3.6. Eq. (3.20) as defined by Irvine and Caughey [80] is of fundamental importance in cable vibration. Using the finite element model, and the case of $\lambda^2 < 4\pi^2$ (specifically no sag and 4 cm sag), the primary vertical motion (V) has no internal nodes along the cable span. When λ^2 is nearly equal to $4\pi^2$, the modal shape also has no internal nodes as in the previous case but in addition to this behavior the frequency identifies the cross-over point in modal behavior (Table 3.2). In this case the modal component is tangent to the static profile of the cable at each support. When $\lambda^2 > 4\pi^2$ the vertical modal plot along the cable length has two internal nodes. This behavior coincided with Irvine and Caughey's theory of vibration where they found that the vertical and longitudinal modal shape change behavior with the non-dimensional parameter λ^2.

In addition, here using the finite element model, it is found that the transversal components modal shapes also changing behavior. The experimental results support the finite element results in the case where $d = 17.13$ cm and show that there are two internal nodes in both the vertical and transverse directions ($\lambda^2 > 4\pi^2$). In addition, it was found both experimentally and numerically that these displacement magnitudes are small when comparing with the primary motion, where the maximum amplitudes are 0.026 and 0.0093 scaled displacement units in the longitudinal and transverse directions, respectively.

As the non-dimensional parameter λ^2 verses the selected sag values is always less than $4\pi^2$ for Cable 2 (Fig. 3.3), the primary modal shape is consistent for all sag values between 0 and 20 cm. And have no integral nodes along the cable span. The coupled longitudinal and transversal components have anti-symmetrical and symmetrical shape. Their displacements magnitude are small comparing to the vertical mode results. And results found experimentally are higher by approximately 64.74% at quarter-span of the cable.

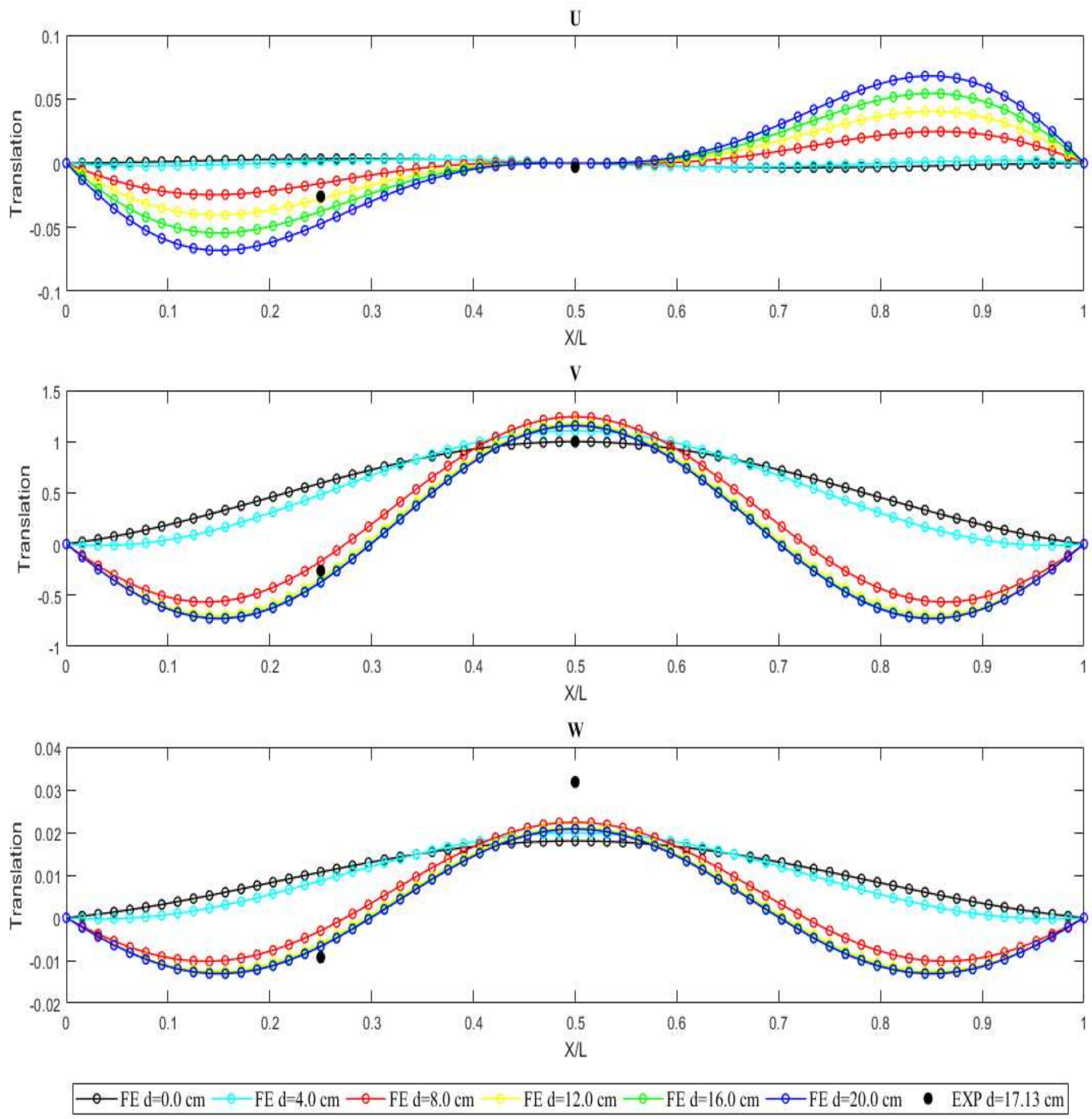

Fig. 3.6 The symmetric in-plane frequency's modal shapes displacements for Cable 1 versus sag values

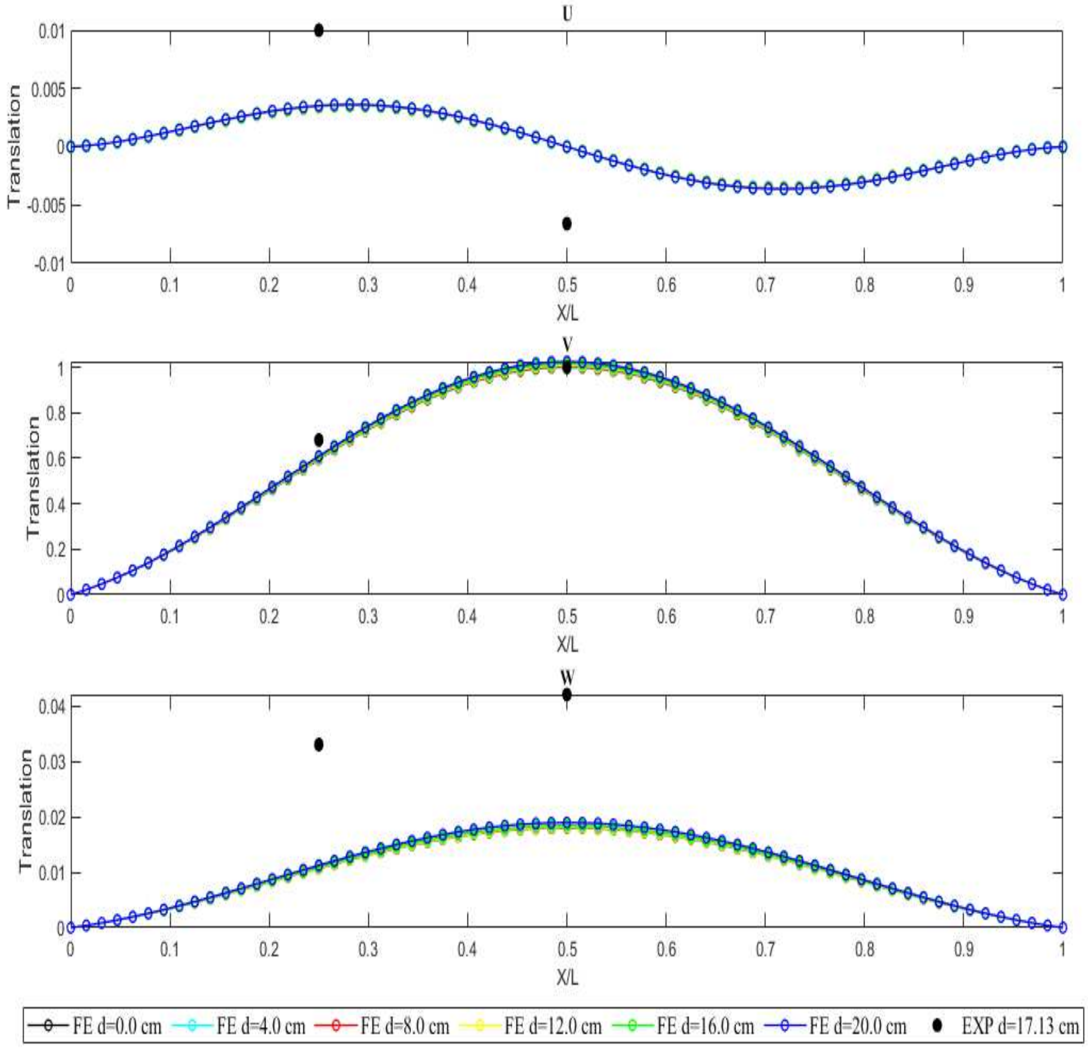

Fig. 3.7 The symmetric in-plane frequency's modal shapes displacements for Cable 2 versus sag values

The anti-symmetric in-plane modes consist of primarily anti-symmetric vertical components, symmetric longitudinal components, and anti-symmetric transversal components as shown in Fig. 3.8 for Cable 1. The finite element results show that the coupled components in U and W become small as the cables sag values decrease. Conversely, the longitudinal displacement increases in magnitude by 79% from 0 to 20 cm. The maximum transverse displacement occurs at the quarter span while it is a minimum at mid-span, with an increase of 72% from no sag to 20 cm.

It was also found experimentally that the transverse displacement (W) is 0.46 for this mode and using the finite element model is between 0.077 to 0.372 unit displacements (depending on the value of sag). This large level of interaction exists because that the second out-of-plane frequency is very close to the first anti-symmetric frequency value, or 2.660 and 2.659 Hz, respectively.

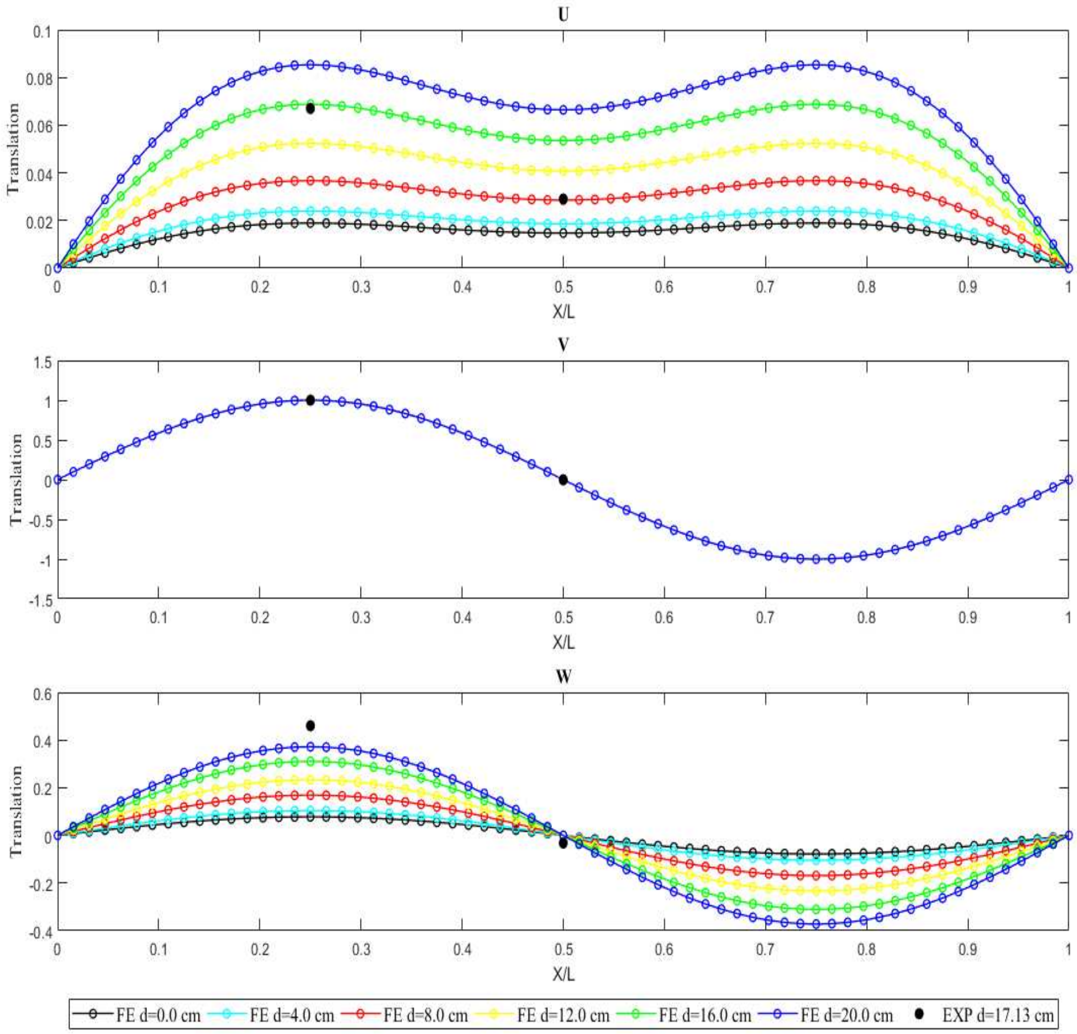

Fig. 3.8 The anti-symmetric in-plane modal shapes displacements for Cable 1 versus sag values

The axial modal shapes are shown in Fig. 3.9 for Cable 1. The primarily symmetric longitudinal component has an anti-symmetric vertical component and symmetric transverse component where the slopes and displacements are zero at the cable mid-span. Both V and W increase with the sag value while W is two orders of magnitude smaller than U. The frequency spectrum changes only slightly with sag. The vertical translation displacement is at a maximum at approximately 0.15 and 0.85 of the cable span, where the peak 0.091 displacement was found relative to the primary longitudinal displacement occurring at the mid span.

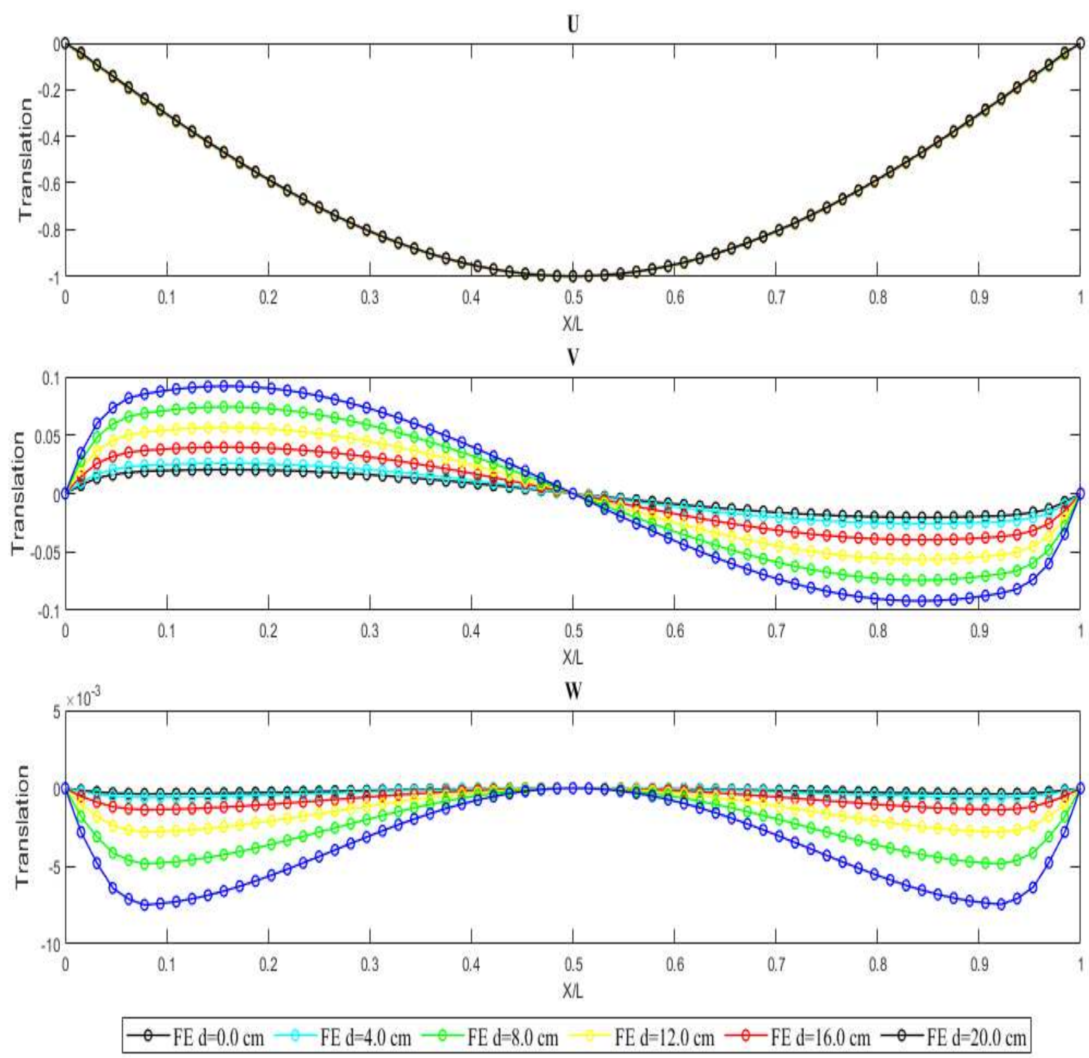

Fig. 3.9 The axial modal shapes displacements for Cable 1 versus sag values

For Cable 1 the torsional mode shapes in Fig. 3.10 show that the rotational displacements are at a maximum at the support locations in all three directions. The coupled motions in the vertical and transversal increases with the sag values. The vertical rotation displacement magnitude θ_Y is higher than the transversal rotation θ_Z, with symmetric and anti-symmetric components, respectively. It was found that rotation displacements at the cable supports increase in the vertical direction by 78% and 92% for the transversal direction.

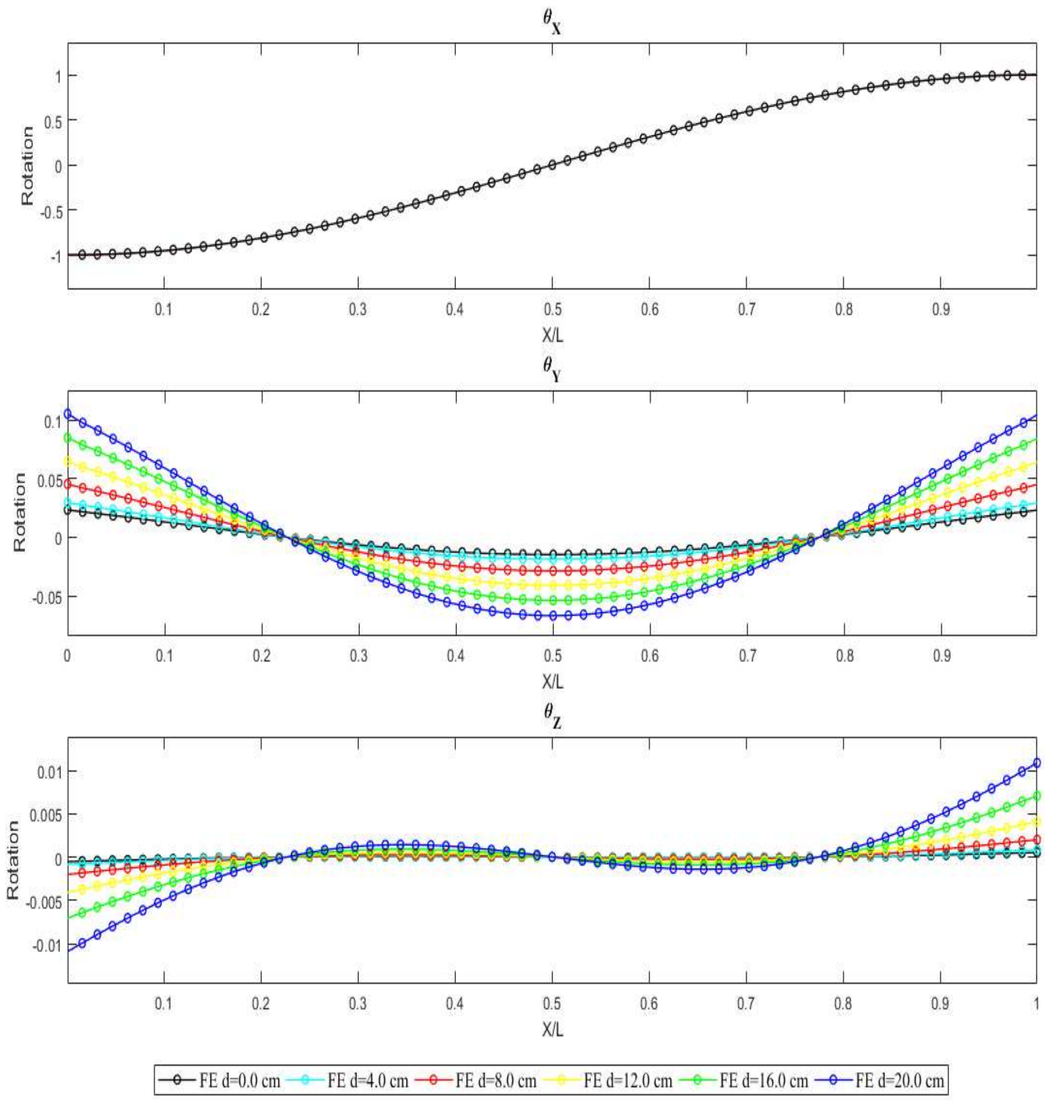

Fig. 3.10 The torsional modal shapes displacements for Cable 1 versus sag values

3.8 Conclusion

The dynamic motion of uniform sagged cable line supported at the same level model is described in three-dimensional showing the interaction between longitudinal, transversal, and vertical translations and rotations. The finite element model considered the torsion effect and sag configuration using six degrees of freedom. Based on the results of this work and supported by results from large scale experimental tests, the preliminary conclusions can be listed as:

1. The analytical solution used to find the natural frequencies is limited, where only the axial characteristic is considered, and the full coupling interactions between different cable coordinate directions are not described. The finite element model proposed here has the advantage of calculating the axial and torsional besides the out-of-plane, symmetric in-plane, and anti-symmetric in-plane frequencies, in addition to find the modal shapes of each showing the coupling interactions between the translation and rotation displacements in the three-dimensions.
2. For cable 1 and 2 used in this work, the out-of-plane, symmetric in-plane, and anti-symmetric in-plane frequencies predicted using the three-dimensional finite element model are within an excellent agreement (less than 0.1%) with the results of the analytical solution and the results obtained experimentally where the tests repeated multiple times for each configuration using accelerations trackers at two points on the cable span.
3. The non-dimensional parameter λ^2 effect was studied using a range of sag values and showed that it greatly impacted the symmetric in-plane mode shapes. The cross-over phenomena in the frequencies were observed using the finite element model. In addition, the modal shape nature changes when λ^2 is less, almost equal, and larger than

$4\pi^2$ not only in the vertical and the longitudinal modes (similar to modes found using the analytical solution) but also in the transversal modes. The experimental for the symmetric in-plane modes for cable with $\lambda^2 > 4\pi^2$ agree fairly well with the normalized ratio predicted using the finite element model where the two nodal points were recorded.

4. The modal shapes were also studied using the finite element model for the out-of-plane and anti-symmetric motion. And it showed that besides the primary motion (transversal or vertical) there is coupling motion in the other two translation directions which has been ignored in the literature. The experimental results obtained for the out-of-plane mode showed that the coupled displacements are small compare to the primary transversal motion, 0.0009 and 0.057 unit displacements for U and V. However, it was verified that there was an interaction even for tight cable (no sag) due to the very small sag generated after the static solution.
5. The large interaction were observed in the anti-symmetric mode. Where numerically and experimentally the transversal displacement W was approximately 30-46% of the primary ant-symmetric vertical motion because it was found that the second out-of-plane frequency is very close to the first anti-symmetric frequency.
6. The axial and torsional frequencies values were consistent with sag variation. However, the modal shapes were influenced by increasing the sag values. The symmetric longitudinal translation mode is coupled with the anti-symmetric vertical and transversal components. The rotation longitudinal torsional mode is coupled with symmetric vertical and anti-symmetric transversal components that are maximum at

the supports. For both axial and torsional, the associated coupled motions increased with sag increasing.

It can be said that the results arising from the models having six degrees of freedom suggest that it is essential to employ the three-dimensional model to have a more reliable prediction of the dynamic behavior. More importantly, the proposed finite element model can be used as a useful design tool because of its good computational efficiency.

CHAPTER 4: EXPERIMENTAL INVESTIGATION OF CABLE VIBRATION DAMPING

4.1 Summary

Cables are flexible structures that are prone to vibration because of their low inherent damping characteristics. In order to mitigate their vibrations, an understanding of the internal damping and influence of support type is a must. The dynamics of axially loaded horizontal sagged cables is studied experimentally. First the dynamic behavior of cables in undamped free vibration is investigated. The main mechanical characteristics, natural frequencies and damping ratios are quantified and identified using the time histories recorded by a sensor mounted on two types of cables, twisted metal and untwisted plastic. The results are obtained using large scale-experiments where harmonic time-varying support is employed. Two boundary conditions are tested, a rigid support and damper that is horizontally oriented. Overall, the experimental results highlight the fundamental characteristics of cable damping and energy dispassion using different boundary conditions. Results showed that the installation of damper in the support reduces the in-plane cable vibration.

4.2 Introduction

Cables are widely used structural elements in many engineering applications. Understanding the cable dynamic behavior and characterization of damping is still attract the scientific community. This kind of structure is subjected to many environmental excitations, for example, wind, rain, and ice. And since it is flexible and has low inherent internal damping, it is susceptible to vibrate easily. These can result in premature cable or connections failure and/or break, correction, and cable life reduction. In addition, cable vibrations have an effect on public confidence in the cable structure's safety. Specifically, the transmission line showed a significant vibration problem which caused by vortex shedding, wake-induced vibration, and galloping [131]. Therefore, energy dissipation is very important when considering the dynamic cable behavior.

As damping properties, understanding and measuring are very significant and critical for such a flexible structure. It is incorporated in many existing and new models in various ways. That reflects the numerous physical mechanisms that is associated with damping, contributing to the energy dissipation of cables. In 1949, Yu [132] started the investigation on internal damping. He noted the hysterics characteristic of internal damping of cables and defined paths as the space curves of the cable. The results indicated that only 5% of the energy dissipation was caused by the solid internal friction and the rest is caused by the friction between the wires. The experiment results showed that an increase in damping is correlated with using a shorter lay length. This model had no sag, constant bending stiffness assumptions, and friction due only to linear proportional to tension, and constant damping independent of tension both are due to the interaction between wires [133]. This model provided an excellent starting point in cable damping investigation for small amplitude.

Many earlier models included damping analytically or using closed form solutions by employing several simple assumptions. The most complex assumption is the interwire friction occurring at the interface of cable wires. In order to simplify it, researchers analyzed the model either with no-slip friction or fully-slip friction. Machida and Durelli [13], Knapp [14], and Kumar and Cochran [22] neglected interwire friction in studying cable damping. Claren and Diana [134,135] investigated the internal friction of strands by introducing a slippage coefficient. No further work in formulating the this coefficient and internal damping of cables was provided [136]. The energy dissipation in multi-layered strand was studied by Hobbs and Raoof [38], where the cable assumed to have layers of orthotropic cylindrical sheets. The integration of cable damping contact forces is challenging, to overcome this issue, one type of contact is used; core-outer wire contact is considered and friction is either neglected or assumed as constant. For an instant, Sathikh [31] studied the six-stranded cables' interwire friction and only considered the core-wire contact.

As the huge increase in cables use in 1990's, the interest in damping mechanisms investigation increased with a desire to find ways for vibration mitigation. Otrin and Boltežar [137] stated that air resistance, internal material damping, and friction caused by the interwar motion were all the mechanism which caused the loss in the energy of cable vibrations. Viscous and structural damping modes were used to quantify these losses. The linear proportional damping models were and are used due to their simplicity, where the damping is proportional to the rate change of the displacement. These models can be used when modeling the air resistance when the cable is vibrating in air. However, the internal damping, as well as the friction effects, are not included and captured in the analysis.

As the purpose of damping models is to determine and quantify the loss in energy physically, it is essential to understand the factors that cause these losses. The available damping models can be categorized to three major categories depending in their mechanisms; friction between the individual wires which modeled using interwire friction, changes in geometry and properties of the cable which modeled as bending stiffness variable, and internal friction within the wires which modeled with internal damping [133]. Usually, the damping value is reported as log decrement, energy dissipated ratio to energy stored, or as a percent of critical damping called damping ratio.

Further, many researchers have studies applying different assumptions and factors and studying their effect on cable damping using analytical, experiment, or simulation using finite element method. Hard and Holben [138] studied the internal damping (self-damping) of tensioned cable, and found that the cable length has no effect on the cable damping, however, the tension effect on the cable is significant; damping decreases as the tension increases [136]. Huang and Vinogradov [139] presented a modal where the inter-wire slip and its influence is taken into consideration in the dynamic behavior analysis. Yamaguchi and Adhikari [140] analytically studied the modal damping characteristics of single structure cable. The energy-based of modal damping was used as the ratio of the modal strain energy to the total potential energy. Michel et al. [66] studied the frictional damping properties of the simple straight strand under axial load using the finite element method. Wei et al. [141,142] used resonance technique to calculate the optical fiber cables damping, their conclusion was that the cable damping first decreases as length increase and then reach a stable value at a certain point. For the free and forced response of untwisted cable the dynamic characteristics were analyzed by Yamaguchi et al. [143], their system had two identical structural sagged cable in parallel connected by another sagged cross cable, for that the damping was characterized using an energy-based method.

Barbieri et al. [144] established a procedure to identify the damping of untwisted cables in order to estimate in a simple way the system damping matrix. This procedure is based on experimental and simulated data. Barbieri [145] designed a noncontact testing for cable vibration, their results stated that cable damping decreases as length and tension increases [136]. Using the wavelet transform approach Casciati et al. [146] found the natural frequencies and damping by introducing a nonlinear finite element model for steel cable wrapped with shape memory alloy wires. Faravelli et al. [147] investigated the mitigation of cable vibration using shape memory alloy and used open-loop actuation and investigate the nonlinear damping of a shape memory alloy, they were able to avoid the nuances and closed-loop control complexity. Maji and Qiu [148] provide results for several tests done on steel and carbon fiber cable under tensile forced, the natural frequency and modal damping ratio were determined. It should be mentioned that these tests were done for straight tight cables with a very small cross-section. In addition, strand cable was analyzed by Jiang et al. [64] using a concise finite element model where local contact, friction, plasticity of the material, as well as load combination effects were taken into account.

Maji and Qiu [136] studied the damping properties of straight carbon fiber cable using simple experiments and a basic finite element model and stated that even though that many researchers have studied cable damping, the internal damping mechanism of cable still has not been fully understood. In addition, all this work enriched the behavior understanding of cable damping, however, the apparent contradiction indicates that it still needs more study. Some of them provided different conclusions on the cable length dependency for cable damping, and that might be the result of using different testing purposes and conditions [136].

A recent survey done by Spak et al. [133] on cable dynamics stated that to capture the realistic behavior of helical cables; damping through the inclusion of friction forces, viscoelastic shear effect, or damping stiffness should be included in cable curvature and wire properties as a function. In addition, in practice, when the internal damping is insufficient to reduce the levels of vibration, Stockbridge-type vibration absorbers are commonly used. In the transmission lines case, Stockbridge dampers dissipate the mechanical energy in wire cables. Therefore, Barbieri et al. [149] done an experiment to study the dynamic of new cables with and without using Stockbridge dampers and compare it with one-dimensional linear and nonlinear finite element model.

In order to reduce the problematic vibration in cables, dampers are usually used near the fixed supports. Many studies have been conducted to understand the dynamics behavior with the use of different types of dampers and mostly on taut cables. Lazar et al. [150] stated that there are limitation to the effectiveness of the use if dampers (such as Stockbridge) as they are mounted on the cables due to the installation is restricted to be close to the end of the cable.

Many of the previous experimental studies for cable damping are limited due to the simple setup or small scale testes, cable geometry, or boundary conditions. Moreover, it was shown that changing the cables design is not expected to significantly improve its damping [66]. In this work, the authors use a large-scale experimental work is in order to identify the internal damping of two types of horizontal cables and their motion under using different types of support, with and without damper. The study is applied into two cables, one is a twisted metal cable and, the other is untwisted isotropic plastic cable. Several conclusions are drawn from the time history data obtained using sensors at mid-span of cables experimentally.

4.3 Experimental Model Setup

The main objective of this work is to analyze the dynamic behavior of two types of cables focusing on finding the damping characteristics and the different associated motions. That is done in order to understand the behavior of cables undergoing vibrations which is essential to comprehend how the cables will respond to other more excitation. To achieve that, a procedure is used based on experimental work obtained by dynamic tests. In designing the experimental apparatus, a number of challenging tasks had to be resolved which results in having a reliable investigation system for such a flexible structure. The overview of the experimental setup is presented in Fig. 4.1. The large two beams give the system stability where the two columns are fixed vertically.

The basic components of the cable testing system are schematically displayed in Fig. 4.2 with end support details. The two-column supports are at the same level and used to pass the ends of the cable and then clamped using a c-clamp. Each cable, first, fixed to the left clamp above the actuator and then the right support clamp where it is initially not tightened (until reaching the sag value and tension force required). Two conditions are used in the right support, one, the cable passes the rigid column and then tightened. The second, when the cable is fixed to the c-clamp that is attached to the air dashpot in Fig. 4.3 [151]. The dashpot is oriented horizontally. These are used to maintain the applied tension force through the tests.

Fig. 4.1 Experimental setup where cable is hanging horizontally

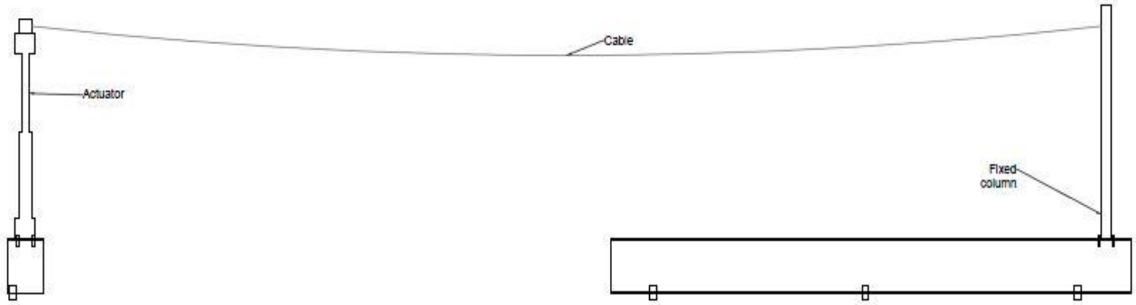

Fig. 4.2 Schematic view of the set with support details

Fig. 4.3 Air dashpot (damper) used showing attached c-clamp where the cable pass and then tightened

It is known when a system is subjected to harmonic excitation, it is forced to vibrate at the same frequency as of that excitation. Using this idea the cables of interest are forced to vibrate to reach to the resonance and get the largest amplitudes, and then find the damping and motions that will be studied. For that, the left end of the cable is supported by A MTS's 243.20 hydraulic actuator [127] in Fig. 4.4 that has a stroke length of 25.4 cm. It is used to apply and simulate a harmonically time-varying support motion during the tests that is moving vertically. The actuator is driven by a power control unit (MTS 407 controller [128]) as shown in Fig. 4.5 , and this has a function generator with a controllable frequency capable of sending the simplest form of periodic motion. The other fixed support (column) is a 7.7 m away from the actuator, which is fixed to a rigid structure (beam) with precisely the same height.

Fig. 4.4 MTS's 243.20 hydraulic actuator used

Fig. 4.5 MTS 407 controller

For each configuration, MetaTracker sensor [129] Fig. 4.6 is mounted to the cable at the mid-span. The sensor weight is 5.57g, and its dimensions are length 30mm x width: 25mm x height: 5mm. And, all the recorded data are sent from the tracker using Bluetooth. This device gives the acceleration and angular velocity records in three-dimensions. Before using the MetaTrcker to capture the cable motion, it was tested by doing a simple pendulum experiment to verify the sensors' results and the data analysis processing with the known analytical method.

Fig. 4.6 Sensor mountain on the cable which contains accelerometer and gyroscope [129]

Cable samples used in the experimental work are twisted metal: six-stranded Aluminum Conductor Steel Reinforced (ACSR) Fig. 4.7, and a section of clear plastic hollow circular tubing and it is untwisted Fig. 4.8. The assumption was made that material are theoretically to be homogenous and linearly elastic, a summary of the cables geometry and mechanical properties are listed in Table 4.1.

Table 4.1 Cable 1 and 2 properties

Item	Cable 1	Cable 2
Core Cable Radius R_c (mm)	2.25	-
Outer Cable Radius R_w (mm)	2	-
Total Area A (mm^2)	91.30	0.576
Unit Mass m (kg/m)	0.35	0.20
Modulus of Elasticity E (GPa)	74.2	8.27
Shear Modulus G (GPa)	37.1	4.135

Length L (m)	7.7	7.7
sag d (cm)	17.4	17.4

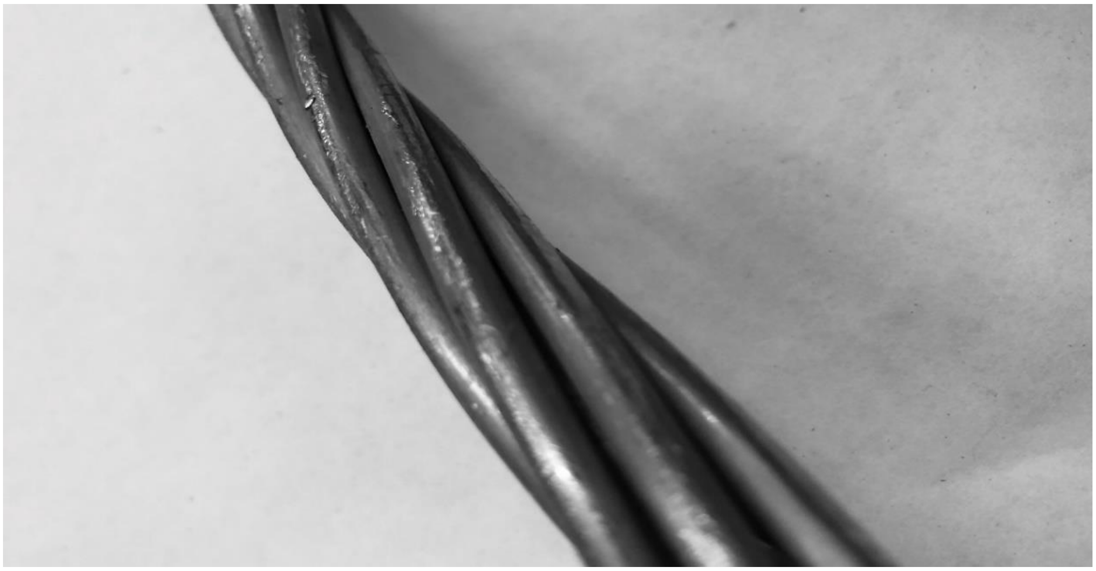

Fig. 4.7 Cable 4.1, Aluminum Conductor Steel Reinforced cable (ACSR)

Fig. 4.8 Cable 2, a circular plastic tube

4.4 System Identification/Experimental Procedure

The cables were excited to vibrate using the actuator at one end. The investigation includes studying the damping ratios and motions under different scenarios. Therefore, tests were conducted under two different boundary conditions for each cable tested.

The actuator is set to excite the system; using the controller, a set of frequencies is tested to force the cable to vibrate at the excitation frequency. If the exciting frequency coincides with the natural frequency of the cable resonance, the results are then collected.

First, the cable is hanging fixed between the rigid support and other support where it is fixed to the actuator. For each cable, the out-of-plane and in-plane natural frequency of the cable were obtained by recording the frequency from the controller when the peak response was observed. The tracker will then record the harmonic vibration of the cables. Then for the same frequencies, the same procedure is repeated where the air dashpot is used.

Second, for the same frequencies used, using the controller, the actuator motion will then be suspended, and the sensor records the decay data of the cables.

Damper are often used near the supports to suppress the problematic vibrations. Even through, the mechanics which cause the vibrations are not fully understood, the effectiveness of attaching damper close to the supports showed a reduction in the vibration amplitude [152]. Therefore, third, left support (actuator) gives a single sine-wave excitation of a fixed amplitude (frequency of the first and second scenario). For this, only in-plane displacements is found. Results are obtained with and without air dashpot attached.

For all scenarios, the acquisition duration for each reading ranges from 10 to 50 seconds, and the sampling frequencies for the measured acceleration are $f_{s-acceleration} = 12.5$ Hz and $f_{s-angular-velocity} = 20$ Hz for the angular velocity. For each cable configuration, a set of tests are carried out. When only rigid support is used, the tests are repeated 20 times.

4.5 Data Processing

The responses data recorded obtained from the MetaTracker are in the form of harmonic signals that are digitized to an analog output signal that are sent to a phone using Bluetooth, and are post-processed by means of MATLAB. The accuracy of the data gained depends on many factors, including imperfection of maintaining the cable tension, disturbance, and trackers positioning and other arrangements. These effects are minimized by repeating the tests several times which led to the final results presented.

To facilitate the results, the frequency of each single has to be computed. To do so, the Fast Fourier Transform algorithm can be used, which is a fast version of the Discrete Fourier Transform by the mathematician J. Fourier (1768-1839), where he showed that periodic motion can be represented using a series of sines and cosines [153]. This method transforms the signal, which is in the time domain, to frequency domain representation. MATLAB has FFT function which is a very effective tool and minimizes the computation time that computes the Discrete Fourier Transform for any given signal. The FFT is symmetric when the region between 0 and sampling frequencies $f_{s-acceleration}$ and $f_{s-angular-velocity}$ are examined, and that adds redundant information. So, data between $0.5 f_{s-acceleration}$ and $f_{s-acceleration}$ as well as $0.5 f_{s-angular-velocity}$ and $f_{s-angular-velocity}$ is a mirror image of data between the first half, so it will be deleted. The maximum frequency found will be used in the next step of the analysis.

As known, the harmonic motion is represented as a projection on a straight line of a moving point on a circle with constant speed, and that can be represented from the results of the acceleration from the data obtained by the MetaTracker and then integrate to get the velocity and the displacement, and all of which are harmonic using same frequency:

$$\ddot{W} = \ddot{W}_{data} \sin(\omega t) \quad (4.1)$$

$$\dot{W} = -\frac{\ddot{W}_{data}}{\omega} \cos(\omega t) \quad (4.2)$$

$$W = -\frac{\ddot{W}_{data}}{\omega^2} \sin(\omega t) \quad (4.3)$$

A similar methodology was used for the other dimension in getting the V displacement values.

MATLAB post-processing code was also used by applying the logarithmic decrement method to determine the internal damping ratio of the obtained history signals, the damped free oscillation and the internal damping ratios for the considered cables ($\zeta < 1.0$), for both the out-of-plane motion and in-plane symmetric motion.

4.6 Experimental Results and Discussion

At the measuring point (mid-span), the spectrum of the signal and time-history responses is obtained. Since the process is repeated 20 times for both cables tested for either out-of-plane and in-plane motions, for illustration, Fig. 4.9 shows one result example obtained by the sensor for a symmetric in-plane motion (the results are normalized to the peak motion). The vertical dash line represents where the actuator motion was suspended. From that, the frequency is found using FFT (from motion before the line), and the damping ratio found using the logarithmic decrement method (from motion after the line) using the given harmonic motion.

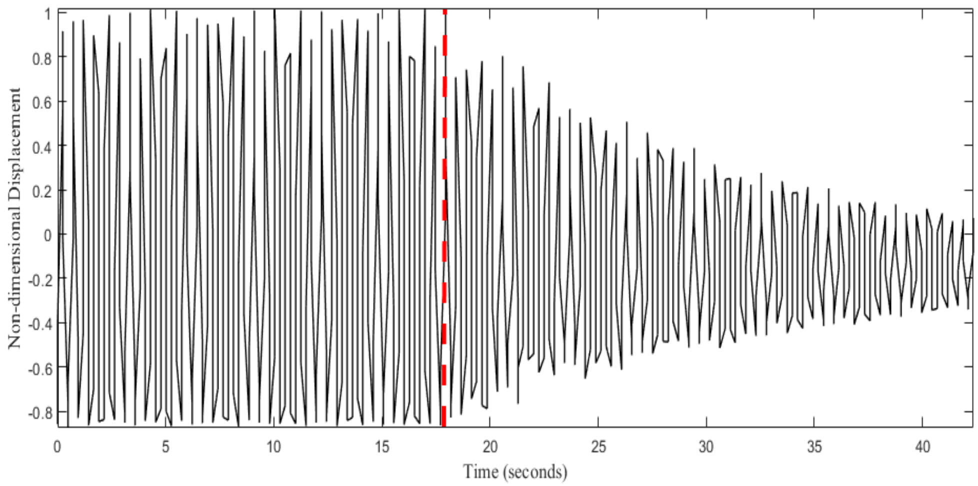

Fig. 4.9 Cables non-dimensional displacements at mid-span before and after actuator motion

Cable 1 and 2 out-of-plane and in-plane frequencies are shown in Table 4.2, that is denoted as ω and found as $f = \frac{\omega}{2\pi}$, are compared with finite element model results from ABAQUS. And, the well-known analytical model for sagged cables given by Irvine and Caughey [80] and can be computed using

$$f_o = \frac{1}{2\pi}\sqrt{\frac{H}{m}} \quad (4.4)$$

$$f_s = \sqrt{\frac{\beta_i^2 H}{m}} \quad (4.5)$$

Where f_o is the out-of-plane frequency, f_s is the symmetric in-plane frequency, H is the horizontal component of the cable tension, m is the mass per unit length, and β_i value can be found from a transcendental equation [80]. From that, the natural frequencies found experimentally have an excellent agreement with the ABAQUS and analytical results. The out-of-plane and the symmetric in-plane frequencies are within approximately 0.95% and 1.95% error, respectively, for both cables.

Table 4.2 The natural frequencies for Cable 1 and 2 using different approaches

	Cable 1			Cable 2		
	Irvine and Caughey	ABAQUS	Experiment (Median)	Irvine and Caughey	ABAQUS	Experiment (Median)
Out-of-Plane f_o(Hz)	1.329	1.328	1.329	0.838	0.837	0.830
Symmetric In-plane f_s(Hz)	3.791	3.750	3.825	1.505	1.495	1.500

For both cables, the logarithmic decrement method was used to analyze the signal history results obtained using the sensor. The damping ratios for out-of-plan and symmetric in-plane motion for 20 tests for cable 1 and 2 are shown in Fig. 4.10 and Fig. 4.11. From that, the median of the samples is used and presented in Table 4.3. From that, the damping ratio for cable 1 is smaller by 61.7% and 77% for the out-of-plane and symmetric in-plane motion of cable 2. This large percentage is present due to the difference in materials and geometry of the cables tested.

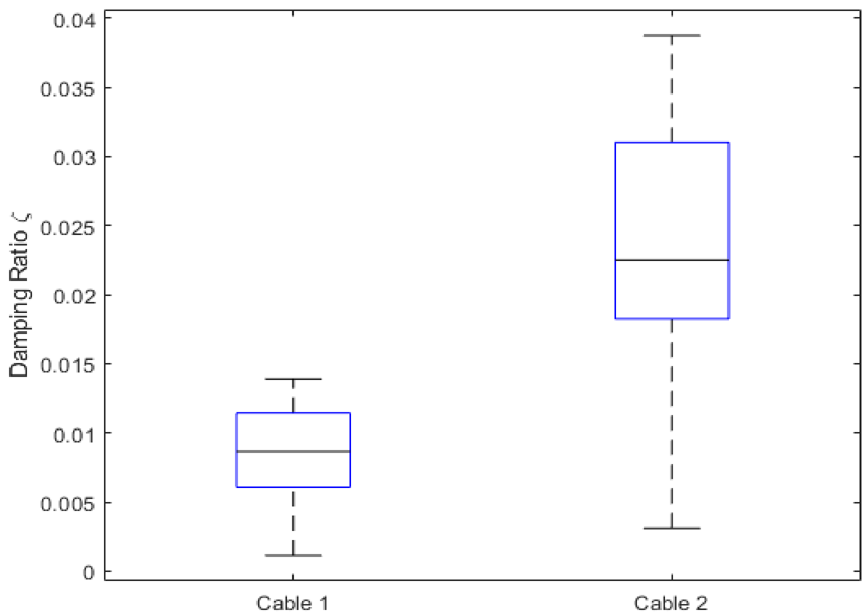

Fig. 4.10 Damping ratios for Cable 1 and 2 undergo out-of-plane motion

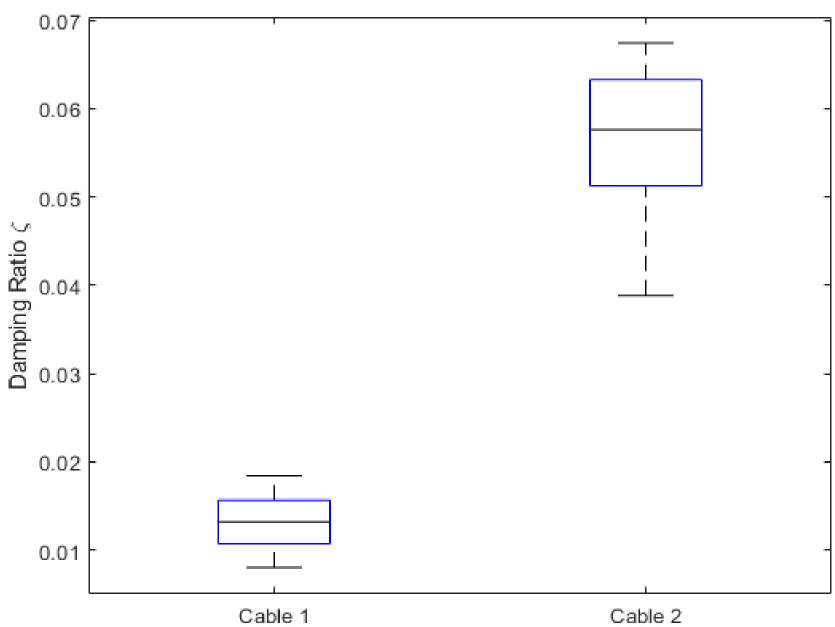

Fig. 4.11 Damping ratios for Cable 1 and 2 undergo symmetric in-plane motion

Table 4.3 The damping ratios median values for Cable 1 and 2 found experimentally

	Cable 1	Cable 2
Out-of-Plane ζ	0.0086	0.0225
Symmetric In-Plane ζ	0.0132	0.0576

Using these frequencies and damping ratios results, for illustration, the free vibration responses (out-of-plane and symmetric in-plane) of Cable 1 and 2 are presented in Fig. 4.12 and Fig. 4.13. For simplification, the underdamped vibration (since $\zeta < 1.0$), one-degree of freedom equation is used [130]

$$W(t) = e^{-\zeta f_o t}(W_0 \cos(f_{o-d} t) + \frac{\zeta f_o W_0}{f_{o-d}} \sin(f_{o-d} t) \qquad (4.6)$$

Where f_{o-d} is the out-of-plane damped frequency, and the initial transversal is W_0 , and it was given a value of one. Similarly, the vertical displacements V were also found.

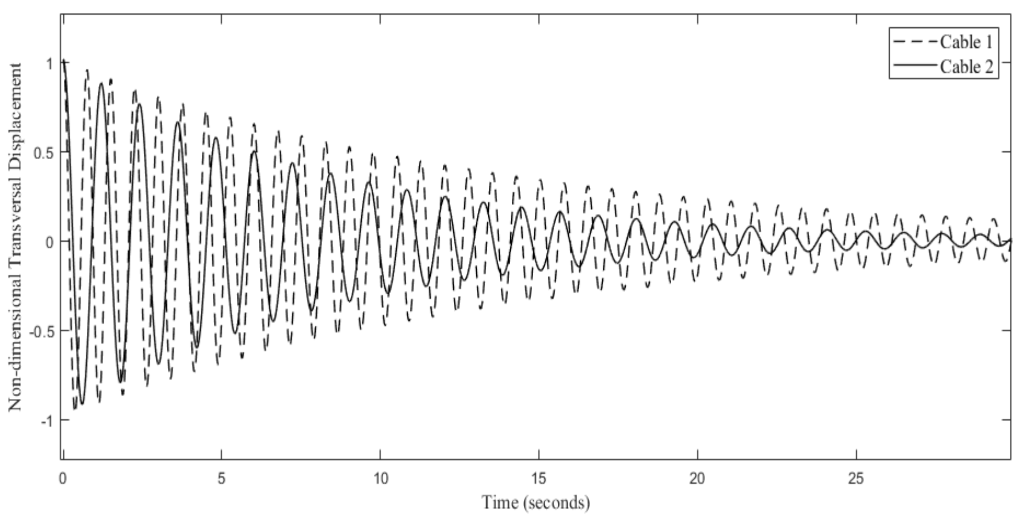

Fig. 4.12 Underdamped transverse free vibration of Cable 1 and 2

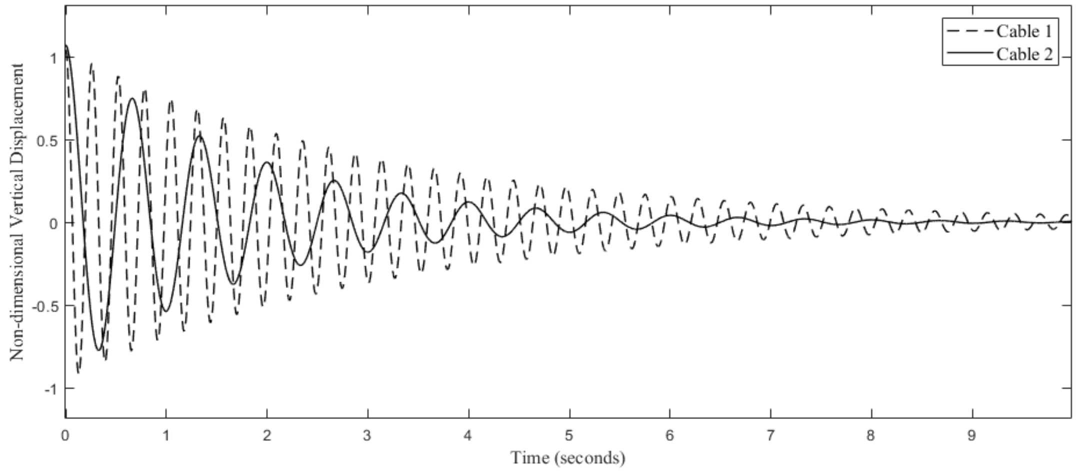

Fig. 4.13 Underdamped vertical free vibration of Cable 1 and 2

The symmetric in-plane motion was captured for Cable 1 and 2 using a single sine wave excitation with and without the horizontal air dashpot damper. Figure 4.14 and 4.15 shows the motions, and it can be seen that the peak value decreases by 27% and 20% when the damper is used for cable 1 and 2, respectively. As expected, Cable 2 displacements quickly dissipated since the damping value is large comparing to Cable 1 (Table 4.3).

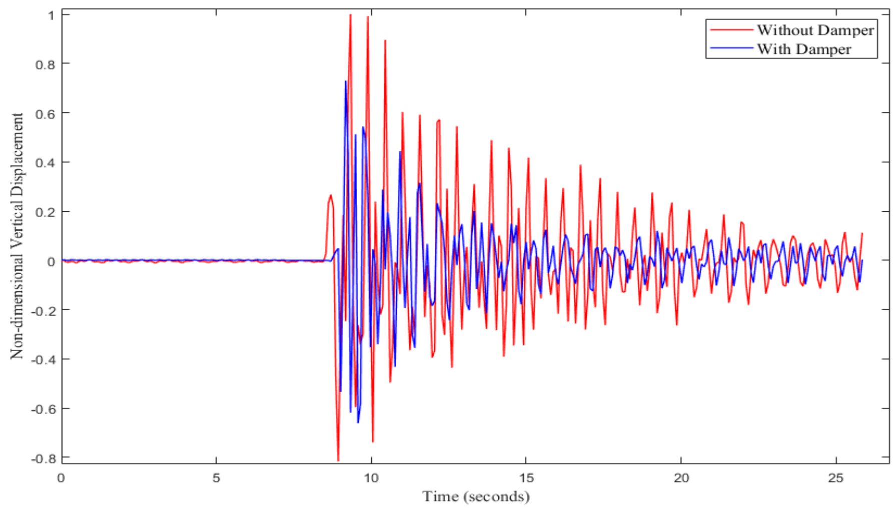

Fig. 4.14 Comparison of the peak motion results from single sing wave for Cable 1 with and without using air dashpot damper

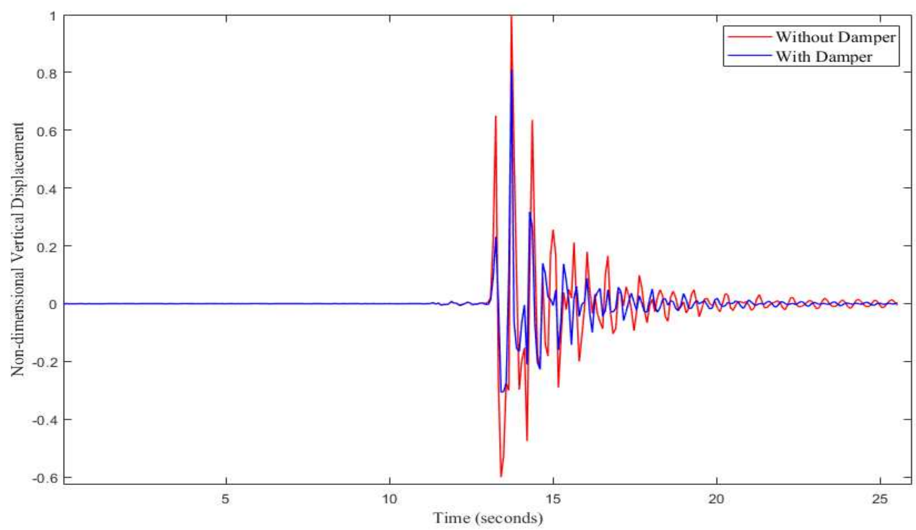

Fig. 4.15 Comparison of the peak motion results from single sing wave for Cable 2 with and without using air dashpot damper

4.7 Conclusion

The free vibration and mitigation of horizontal sagged cables have been investigated experimentally using large-scale dynamic tests. Different boundary conditions were examined to study the cable motion response. Time history data obtained using a sensor showed that the internal damping ratio for out-of-plane and in-plane heavily deepened on the geometry and material of the cable. The experimental tests captured the cable vibration with and without an air dashpot damper. Results demonstrated that the installation of the damper in the cable support decreases cable motion. For instant, the reduction in the in-plane displacements motion was found to be 27% when the damper was used.

CHAPTER 5: MODAL DYNAMICS OF TWISTED CABLES

5.1 Summary

Understanding the dynamic behavior of twisted cables is of great interest became of the wide increase in their uses in various applications. In this work, an efficient numerical procedure is presented to generate the primary elastic stiffness coefficients using elasticity theory where the three-dimensional cable is reduced to a one-dimensional model. The cables are then subjected to axial loads in three-dimensional space. The model gives stiffness coefficients that are in good agreement with seven known analytical models for angles below the maximum lay angle of the cable. The free vibration behavior of these cables is then analyzed using a finite element model, where the ends of the sagged cable are fixed at the same level. The natural frequencies and modal shapes are also found using extensive experimental tests. The frequency spectrum and the six translations and rotations are analyzed and compared with existing analytical solutions and commercial finite element results. Three practical examples are used to demonstrate the validity and applicability of the finite element and experimental models, for twisted and untwisted cables. The results show that cable elasticity, twist coupling and initial sag play a considerable role in the modal coupling behavior. The results also suggest that some simplified models may not be adequate to fully understand the dynamic behavior of twisted cables.

5.2 Introduction

Cable structures have been widely used in a large variety of tensile structures including cable-supported bridges, large-span roofs, marine and offshore structures, guy lines for towers, and power supply lines. This is in large part a use of their capability of transmitting force, carrying payloads, and conducting signals as well as their aesthetic appearance. An increased interest in cables has required a more thorough and detailed investigation of cable mechanics. One significant characteristic of twisted cables is that their static response is coupled. This means that when a cable has a twist along its length, it exhibits coupled extensional-torsional behavior. When an axial load is in action the cable undergoes simultaneous extensional and rotational displacements. Similarly when torque is applied, both rotational and extensional displacements exist. This behavior has a critical impact on the cable's dynamic response but it has received relatively little attention. The full effect of twist on the coupling between extensional-torsional behavior on longitudinal, vertical, and transverse motion has to be fully studied. In general, six types of waves will propagate through the cable. Three characterize the extensional-compressive deformation and the other describe primary torsional deformation. However, the interaction and superposition of these modal deformations will make the overall cable dynamics quite complicated.

Many reports in the literature have been devoted to working on characterizing the helical nature of cable and the static response to different loading scenarios. The analysis has frequently been performed by modeling the cable as a perfectly flexible element, primarily reacting only to axial forces. However, it is becoming increasingly necessary to consider additional stiffness contributions to totally represent the cable’s important features. Cable analysis can be subdivided into mechanical models that describe the wires inside the cable into either discrete which is based on modeling wires individually as thin rod or curved beams, or semi-homogenization formulations which is a method based on replacing the wire layers with equivalent elastic continuum which presented as a thin orthotropic cylinder. The early theoretical work on the mechanical behavior of cable appeared in the 1950s by Hruska [8,9]. Machida and Durelli [13] investigated the bending and torsional effect on the stiffness matrix of the outer wires. The bending and twisting effects were included but the symmetry of the stiffness matrix derived was lost. Knapp [10] extended the

Hruska [8,9] model for a rigid core and McConnell and Zemke [11] included the torsion stiffness effect of the outer wires.

More sophisticated analytical models have been based on beam theory, including different assumptions about geometry and wire contact. Costello and Phillips [15] and Huang [16] presented basic strand models along with Velinsky [18] and Phillips and Costello [19] where the internal wire rope was included. Costello [20] presented a linear theory that included the effect of curvature and twist. Kumar and Cochran [22] extended this theory that resulted in a closed-form expression for the stiffness matrix terms, but stiffness matrix symmetry was again lost. Jolicoeur and Cardou [26] compared the results of the mechanical response for a single straight rope which was predicated by the Costello and Phillips [15] model with the simple model provided by Hruska [8,9], This comparison showed that the fiber model was not appropriate and that both twisting moment and angle have to be taken into account. Costello and Phillips [15] showed a good prediction with the experimental results of Utting and Jones [23,24], who introduced a model that included contact deformation (which also called wire flattening) and friction effects. Labrosse [27] presented an analytical method that predicted the overall behavior of a simple straight wire subjected to tension, bending and torsion. This model excluded the Poisson's ratio and included the motion between the core and the wires where the latter were considered as curved beams. Using discrete thin rod theory, additional studies were completed by Sathikh et al. [154], and more recently by Argatov [32] proposing a better formulation that considered the contraction between the outer wires and the core wire.

A second class of method, which is usually called homogenization, was used and introduced a semi-continuous model. Hobbs and Raoof [38] used this approach for multilayered cables where each layer was modeled as an equivalent orthotropic sheet. This methodology was extended and expanded by Hobbs and Raoof [38], Raoof [39], [40], Raoof [41], Raoof and Kraincanic [42], and Mohammed and Ivana [43]. Raoof and Kraincanic [106] stated after comparing the semi-continuous models and the thin rod models analysis of cable that the thin rod theory was more reliable when the wire strand diameter was small or for one or few layers of external wires. Semi-continuous models are especially advantageous when the cable is made with a large number of wires [45].

Many previous formulations take changes in cable geometry into account by stating the mechanical problem in a non-linear geometric framing and then linearizing the results. However, this usually results in a non-symmetric stiffness matrix that violates Betti's reciprocal theorem. Karathanasopoulos and Kress [35] addressed this and found a symmetric matrix by proposing a model to study the response of helical rods under axial-torsional loads where radial contraction was included. In this model the formulation of the radial strain was considered as an external load (Poisson and flattening effects were not induced). Karathanasopoulos et al. [36] used this model to study the effect of thermal loads on braided conductors. Foti and Martinelli [155] developed a model to evaluate the axial-torsional response of a single layered strand considering the deformability of the internal contact surfaces and derived a symmetric stiffness matrix.

In studying the vibration of cables, the literature has demonstrated that as more complex theories of cable stuffiness take more factors into consideration to derive the governing equations of motion, these become more complex and obtaining exact analytical solutions can be challenging. The use of numerical methods allows a more feasible calculation of natural frequencies and mode shapes. The interesting problem of how extension, torsion, and bending deformations interacting in twisted cables, as well as the problem of how resonance occurs, remains largely unsolved [156]. The dynamics of untwisted cables has a long and very rich history, which has been documented by Irvine and Caughey [80], who also did remarkable work in developing a novel linear theory for the free vibration of uniform untwisted cables in both out-of-plane and in-plane motion. Many early models including Irvine and Caughey studied only axial loading and ignored the torsional displacements associated with cable dynamics.

Samras et al. [101] initiated studies of coupling and emphasized the importance of taking the coupled extensional-torsional behavior into account. The interaction between transversal (out-of-plane), vertical (in-plane), and torsional motions for sagged cables has been studied for untwisted cables using a number of simplified theories. Nigol and Power [89] and Desai et al. [90] described the coupling between vertical motion and torsion. Jones [91] studied the coupled vertical and horizontal motion, and Yu [88,93] proposed analysis methods for the longitudinal, vertical, and torsional coupling. Rega [116,117] and Thai and Kim [124] discussed the main features and problems associated with the nonlinear vibration analysis suspended cables. Alkharisi and Heyliger [157] found the effective mass and stiffness components for coupled cables using constants that are derived from three-dimensional elasticity. These were used to study vibration behavior with both analytical and finite element models for homogenous and composite cable geometries.

Dynamic experiments on horizontal sagged cables (untwisted) subjected to harmonic time-varying support are limited in the literature besides the large amount of the numerical investigations. Among these experiments, Perkins [118] model, who stated that the investigations of nonlinear dynamics of cables are largely unsubstantiated by experimental results, therefore, presented a two-degrees of freedom analytical model that agreed with experimental results for which varying support motion amplitude lead to non-planar internal resonance. Koh and Rong [158] accounted for three translation displacement motions where a quantitative agreement for numerical and experimental results are found as regards the dynamic tension of non-resonant cable.

Although twisted cables have been used as structural members for a long time, the theoretical and experimental work completed to analyze and understand their dynamic behavior has fallen behind their applications when comparing with other studies on commonly used members. In this work, a finite element cable model using stiffness coefficients derived from elastic theory is presented and compared with experimental results. Several dynamic tests were completed to accurately predict and measure the dynamic motion and resonances considering the free vibration analysis with a focus on the coupled extensional and torsional actions in the three-dimensions. In addition, the coupling levels are quantified for three different types of twisted and untwisted cables and the effects of lay angles and sag variation on the cable dynamics are studied.

5.3 Mechanics of Twisted Cables

Attention in this paper is confined to finding the natural frequencies and corresponding mode shapes of twisted cables, both numerically and experimentally, that are mainly a function of the mass and the stiffness of the cable. The mechanics of the twisted cables will be incorporated thoroughly to represent an accurate model of the underlying physics. Because the primary source of nonlinear behavior of the cable is the initial geometric stretch prior to dynamic analysis and other combined effects, the helical geometry and sag of the twisted cable make the problem more complicated. The cable can be a complex geometrical structure composed of many individual wires, and the goal of this model is to capture the dominant behavior without making the model unnecessary complex.

5.3.1 Geometry

For twisted cables, the focus here will be to investigate so-called six-stranded cables, which usually have a straight core wire surrounded by a layer of similar outer wires. These wires are laid at an angle which is known as the lay angle α. These angles are used to quantify the amount of twist that the layered cables possess around the core (defined using Cartesian basis) as shown in Fig. 5.1. The discrete model is better suited for simple geometries than the homogenous models and used during the analysis of the present study.

Fig. 5.1 Geometry of the strand with a single layer

The wire geometry in Fig 5.2 can be described using a curvilinear system shown to characterize the vector $R(s)$ defined using Cartesian basis X, Y, Z (following Lee [3]) as:

$$R(s) = \begin{pmatrix} R_h \cos\varphi \\ R_h \cos\varphi \\ b\varphi \end{pmatrix} \qquad (5.1)$$

Where,

$$\varphi = \frac{s}{\gamma}\ ,\ \gamma = \sqrt{a^2 + b^2}\ ,\ b = a\tan\alpha \qquad (5.2)$$

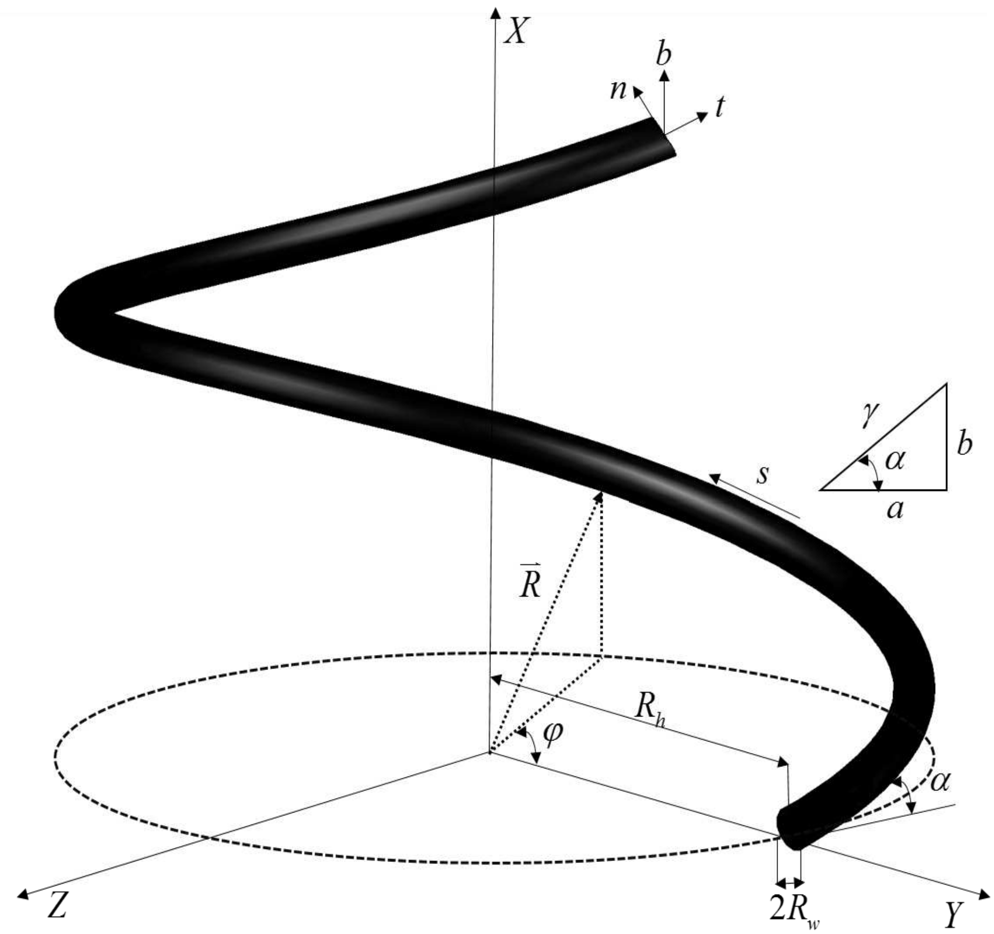

Fig. 5.2 Helix geometry of an individual wire

In the equations above, R_h represents the helix radius, b is the helix rise along the central Cartesian axis X, and γ is the helix curvilinear length per unit angular φ. In Eq. (5.2), *b* is related to the helix radius through the tangent of the angle α, where the core helix cross-section radius is R_w. The helix curvature κ and tortuosity τ are defined as:

$$\kappa = \frac{R_h}{\gamma^2}\ ,\ \tau = \frac{b}{\gamma^2} \qquad (5.3)$$

The length of the curvilinear helix *s* of non-unit angular evolution φ and its projection on the X axis, defined as h, are both related to R_h and α by the relations:

$$h = s\sin\alpha \ , \ R_h\varphi = s\cos\alpha \qquad (5.4)$$

The pitch length, which is denoted by *P* when the six-stranded cable is straight (with no sag), can be found using the expression

$$P = \frac{2\pi R_h}{\tan\alpha} \qquad (5.5)$$

Where

$$R_h = R_c + R_w \qquad (5.6)$$

The wires centerline is a helical curve of radius R_h, where R_c is the core radius, and R_w is the radius of the wire.

It is essential to know the maximum lay angles of the cables used in this study since this value will influence overall cable behavior. This can be found using [155]:

$$\alpha_{max} = \arccos\left(\sqrt{\frac{\tan^2(\frac{\pi}{2}-\frac{\pi}{6})}{(1+\xi_0^{-1})^2-1}}\right), \xi_0 = \frac{2R_w}{2R_c} < 1 \qquad (5.7)$$

The next step in this analysis is to represent the kinematic response of a cable cross-section in a three-dimensional elasticity context to find the effective one-dimensional stiffness coefficients. A small length of the twisted cable is described by a single layer of three-dimensional continuum elements, where the element length h is chosen so that it is always 10% less than the cable's pitch length. Once the cable domain is cut at a certain length, the front face local coordinates (i.e., how this face rotates around its center) must be calculated using the geometries properties of the twisting cable, these nodes now at the cut have different angle than the original lay angle, therefore identifying where the nodes located is essential for applying boundary conditions. To compute this transformed lay angle, the following equation can be used

$$\Theta_e = \frac{360}{(\frac{P}{h})} \qquad (5.8)$$

additional details about cables construction and topology can be found in Feyrer [7], while insight into the geometries modeling of the helical assemblies has been provided by Lee [3].

5.3.2 Finite Element Modeling Basis

The governing differential equations of equilibrium in a Cartesian coordinate system of plan elasticity for a hexahedron shapes. It can be expressed in indicial form as:

$$\sigma_{ij,j} + f_i = 0 \qquad (5.9)$$

Where $\sigma_{ij,j}$ are the component of stress, and f_i are the body force vector components in X, Y, and Z directions. For small displacements, the strain-displacements relations are represented as:

$$\varepsilon_{ij} = \frac{1}{2}(u_{i,j} + u_{j,i}) \qquad (5.10)$$

The generalized Hooke's law can be used as the constitutive relation using the elastic stiffness tensor C_{ijkl} components (function of the properties of individual wires) in Eq. (5.11):

$$\sigma_{ij} = C_{ijkl}\varepsilon_{kl} \qquad (5.11)$$

Regardless of how many layers or shapes are considered, the design of helical, straight cables includes coupling between extensional and torsional forces and displacements. This relationship can be represented, in matrix form, while undergoing static axial deformation as:

$$\begin{Bmatrix} F_X \\ M_X \end{Bmatrix} = \begin{bmatrix} k_{\varepsilon\varepsilon} & k_{\varepsilon\theta} \\ k_{\theta\varepsilon} & k_{\theta\theta} \end{bmatrix} \begin{Bmatrix} u_{X,X} \\ \theta_{X,X} \end{Bmatrix} \qquad (5.12)$$

Here F_X is the axial force, M_X is the axial twisting moment, $u_{X,X}$ is the axial strain, $\theta_{X,X}$ is the twist per unit length, $k_{\varepsilon\varepsilon}$ is the axial stiffness, $k_{\varepsilon\theta}$ and $k_{\theta\varepsilon}$ are the coupling stiffnesses (these are equal to zero in case of the untwisted cable) and $k_{\theta\theta}$ is the torsional stiffness. These are all effective one-dimensional relations, and these must be a transition between the three-dimensional behavior of the cable and the effective one-dimensional relation shown in Eq. (5.12).

Linear three-dimensional elasticity elements represented as hexahedral solids are used in the finite element analysis to predict the mechanical behavior of six-stranded straight wire. Each node in the hexahedron element has three degrees of freedom in the X, Y, and Z directions as displacements (u), (v), and (w), respectively. To find the overall mechanical behavior of six-stranded cables represented in the stiffness coefficients in Eq. (5.12), two sets of boundary conditions are sequentially imposed: 1) at one end, all nodal displacements in X, Y, and Z directions are prescribed to be zero, meaning this face is fully clamped. At the other end of the control segment, a unit displacement is imposed in the axial direction ($u = 1$), which all other displacements are set to zero. From this condition, $k_{\varepsilon\varepsilon}$ and $k_{\theta\varepsilon}$ can be computed from the total forces and moments required to hold this deformation. Then, 2) at one end, all node displacements are set to be zero, and on the other face nodal displacements in the Y and Z directions, are imposed to represent a unit rotation while the displacement in the X direction is set to zero. From this configuration, $k_{\varepsilon\theta}$ and $k_{\theta\theta}$ are found from the total forces and moments. The coupling terms in the stiffness matrix should be symmetric to satisfy the Maxwell Betti reciprocal theorem. In many of the methods used to derive these measures, unequal values are obtained and are then averaged. In this work, using this method, the discrepancies in the coupled terms were found less than 4% different.

The mass matrix for the one-dimensional model, where the kinetic energy terms are represented, can be expressed as the 2×2 matrix

$$[M]=\begin{bmatrix} m_{\varepsilon\varepsilon} & m_{\varepsilon\theta} \\ m_{\theta\varepsilon} & m_{\theta\theta} \end{bmatrix} \tag{5.13}$$

Where

$$m_{\varepsilon\varepsilon}=\int_V \rho dV \tag{5.14}$$

$$m_{\theta\theta}=\int_V \rho r^2 dV \tag{5.15}$$

These terms depend on the pointwise mass density ρ, r is the distance from the polar origin of the six-stranded wire to any arbitrary location in the cable cross-section, and V is the total volume of the control volume segment of the cable. The off-diagonal elements of the mass matrix are zero.

To evaluate the validity of the present approach, the stiffness coefficients and their numerical convergence for the twisted cable were compared with analytical models available. The models of Hruska [8,9], Machida and Durelli [13], Knapp [10], McConnell and Zemke [11], Kumar and Cochran [22], Labrosse [27], and Sathikh et al. [154] were each applied to the present geometry and compared with the three-dimensional elasticity approach proposed here. The comparisons are very good and are shown in a later section.

5.4 Free Vibration Analysis

Four approaches are used in this paper to find the natural frequencies and the corresponding modal shapes for untwisted and twisted sagged cables where the supports are fixed at the same level. The first involves the one-dimensional finite element model that uses the effective mass and stiffness described in the previous section. The second approach uses the standard commercial finite element program ABAQUS [159]. The third approach uses the limited analytical solutions available in the literature. The fourth is a sequence of experimental tests. Each of these are described below.

5.4.1 Finite Element Model

The sagged cable is represented using n nodal points. Each node has six degrees of freedom in the three-dimension as shown in Fig 5.3. The stiffnesses and mass coefficients derived in section 5.3 are represented in the global coordinate system domain. The equation of motion is derived from the static configuration first determined about the geometrically nonlinear equilibrium state using the initial sag value d and applying the boundary conditions at the ends. Since the sag to span is small, the equilibrium shape can be approximated by a parabola [158]. The gravity load of the cable is considered in its initial parabola profile configuration. The equilibrium expression is discretized over its length using an assembly two-node one-dimensional elements. Each element is referred to the global X, Y, Z axes and the initial intrinsic coordinates, S, as presented in Fig. 5.3. The equilibrium state from self-weight is found by iterative solution of the resulting nonlinear equations. When the total stiffness is updated and the cable reaches its equilibrium shape, the free vibration analysis is initiated. The natural frequency and modal shapes are found by solving the standard linear eigenproblem about the deformed equilibrium state.

$$\left([K_t]-\omega^2[M]\right)\begin{Bmatrix} U_X \\ U_Y \\ U_Z \\ \theta_X \\ \theta_Y \\ \theta_Z \end{Bmatrix}=0 \qquad (5.16)$$

Here $[K_t]$ and $[M]$ are the $N\times N$ global stiffness and mass matrices of the cable structure, respectively, this is formed after employing the standard assembly procedure over all discretized elements. The eigenvalue is the natural frequency and denoted as ω and found as $f=\frac{\omega}{2\pi}$ in Hz, where U_X, U_Y, and U_Z are the global translations, and θ_X, θ_Y, and θ_Z are the global rotation displacements in the X, Y, and Z directions, respectively. The external dynamic load has been specified to be zero to study the free vibration behavior. The endpoints of the cable correspond to pinned-pinned boundary conditions.

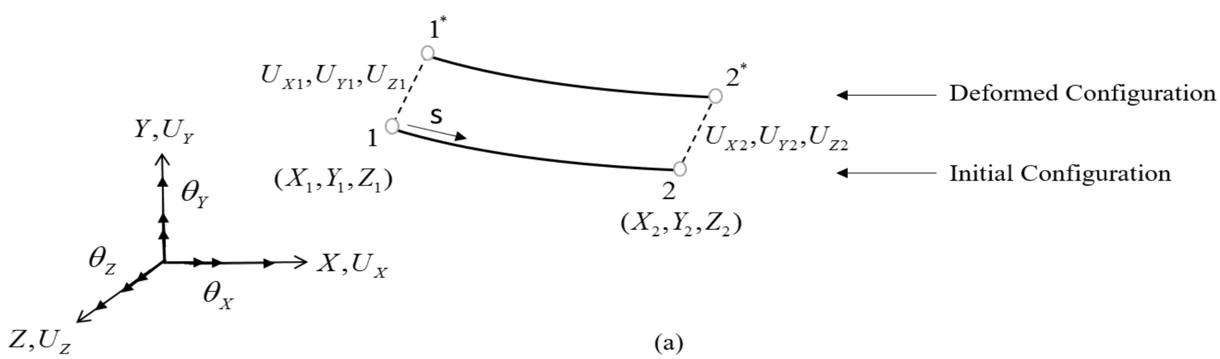

(a)

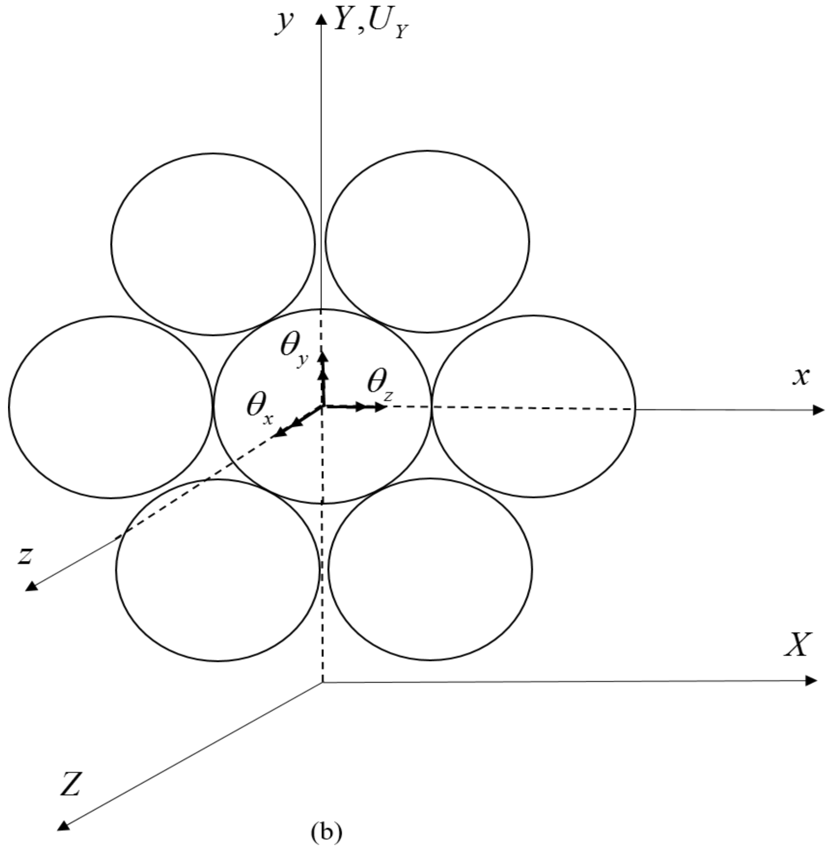

Fig. 5.3 Characteristics of the cable element: (a) two nodes parabolic and (b) reference cross-section

The total element stiffness matrix is derived in the global coordinate system directly as

$$\left[K_t\right] = \left[K^e\right] + \left[K^g\right] \quad (5.17)$$

Here $\left[K^e\right]$ is the elastic stiffness matrix and $\left[K^g\right]$ is the initial stress (geometric) matrix. The elastic stiffness is the modified form of the conventional symmetric truss stiffness matrix that includes axial/torsional coupling, where the stiffness coefficients derived in section 5.3 are used. The local elastic stiffness contains only the axial, torsional, and coupling stiffness and are defined in the local system as

$$
\left[k^e\right]=\begin{bmatrix}
\frac{k_{\varepsilon\varepsilon}}{L_e} & 0 & 0 & \frac{k_{\varepsilon\theta}}{L_e} & 0 & 0 & -\frac{k_{\varepsilon\varepsilon}}{L_e} & 0 & 0 & -\frac{k_{\varepsilon\theta}}{L_e} & 0 & 0 \\
0 & 0 & 0 & 0 & 0 & 0 & 0 & 0 & 0 & 0 & 0 & 0 \\
0 & 0 & 0 & 0 & 0 & 0 & 0 & 0 & 0 & 0 & 0 & 0 \\
\frac{k_{\theta\varepsilon}}{L_e} & 0 & 0 & \frac{k_{\theta\theta}}{L_e} & 0 & 0 & -\frac{k_{\theta\varepsilon}}{L_e} & 0 & 0 & -\frac{k_{\theta\theta}}{L_e} & 0 & 0 \\
0 & 0 & 0 & 0 & 0 & 0 & 0 & 0 & 0 & 0 & 0 & 0 \\
0 & 0 & 0 & 0 & 0 & 0 & 0 & 0 & 0 & 0 & 0 & 0 \\
-\frac{k_{\varepsilon\varepsilon}}{L_e} & 0 & 0 & -\frac{k_{\varepsilon\theta}}{L_e} & 0 & 0 & \frac{k_{\varepsilon\varepsilon}}{L_e} & 0 & 0 & \frac{k_{\varepsilon\theta}}{L_e} & 0 & 0 \\
0 & 0 & 0 & 0 & 0 & 0 & 0 & 0 & 0 & 0 & 0 & 0 \\
0 & 0 & 0 & 0 & 0 & 0 & 0 & 0 & 0 & 0 & 0 & 0 \\
-\frac{k_{\theta\varepsilon}}{L_e} & 0 & 0 & -\frac{k_{\theta\theta}}{L_e} & 0 & 0 & \frac{k_{\theta\varepsilon}}{L_e} & 0 & 0 & \frac{k_{\theta\theta}}{L_e} & 0 & 0 \\
0 & 0 & 0 & 0 & 0 & 0 & 0 & 0 & 0 & 0 & 0 & 0 \\
0 & 0 & 0 & 0 & 0 & 0 & 0 & 0 & 0 & 0 & 0 & 0
\end{bmatrix} \quad (5.18)
$$

Here L_e is the new element length after the initial nonlinear static deformation and can be found using

$$L_e=\sqrt{(X_2-X_1)^2+(Y_2-Y_1)^2+(Z_2-Z_1)^2} \quad (5.19)$$

Here X_2, Y_2, and Z_2, and X_1, Y_1, and Z_1 are the global coordinates of the nodes at the element endpoints.

The initial stress stiffness matrix is associated with the forces employed by the stressed element associated with the direction changes of the element when displaced into its equilibrium state. This can be described in the local coordinate system as

$$\left[k^{g}\right]=\frac{F_a}{L_e}\begin{bmatrix} I & O & -I & O \\ O & O & O & O \\ -I & O & I & O \\ O & O & O & O \end{bmatrix} \quad (5.20)$$

Where F_a is the axial force at the beginning of each incremental step reaching its final value at the static equilibrium position, and I is a 3×3 unit matrix and O is a 3×3 null matrix.

Similarly, the mass matrix is discretized over the cable length. The mass terms defined in Eq. (14) and (15) and are used and the element mass matrix becomes

$$[m]=\frac{L_e}{6}\begin{bmatrix} 2m_{\varepsilon\varepsilon}I & O & m_{\varepsilon\varepsilon}I & O \\ O & 2m_{\theta\theta}I & O & m_{\theta\theta}I \\ m_{\varepsilon\varepsilon}I & O & 2m_{\varepsilon\varepsilon}I & O \\ O & m_{\theta\theta}I & O & 2m_{\theta\theta}I \end{bmatrix} \quad (5.21)$$

All matrices defined in this section are then mapped to the global coordinate system using a transformation matrix using a procedure similar to typical structural elements. The cable element is then oriented in three-dimension using the angles between the local and global coordinate system. The undamped free vibration problem in Eq. (5.16) is then solved.

5.4.2 ABAQUS

All cables studied here were also modeled using a commercial finite element program, ABAQUS [159]. The cables were given their initial configuration in the X, Y plane; however, after adding one more node using truss elements to stabilize it (using imaginary elements that have very small stiffness value), and solving the nonlinear geometry of the deformed cable, the model is shown in Fig. 5.4 as in the case of the finite element model developed in the previous section. The sag value under the nonlinear analysis increases due to considering its own weight and the effect of axial stretching The cable will then be in equilibrium in a parabolic shape for solving the vibration problem. Only the translation displacements are fixed at the supports since the cable element in ABAQUS can only consider axial motion and has lack of ability to model either twist or axial-torsional coupling. In this model the cable is assumed to have circular cross-section.

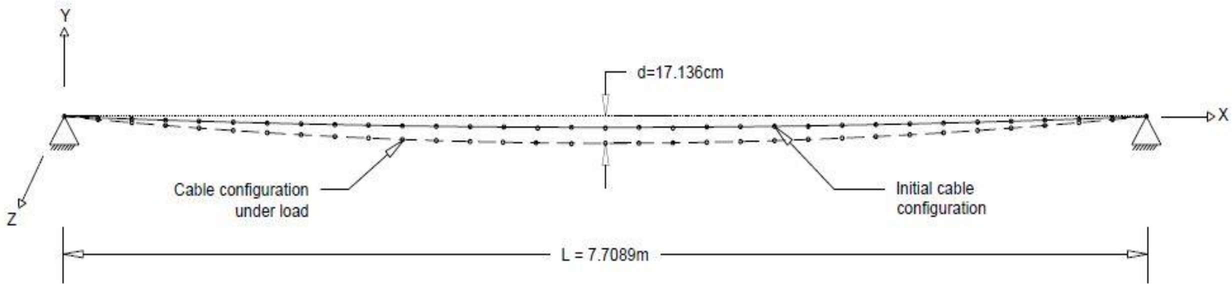

Fig. 5.4 Two-dimensional cable model initial configuration in ABAQUS

5.4.3 Analytical Solutions

Irvine and Caughey [80] have solved for the out-of-plane, symmetric in-plane, and anti-symmetric in-plane frequencies using

$$f_o = \frac{1}{2\pi}\sqrt{\frac{H}{m}} \quad (5.22)$$

$$f_{an} = \frac{2}{2\pi}\sqrt{\frac{H}{m}} \quad (5.23)$$

$$f_s = \sqrt{\frac{\beta_i^2 H}{m}} \quad (5.24)$$

Here the horizontal component of the cable tension is H, m is the mass per unit length, and β_i value can be found from a transcendental equation [80].

The non-dimensional parameter λ^2 has been introduced by Irvine and Caughey [80] in their linear theory for cable vibration and is of great used when classifying the type of cable vibration, and can be computed using Eq. (5.25)

$$\lambda^2 = \left(\frac{8d}{L}\right)\frac{L}{\left(Hl / EA\right)} \quad (5.25)$$

Here E is the modulus of elasticity, A is the cross-sectional area, and L is the cable length. And l can be computed using

$$l = L\left\{1 + 8(\frac{d}{L})^2\right\} \qquad (5.26)$$

This non-dimensional parameter λ^2 accounts for the geometric and elastic properties of the cable. When λ^2 is less, equal, and greater than $4\pi^2$ the symmetric in-plane frequency is lower, equal, and higher than the anti-symmetric in-plane frequency, respectively. In this work the sag used is $d = 17.136$ cm which resulted in $\lambda^2 > 4\pi^2$. It was also been found by Irvine and Caughey [80] that when this parameter is large, the symmetric in-plane mode shape will have two internal nodes.

The axial and torsional frequencies of the proposed finite element model are compared with the analytical solution of a straight and solid circular section under axial or torsional vibration given by

$$f_a = \frac{1}{2L}\sqrt{\frac{E}{\rho}} \quad (5.27)$$

$$f_t = \frac{1}{2L}\sqrt{\frac{G}{\rho}} \quad (5.28)$$

Here G is the shear modulus. These frequencies expressions are very special cases of no sag, which are outside of the scope of the present work but are given here for comparison.

5.4.4 Experimental Model

A series of experiments were used to measure the natural frequencies and corresponding modal shapes of untwisted and twisted cables. The cable length was fixed at $L = 7.709\ \mathrm{m}$. An MTS 243.20 hydraulic actuator [127] (with a stroke length of $25.4\ \mathrm{cm}$) has the ability to simulate a harmonically time-varying support motion in the vertical direction driven via a power control unit (MTS 407 controller [128]). The focus of these tests was on the out-of-plane, symmetric in-plane, and anti-symmetric in-plane frequencies. The overview of the experimental setup is shown in Fig 5.5. The sagged cable is hanging with both ends at the same level.

For each cable configuration and expected resonant frequency, a total of 20 tests were conducted. A MetaTracker sensor [129] was used to obtain the vibration data. This is a mountable device that gives the acceleration records, including the acceleration time history signal for $\ddot{U}_X$, $\ddot{U}_Y$, and $\ddot{U}_Z$ which are longitudinal, vertical, and transverse motions that are parallel to X, Y, Z axes, respectively. It also includes a gyroscope which gives the angular velocity time history signal in the three-axis $\dot{\theta}_X, \dot{\theta}_Y$, and $\dot{\theta}_Z$. Sensors were located at mid-span and the quarter span of the cable length for all tests. For finding the out-of-plane, symmetric in-plane, and anti-symmetric in-plane modes, A total of 180 tests was completed for the three cables tested. For each test, twelve data sets were collected (six acceleration and six angular velocity data files retrieved) from the two tracker used on the cable.

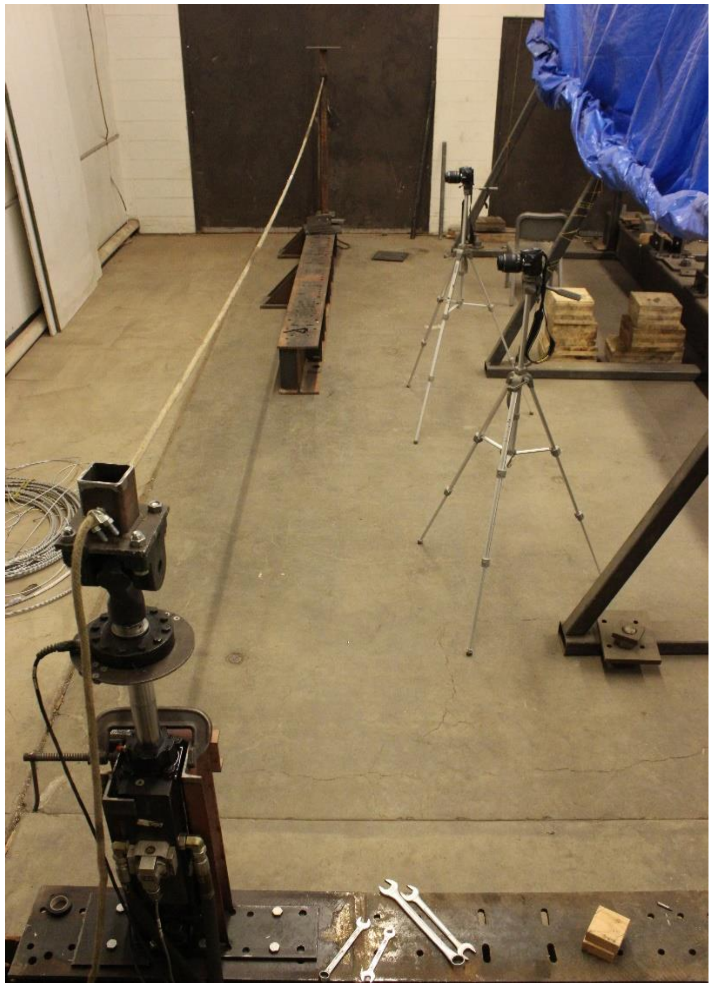

Fig. 5.5 Experimental setup for the sagged untwisted and twisted cables study

For the twisted cables, the actual lay angles α_{actual} used to compare with the numerical model given P were found using

$$\alpha_{actual} = \arctan(\frac{2\pi R_h}{P}) \qquad (5.29)$$

5.5 Applications

Numerical examples of both untwisted and twisted cables were used to facilitate experiments and compare with the developed finite element formulations. Identical material and geometrical properties were used for both experiments and simulations. Table 5.1 shows the properties for Aluminum Conductor Steel Reinforced (ACSR) and Aluminum Conductor Aluminum Reinforced (ACAR) cables denoted as Cables E_1 and E_2. A section of clear plastic hollow circular tubing was used as the sole case of an untwisted cable, and is denoted as E_3.

Table 5.1 Twisted and untwisted cables properties

	Twisted		Untwisted
Item	Cable E_1	Cable E_2	Cable E_3
Core Cable radius R_c (mm)	2.25	1.25	-
Outer Cable Radius R_w (mm)	2	1	-
Total Area A (mm^2)	91.30	23.75	0.576
Unit Mass m (kg/m)	0.35	0.06	0.20
Modulus of Elasticity E (GPa)	74.2	69	8.27
Shear Modulus G (GPa)	37.1	34.5	4.135

5.6 Results and Discussion

5.6.1 Cable Stiffness

A lay angle of varying value was chosen for all twisted cables. And, the stiffness coefficients obtained using the three-dimensional elasticity finite element model for the straight twisted cable were examine with the seven one-dimensional analytical solutions available. The stiffness coefficients are can be expressed in non-dimensional form as

$$\bar{k}_{\varepsilon\varepsilon} = \frac{k_{\varepsilon\varepsilon}}{E\pi R_h^2}$$

$$\bar{k}_{\varepsilon\theta} = \frac{k_{\varepsilon\theta}}{E\pi R_h^3}$$

$$\bar{k}_{\theta\varepsilon} = \frac{k_{\theta\varepsilon}}{E\pi R_h^3}$$

$$\bar{k}_{\theta\theta} = \frac{k_{\theta\theta}}{E\pi R_h^4} \qquad (5.30)$$

The elastic stiffness matrix coefficient were obtained for each lay angle between 0 and 30 degrees, which spaces the usual practical range for cables E_1 and E_2.

The axial stiffness $\bar{k}_{\varepsilon\varepsilon}$ versus lay angle α for each model of cable E_1 are shown in Fig. 5.6. The stiffnesses found using the present model possesses the same general trend in decreasing as the lay angles increases. Without exception, the present model gives stiffnesses lower than the simplified models by between 2-28%. The total magnitude decrease between 0 and 30 degrees is about 47%. The maximum lay angle for this particular cable is 22.5 degrees. Results from the one-dimensional analytical models are nearly coincident except the results from the model of Knapp [10], where the compressibility is included, and those of Kumar and Cochran [22], which is the only one-dimensional analytical model that considers Poisson effect.

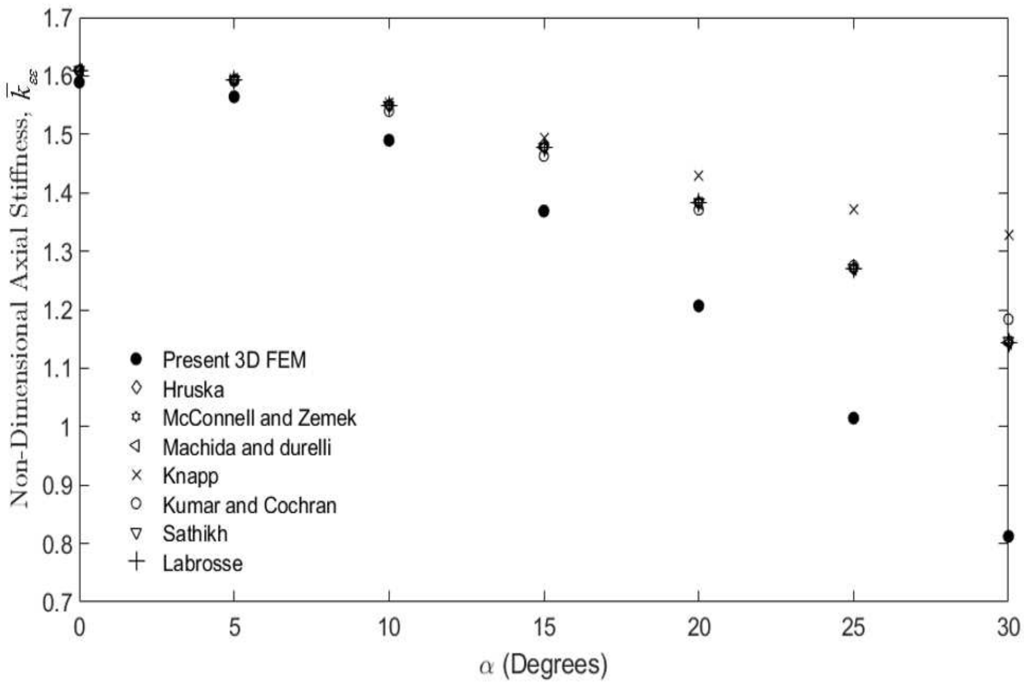

Fig. 5.6 Axial stiffness $\bar{k}_{\varepsilon\varepsilon}$ for cable E_1 (ACSR) versus lay angle α for the present 3D FEM and comparative one-dimensional analytical models

The variation of the non-dimensional coupling terms $\bar{k}_{\varepsilon\theta}$ and $\bar{k}_{\theta\varepsilon}$ with lay angle are detailed in Fig. 5.7 and Fig. 5.8, respectively. The present model gives results that are slightly higher than those provided by most of the one-dimensional models. Among the analytical models, only Hruska [8,9], Sathikh et al. [154], and Labrosse [27] lead to a symmetric matrix form. The agreement for the present finite element model for lay angles less than 20 degrees is very good with most of the different one-dimensional analytical models. The coupling stiffnesses $\bar{k}_{\varepsilon\theta}$ and $\bar{k}_{\theta\varepsilon}$ are within approximately 4% of each other for all the lay angles studied in the elasticity model.

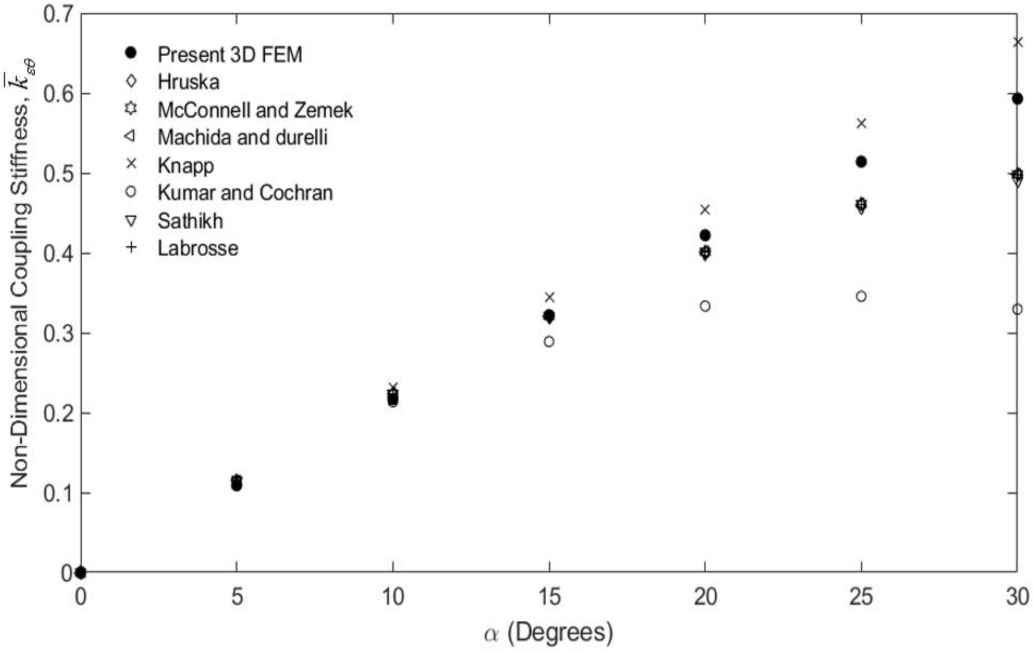

Fig. 5.7 Coupling stiffness $\bar{k}_{\varepsilon\theta}$ for cable E_1 (ACSR) versus lay angle α for the present 3D FEM and comparative one-dimensional analytical models

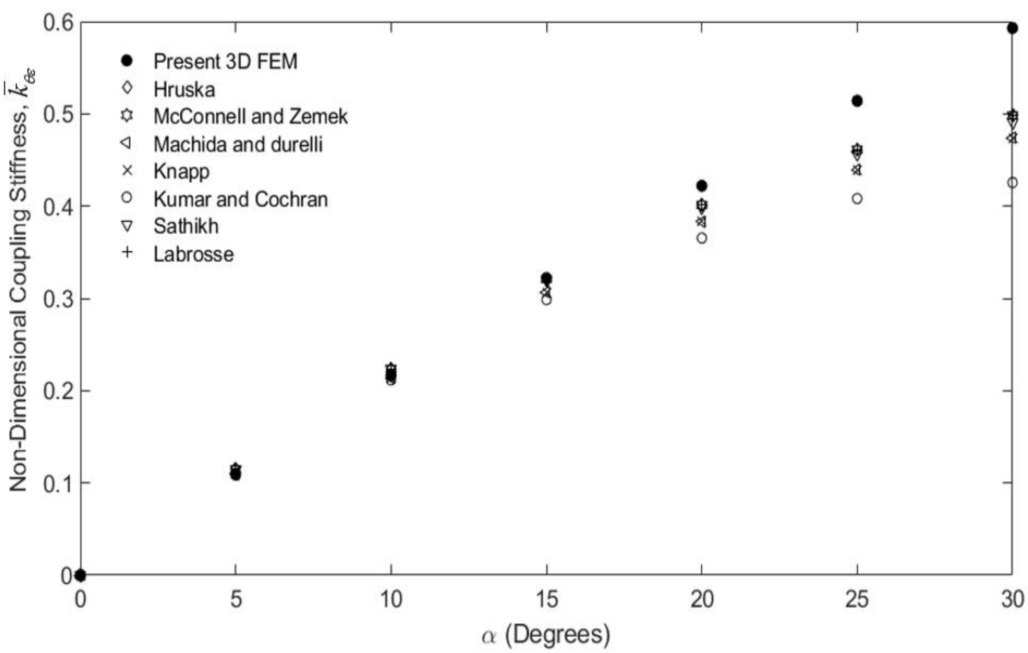

Fig. 5.8 Coupling stiffness $\bar{k}_{\theta\varepsilon}$ for cable E_1 (ACSR) versus lay angle α for the present 3D FEM and comparative one-dimensional analytical models

Fig. 5.9 shows the non-dimensional torsional term $\bar{k}_{\theta\theta}$ versus lay angle. The original model of Hruska [8,9] model gives appreciably lower value than all other models. This is because in torsional stiffness the outer wires is neglected in this model. Other than Hruska [8,9] model, the present three-dimensional finite element model is within the bounds of the remaining simple one-dimensional models. In addition, an increase in the lay angle increases the torsional stiffness. For the present finite element model, the torsional stiffness magnitude increase by approximately 80% between 0 to 30 degrees.

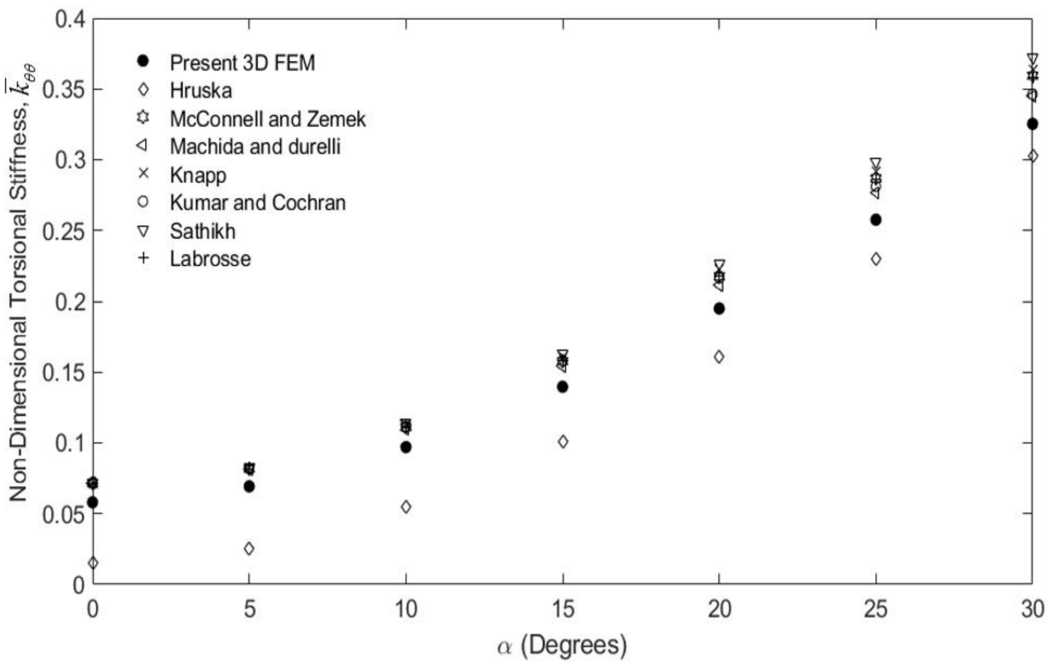

Fig. 5.9 Torsional stiffness $\bar{k}_{\theta\theta}$ for cable E_1 (ACSR) versus lay angle α for the present 3D FEM and comparative one-dimensional analytical models

For the twisted cable E_2 similar trends were found using the present three-dimensional finite element model in comparison with the analytical models, with smaller magnitudes of stiffness in general compared to cable E_1 because of to its small cross-sectional area and material properties. Table 5.2 shows the non-dimensional axial, coupling, and torsional terms versus lay angles between 0 and 30 degrees. For cable E_3, $k_{\varepsilon\varepsilon} = 4.76E+03$ kN, $k_{\theta\theta} = 2.19E-04$ $N \cdot m^2$, and $k_{\varepsilon\theta} = k_{\theta\varepsilon}$ are zero (the cable deformations are uncoupled).

Table 5.2 Non-dimensional stiffness coefficients for cable E_2

Lay Angle (degrees)	$\bar{k}_{\varepsilon\varepsilon}$	$\bar{k}_{\varepsilon\theta} = \bar{k}_{\theta\varepsilon}$	$\bar{k}_{\theta\theta}$
0	1.4754	0	0.0501
5	1.4526	0.0971	0.0601
10	1.3849	0.1922	0.0848
15	1.2750	0.2831	0.1228
20	1.1282	0.3669	0.1722
25	0.9544	0.4398	0.2283
30	0.7707	0.4966	0.2888

5.6.2 Cable Dynamics

Using the elements of effective mass and stiffness, the finite element method model and experimental approaches were used to find the natural frequency and modal shapes for the fixed-fixed cable where both the twisted and sag value are included and compared with known results for the special case of the untwisted cable. In addition, the undamped free vibration problem was also solved for the same cables described in Table 5.1 using both ABAQUS and Irvine and Caughey [80] model and straight circular section analytical solutions. Out-of-plane, symmetric in-plane, anti-symmetric in-plane, axial, and torsional motions were all considered. In addition, the actual lay angles α_{actual} for cables E_1 and E_2 were found using Eq. (5.29). For given pitch lengths of P measured of 190 and 110 mm (see Fig. 5.10 for cable E_2 pitch length), from that the actual angles are found to be 8 and 7.32 degrees for cables E_1 and E_2, respectively.

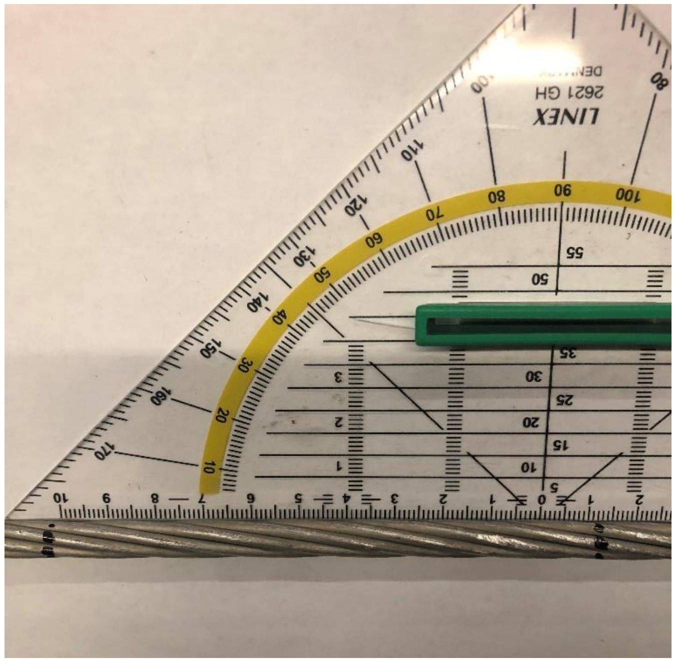

Fig. 5.10 Cable E_2 (ACAR) pitch length found to be 110 mm from the outer wire takes a full turn around the circular core wire

The computational finite element model was used first to solve the static problem given an initial sag ($d = 17.136\text{cm}$), and was then used to solve the undamped free vibration problem in three-dimensions using the final cable configuration where axial stretching and cable weight are included. Likewise, in the ABAQUS model, the nonlinear geometry were found first, followed by the solution of the vibration problem where torsional stiffness and coupling was not included. The eigenproblem for the natural frequencies and corresponding mode shapes were calculated using the two-nodded element approximation. Convergence of 4, 8, and 16 elements were tested for cables E_3 (untwisted) with the analytical results, 16 element model showed less than 0.5% error (study details are not shown here), therefore, a total of 16 elements were used throughout the present finite element model.

The present finite element frequencies were compared with the analytical solutions, the ABAQUS model, and the results obtained experimentally. These comparison are shown in Table

5.3 for cable E_1 . The natural frequencies found using the present model have an excellent agreement when the 16 elements are used to the cable model. There are differences between the finite element and the analytical models solutions for the axial and torsional frequencies, because of the actual lay angle of cable E_1 (8 degrees). When the lay angle is equal to zero the axial frequency from the finite element results is almost equal to the analytical results, and the torsional frequency from the finite element model is 12% lower due to the Poisson ratio effect when calculating the torsional stiffness (the $\alpha = 0$ results presented later in this section).

Table 5.3 The natural frequencies for Cable E_1 using different approaches

	Frequency $f\,(\mathrm{Hz})$				
	Irvine	Circular Section	ABAQUS	Experiment (Median)	Present Finite Element Model
Out-of-Plane	1.329	-	1.328	1.329	1.330
In-plane symmetric	3.791	-	3.750	3.825	3.847
In-plane anti-symmetric	2.658	-	2.643	2.662	2.674
Axial	-	280.051	-	-	235.197
Torsional	-	198.026	-	-	197.764

The accuracy of the data gained from the experimental tests depends on many factors these include 1) the imperfection of initiating and maintaining the cable tension, 2) disturbances and positing of the trackers. These effects are minimized by repeating the tests several times for each frequency and cable, which leads to the results presented. As an illustration, Fig 5.11 shows the frequency results found for cable E_1 experimentally in box plot, where 20 tests have been conducted for each frequency, the horizontal line across the box is the median which is used in the comparison.

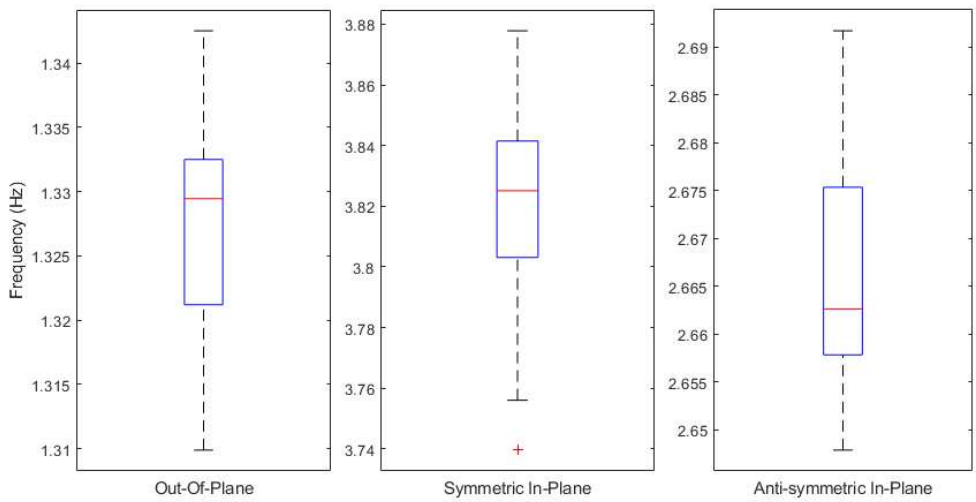

Fig. 5.11 Cable E_1 frequencies obtained experimentally and presented in boxplot, specifically give the median value which is represented by the line across in the interquartile range, it is used in the comparison with other approaches

The present finite element frequencies were also compared with the experimental work for the remaining twisted and untwisted cables studied here and are presented in Table 5.4. The actual lay angle and sag value were used in this comparison.

Table 5.4 The natural frequencies for Cables E_2 and E_3

	Frequency f (Hz)			
	Cable E_2		Cable E_3	
	Experiment (Median)	Present Finite Element Model	Experiment (Median)	Present Finite Element Model
Out-of-Plane	1.331	1.332	0.830	0.835
In-plane symmetric	3.832	3.857	1.500	1.503
In-plane anti-symmetric	2.660	2.678	1.612	1.639
Axial	-	280.011	-	10.129
Torsional	-	225.089	-	6.981

For twisted cables E_1 and E_2, the effect of lay angle on the dynamic cable behavior was also assessed. For angles between 0 to 30 degrees, Table 5.5 shows the frequency spectrum for cable E_1 with the angle changes. The out-of-plane frequencies slightly decrease with lay angle increase, but the change is only 0.35% from 0 to 30 degrees. The in-plane symmetric frequencies possesses the same trend in decreasing as the lay angles increases (0.63%). In addition, the in-plane anti-symmetric frequencies also decrease. However, as the cables approach the maximum lay angle, the frequencies begin to slightly increase. The axial frequencies generally decrease with a slight increase as α approaches α_{max}. The torsional frequencies consistently and linearly increase with lay angle.

Table 5.5 The natural frequencies for Cable E_1 with lay angle between 0 to 30 degrees

	Frequency f (Hz)						
Lay Angle (degrees)	0	5	10	15	20	25	30
Out-of-Plane	1.331	1.330	1.329	1.325	1.321	1.323	1.326
In-plane symmetric	3.852	3.850	3.844	3.827	3.815	3.819	3.828
In-plane anti-symmetric	2.675	2.675	2.673	2.663	2.656	2.659	2.666
Axial	280.471	255.641	225.973	210.795	203.230	201.484	202.815
Torsional	174.044	184.084	209.026	241.009	274.695	307.563	337.749

For the same cable (E_1), the corresponding modal shapes for the out-of-plane, symmetric in-plane, anti-symmetric in-plane, axial, and torsional frequencies are shown in Fig. 5.12-Fig. 5.16 for lay angles between 0 and 30 degrees. The translational and rotational displacements denoted as U_X, U_Y, U_Z, θ_X, θ_Y, and θ_Z and show the interaction for each type of motion. All modal plots are normalized with respect to the peak translation or rotation displacement.

The results from the experimental tests are also included, where the mid and quarter maximum acceleration and angular velocity records were obtained and processed by integrating to get the translations and rotation displacements. For example, in the longitudinal direction:

$$U = -\frac{\ddot{U}_{data}}{\omega^2}\sin(\omega t) \qquad (5.31)$$

$$\theta_X = -\frac{\dot{\theta}_{X-data}}{\omega}\sin(\omega t) \qquad (5.32)$$

Similar operation are used in the other two directions. From that the peak of displacements value of 20 tests were found, and the median of the data is then used in the modal shape comparison.

Figure 5.12 shows the amplitudes for the out-of-plane frequencies. These are normalized to the primary motion which is the symmetric (out-of-plane) transverse translation U_Z. When the cable is uncoupled (0 degrees), all rotations are all equal to zero. For lay angles between 5-30 degrees, the amplitudes of all the translations and rotations coincide using the three-dimensional finite element model. Because of the twist in the cable, there are non-zero translation and rotation values in all directions. The maximum rotation is in the longitudinal direction where it is 0.72 per unit translation at the quarter span of the cable. The peak experimental value $\alpha = 8$ degrees is 0.55, where in both cases the mode has a symmetrical shape about mid-span. The maximum rotation displacement in the other two directions occur at the mid span with smaller magnitudes compared to the longitudinal rotation. The vertical and transverse rotation results from the finite element model are lower and higher than the experimental results by 25.5 and 36.41%, respectively.

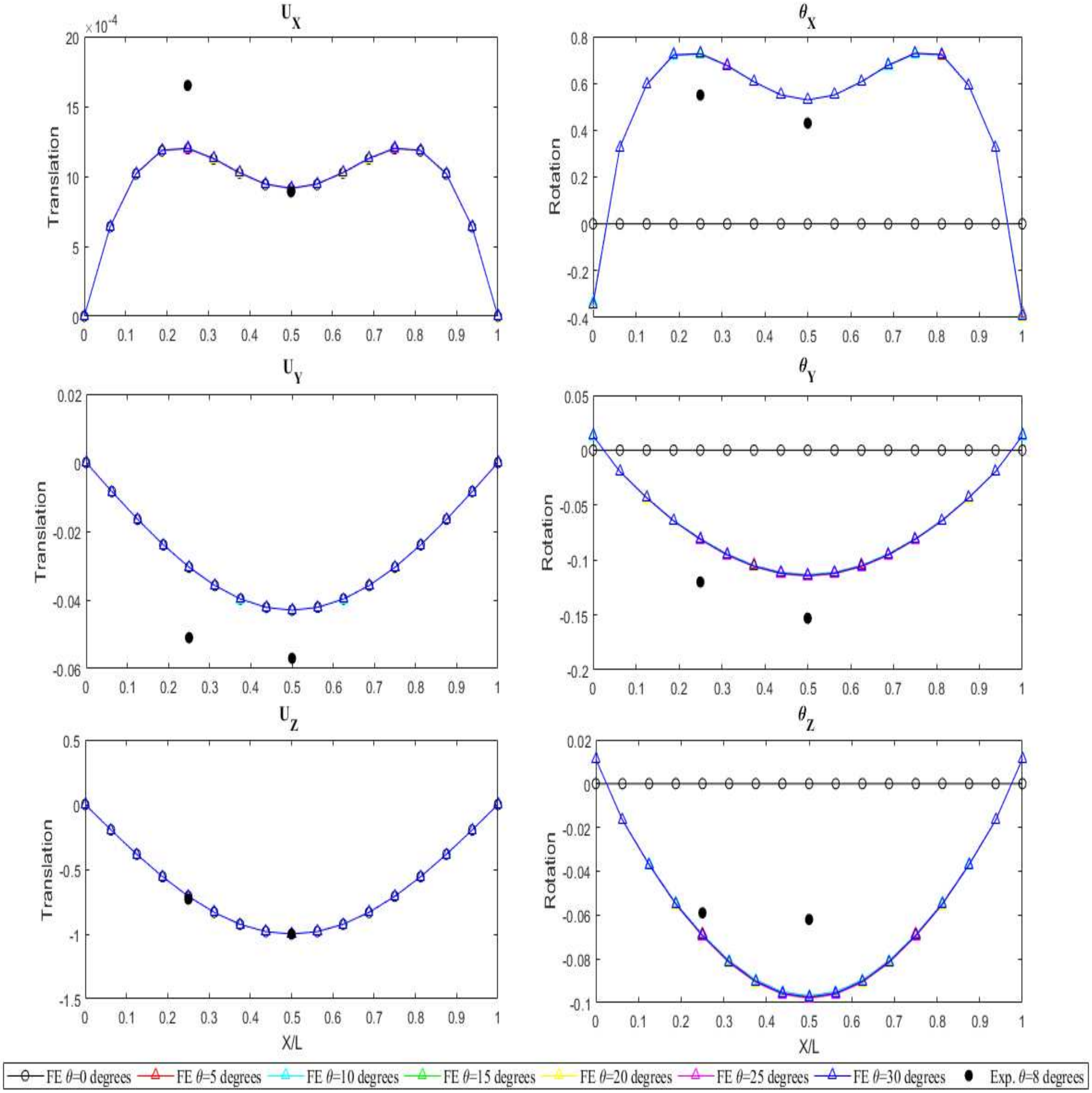

Fig. 5.12 The out-of-plane modal shapes for cable E_1 for the finite element model (FE) with lay angles 0 (uncoupled) and 5-30 (coupled) degrees and experimental results (Exp) for a cable with lay angle of 8 degrees.

In addition, rotations at the cable supports were observed when coupling is exist. The peak rotation was in the X direction and was lower by 35% of the displacement magnitude at the mid span. The coupled translation displacements have very small magnitude comparing with the transversal translation displacement, the peak values are 0.0012 and 0.043 per unit translation for the longitudinal and vertical displacements. These results were validated experimentally with about 27% different between finite element and experimental results.

The symmetric in-plane modal shape is shown in Fig. 5.13. The non-dimensional parameter λ^2 for this cable is greater than $4\pi^2$. Therefore, the frequency for all lay angles is larger than the anti-symmetric in-plane frequency (as shown in Table 5.5). It was found that the symmetric in-plane mode (U_Y) has two internal nodes, which replicated the linear vibration theory defined by Irvine and Caughey [80]. It was also noted in this work that the transversal translation, vertical rotation, and transversal rotation have two internal nodes. each of these behavior was confirmed using the obtained experimental results.

The coupled rotations appear when lay angle is non-zero. The longitudinal rotation θ_X is the maximum and increases 50% of its peak value at the support as the lay angle increases from 5 to 30 degrees. The rotation θ_X for a cable with lay angle 10 degrees at quarter span from the finite element model is significantly lower than the experimental value (66%). The maximum values for the vertical and transverse displacements at mid span are 0.27 and 0.008 per unit translation. These are 33% and 32% higher and lower than the experimental results. Further, the coupled translation displacements U_X and U_Z were also found and are very small but reasonably scaled compared to the primary vertical translation displacement.

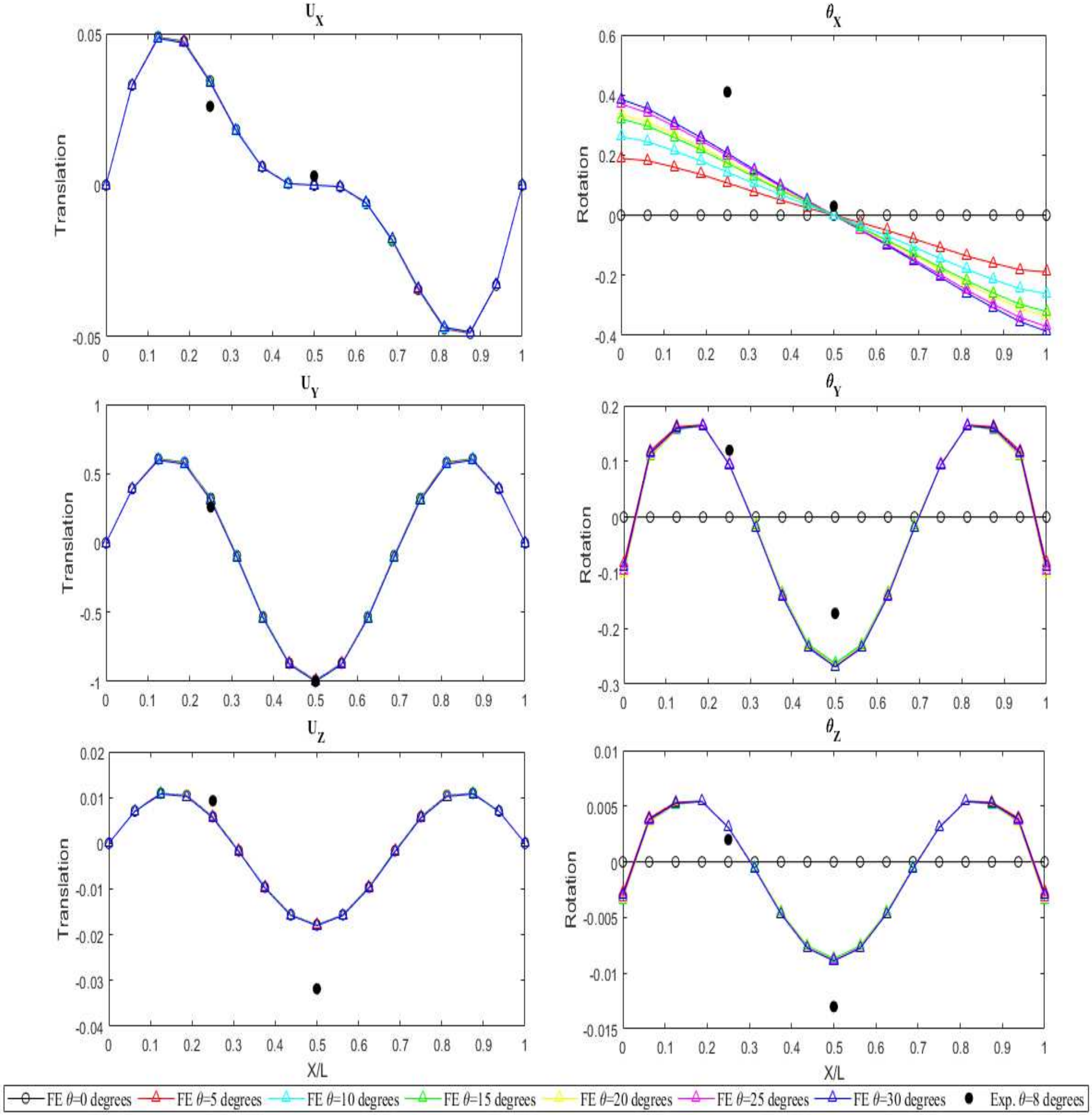

Fig. 5.13 The symmetric in-plane modal shapes for cable E_1 for the finite element model (FE) with lay angles 0 (uncoupled) and 5-30 (coupled) degrees and experimental results (Exp) for a cable with lay angle of 8 degrees.

The anti-symmetric modal shapes for lay angles 5 to 30 degrees are very similar in nature and are shown in Fig. 5.14. The results are normalized to the primary cable motion, which is the vertical translation U_Y. The maximum rotation θ_X is also in the longitudinal direction where it peaks at the cable supports. The mid-span rotation value θ_X is compared with the experimental results (1.31 per unit translation displacement) and it is found that the finite element model results was 50% lower. Using the finite element model and experiments, the coupled vertical and transverse rotations have an anti-symmetric shape. And, it is found using the present model that the vertical rotations are being 78% larger in magnitude than the transverse rotations.

Coupling displacements are also observed in the X and Z axes. Where the transverse translation U_Z is relatively large. The peak displacement occurs at the quarter span and its 31% of the primary motion U_Y. However, the longitudinal displacements U_X is the smallest in magnitude of the two with symmetrical shape. The three-dimensional finite element model results showed that the lay angle variation effect is negligible for this modal shape.

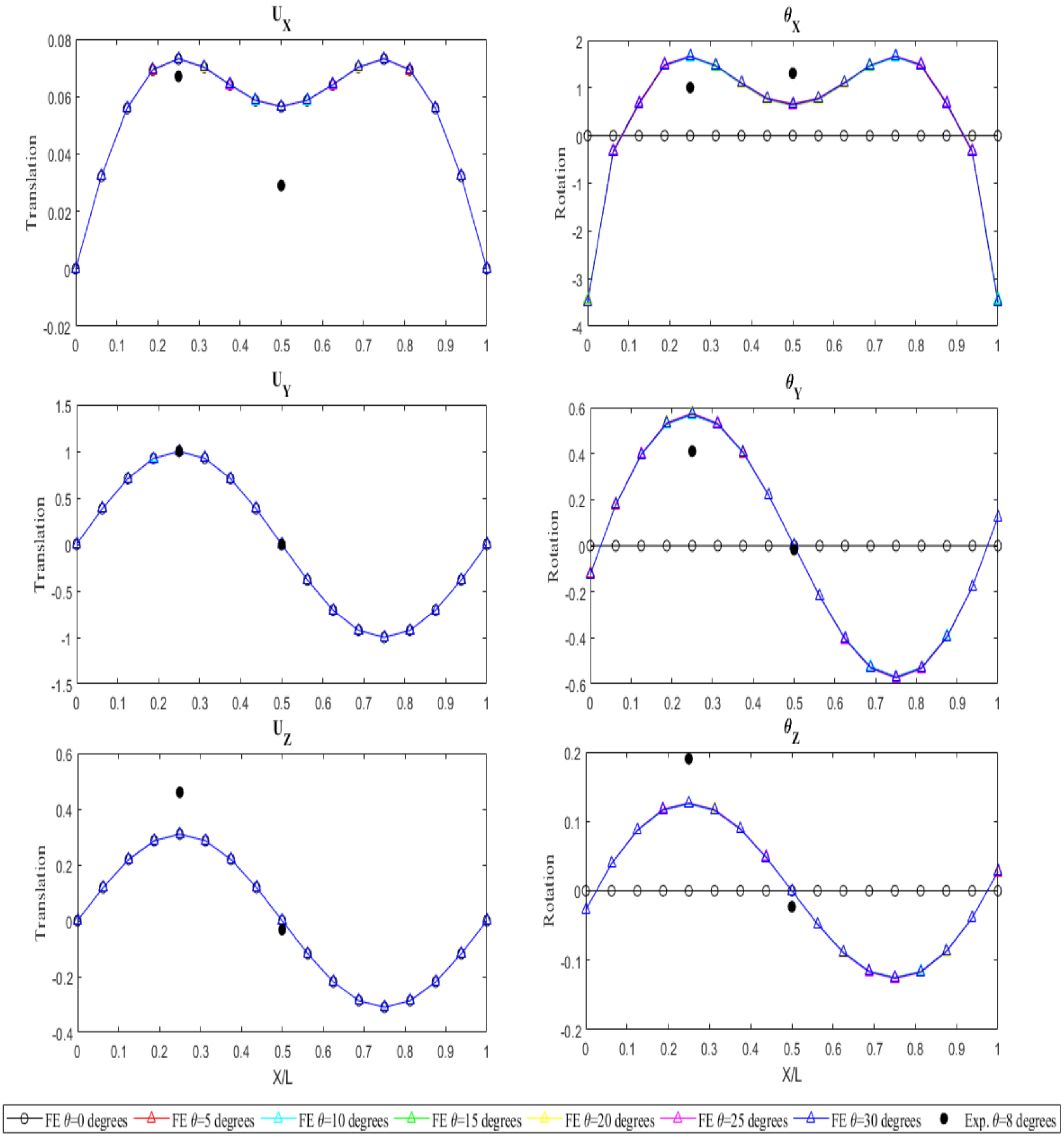

Fig. 5.14 The anti-symmetric in-plane modal shapes for cable E_1 for the finite element model (FE) with lay angles 0 (uncoupled) and 5-30 (coupled) degrees and experimental results (Exp) for a cable with lay angle of 8 degrees.

The axial frequencies are shown in Fig. 5.15 and they are normalized to the longitudinal translation U_X. For the uncoupled (0 degrees) case the rotations θ_X, θ_Y, and θ_Z are all equal to zero. For the coupled case (lay angle 5-30 degrees), the translation amplitudes are generally coincided (different is less than 5% from 0 to 30 degrees), and the rotation values vary with lay angles. The maximum rotation magnitude is in the X direction, with a magnitude that increase with lay angle. The same behavior occurs for the θ_Y and θ_Z at the supports. The vertical rotation displacement are larger than transversal by 90%. The coupled translation displacements U_Y and U_Z are very small comparing to the primary motion with the peak values of those are occurring closer to the supports than mid-span. The maximum values of the displacements are 0.08 and 0.005 unit translation for the vertical and transversal translation displacements, respectively.

The torsional frequencies are represented in Fig. 5.16 and are normalized to the primary longitudinal rotation θ_X. For the uncoupled (0 degrees) case the translations in the X, Y, and Z directions are all equal to zero. The rotations displacements vary with lay angles. The θ_X, θ_X, and θ_X peaks increases with the lay. Lower rotations are found for the θ_Y and θ_Z where the peak value found at the support is 91% lower than the transversal rotation mode. The translations in the three directions are very small in magnitude and these increase with lay angles. The maximum is in the longitudinal direction, where the peak at the quarter span has a value of 0.00144 unit translation when the lay angle is 30 degrees.

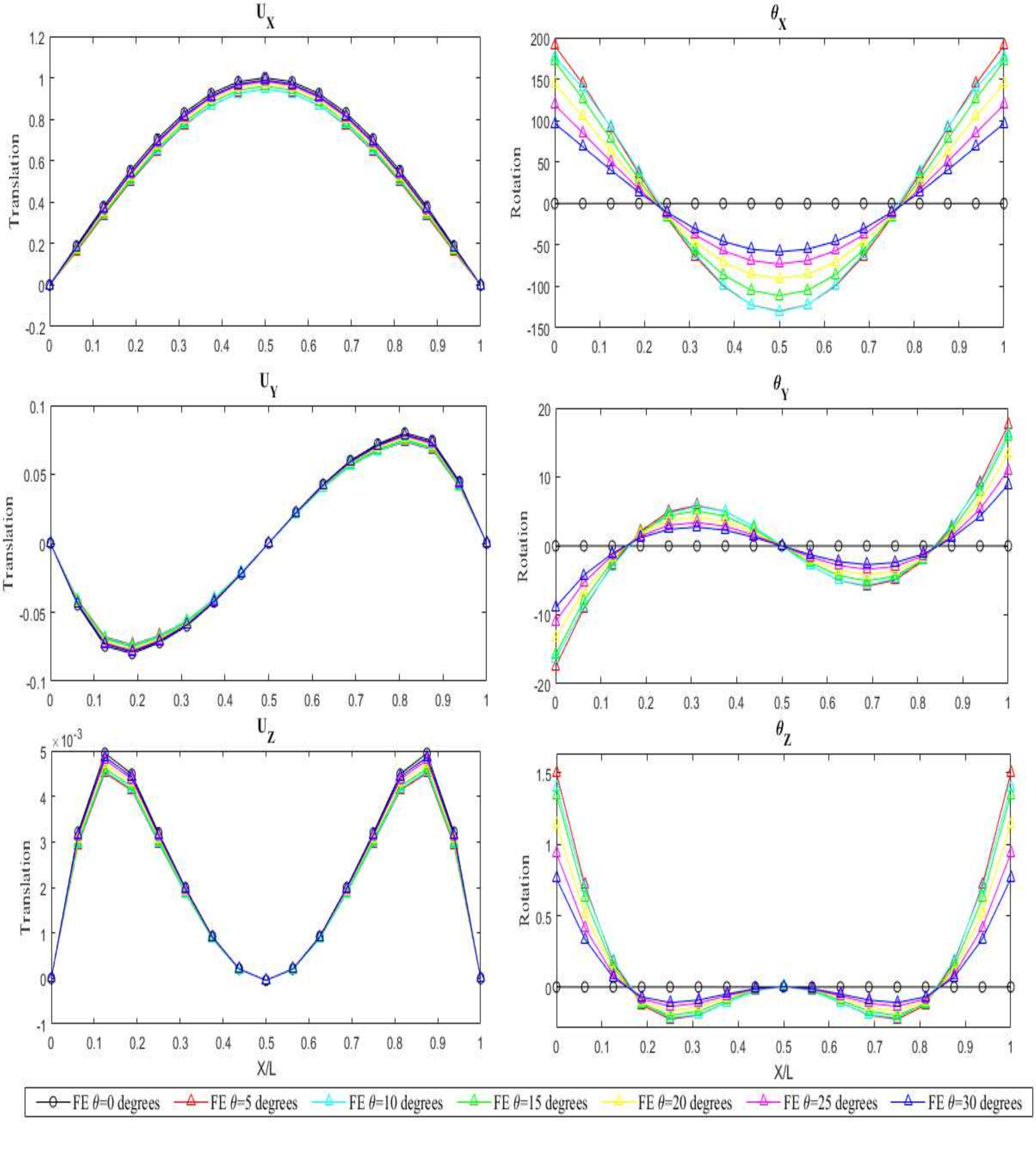

Fig. 5.15 The axial modal shapes displacements for cable E_1 for lay angles 0 (uncoupled) and 5-30 (coupled) degrees.

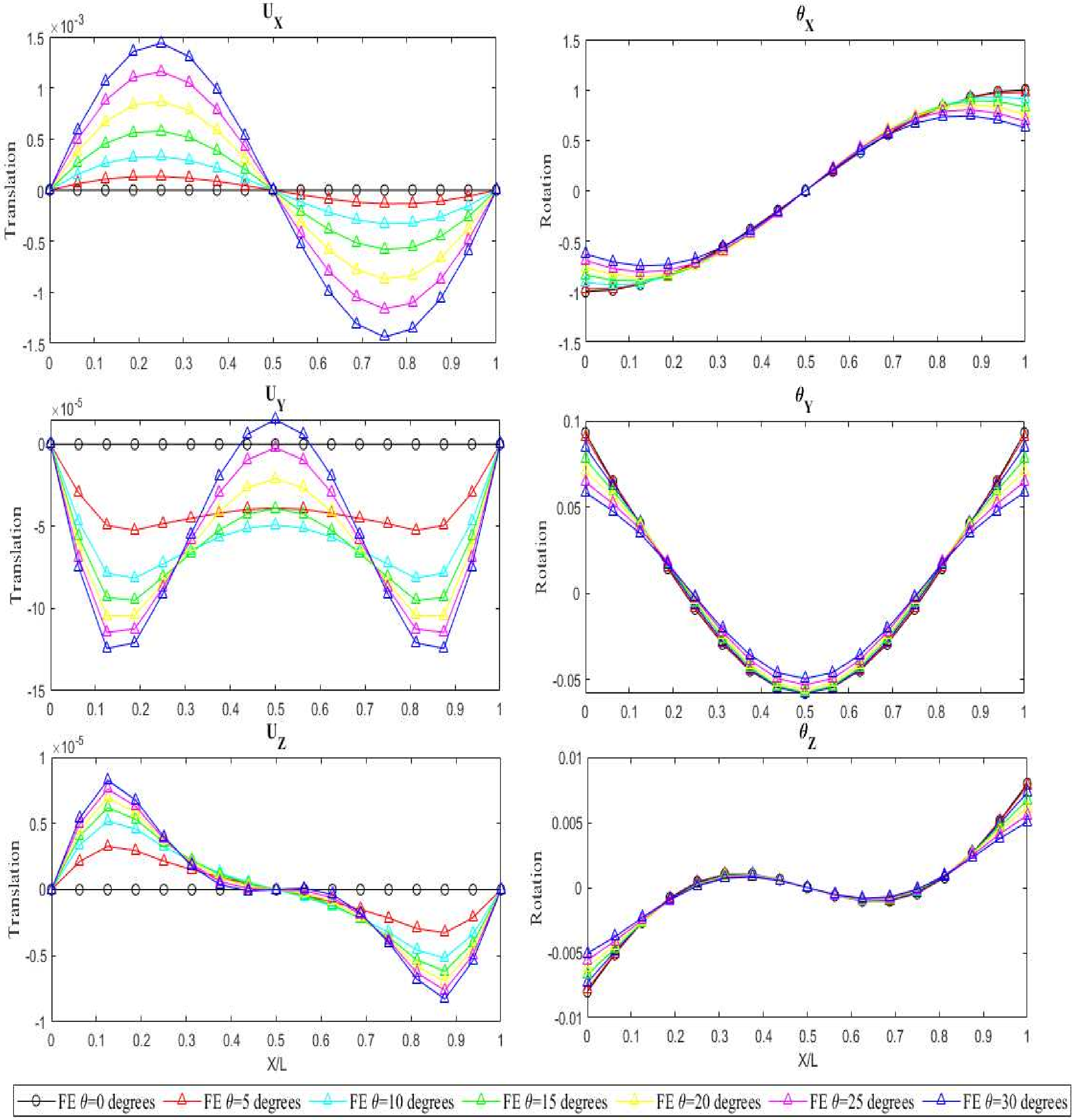

Fig. 5.16 The torsional modal shapes displacements for cable E_1 for lay angles 0 (uncoupled) and 5-30 (coupled) degrees.

5.7 Conclusion

The effective stiffness and mass matrix were calculated using a three-dimensional elasticity method for two twisted cables. These were used to measure the nature of the dynamic motion and resonances considering the free vibrational analysis of cables supported at the same level, using a three-dimension finite element model where the sag is considered, the twisted and the untwisted cables were examined. The finite element model was validated with large experimental work as well as using commercial finite element software and available analytically solution. The lay angle variation effect was tested using the model to study the frequency spectrum and modal shapes. The study showed that the proposed finite element model gives an excellent prediction of the dynamic response for twisted cables, to results in enhancing a safe design and reliable system. In addition, the primary conclusions are:

1. The axial stiffness coefficients for lay angles between 5 to 30 degrees using the elasticity-based approach are slightly lower (4 percent) than those on the one-dimensional models for the actual lay angle of the studied cables. The coupling and the torsional stiffness are generally within the bounds of the simple one-dimensional models.
2. The frequency spectrum, including out-of-plane, symmetric in-plane, anti-symmetric in-plane, axial and torsional frequencies, for twisted and untwisted cables studied are within excellent agreement with the experimental results (the difference is less than 0.5 percent) where actual lay angle was used.
3. Lay angles has a very small (within under 0.4 percent) influence for lower frequency spectrum (out-of-plane, symmetric and anti-symmetric in-plane). In contrary, they have a large (40 percent) influence for axial and torsional models. The axial frequencies are

decreasing linearly with 8 percent rate until the maximum angle of the cable is reached, and it starts to change the behavior. The torsional frequencies are steady linear increase with lay angles.

4. The translation modal shapes are almost completely unaffected by lay angle for the lower frequency spectrum. In addition, the anti-symmetric modal shape have the maximum longitudinal rotation is in this mode (1.31 per unit translation displacement), the results from the finite element model are lower by approximately 50 percent from results obtained using the experiment. And, the rotational modal shape for the symmetric in-plane mode is strongly influenced by lay angle. The other two rotations are not.
5. The translation mode shapes are minimally impacted by lay angle for the axial modes, but all three rotational mode shapes are strongly influenced. This behavior is reversed in the case of torsional modes.

CHAPTER 6: FREE VIBRATION OF AN INCLINED TWISTED CABLE

6.1 Summary

This paper is aimed at simulating and investigating the coupled translations and rotations vibrations occurring simultaneously in inclined sagged strands. The derived three-dimensional models of the single-layered six wires strand stiffness results from the elasticity-based finite element behavior analyses under axial tension and torsion loads is validated through a comparison with the one-dimensional analytical model results. Results found agreed well for the actual lay angle of the cable, and the angles below 20 degrees with the finite elements models where internal contact was not considered. To find the cable natural frequency and corresponding modal shapes the derived primary stiffness and mass matrices are discretized over the inclined sagged cable using a computational efficient finite element model where the two-node cable element have three translational and three rotational degrees of freedom. The phenomena is also studied using extensive experimental tests using same cable geometry and material. Besides to the experiments the finite element model accuracy was tested with a well-known analytical model available from the literature for horizontal cables, and the inclination angle variation are also investigated and compared with the computer finite element software ABAQUS for the same purpose. The results found confirm the correctness of the derived formulation, mathematical, and psychical importance of the six-degrees of freedom finite element model developed and the efficiency in evaluating the coupled cable dynamic behavior. It addition, it highlight the fundamental dynamics of inclined cables and the role of the inclination angle, sag, and weight of the cable.

6.2 Introduction

Cables is widely used in many fields for example as construction, bridge, port, and mining industry. As a results of preforming in high strength and good flexibility due to their remarkable advantage of tensile property, low bending and torsion stiffness [70]. Dynamics of elastic cables have attracted many researchers as the interest in using cable has increased. In many cases where cables play an important role, any failure of the cable may cause a serious accident such casualty and economic loss, showing that in-depth studies on the cable is of great significance. In general, the static response for single or multi-layered strands is coupled. In other words, when a cable has a twist along its length, it will have coupled axial-torsional behavior. When tension load is applied on the twisted cable, two displacements types will propagate, axial and torsional. And, when torsion load is applied axial and rotation displacements will be exist. These phenomena have great impact on the dynamic of cables. And it did not receive enough attention in the literature, where the static response is fully understood. The longitudinal, vertical and transversal translations and rotation motion interaction are effected by the coupling of the twist and make the cable dynamics very complicated. The emphasis in this study is on inclined twisted sagged cables, and the special case of horizontal cables is also investigated.

The study of natural frequencies and mode shapes of cables has a long history. The derivation of the static and dynamic response of horizontal and inclined uniform (untwisted) cables can be found in Cable Structures [74]. In 1953, the fourth order differential equation was driven by Saxon and Cahn, which governed the small amplitude vibration of uniform cables supported at the same level (horizontal) for any sag value [78]. Moreover, other linear cable theories also failed to reconcile with the string theory when the sag set to be zero. In 1974, Irvine and Caughey introduced their linear theory for out-of-plane and in-plane free vibration for horizontal suspended elastic cables [80]. Explicit solutions were driven for the natural frequencies and modal shapes. In detail, they studied the modal cross-over phenomenon in the frequencies. In addition, they presented the non-dimensional parameter λ^2 which accounts for the elasticity and geometry of the cable. The symmetric in-plane frequencies and modes varied with this parameter, the existent of the cross-over points when the frequencies of the symmetric in-plane modes are equal to those of the neighbor antisymmetric in-plane modes. Their results agreed well with the results of simple experiments for uniform cables excited in a manner that it demonstrated the modal cross-over phenomena.

Irvine [84] extend the work, and applied the introduced linear theory of horizontal cable on inclined cables. The addition was simply using a coordinate transformation to the cable chord. However, in this work he ignored the weight component which is parallel to the cable chord. Henghold et al. [115] analyzed the free vibration of a single span cable using three-dimensional nonlinear finite element technique. In their work they developed an empirical formula that gave an approximation to the lowest natural frequency. More work into finding solution for the free vibration of an inclined extensile sagged cable was by Triantafyllou [85], in his work weight component and spatial variability of dynamic tension were taking into account. In addition, he showed that the inclined cables differ than the horizontal cables regarding properties, stating that it cannot be obtained by simply extending the horizontal cable results. He concluded that inclined cables rather than having modal cross-over in the frequencies, an avoided crossing occurs due to the cable unsymmetrical configuration.

Nevertheless, the Irvine's theory was validate by confirming for a range of parameters. In addition, the weight component from other point of views was studied by many scholars; Triantafyllou and Grinfogel [86] where they extended Triantafullou's work and drive a simple approximate formulas for the inclined cables. Perkins and Mote [160] provided three nonlinear equations of the cable vibration based on Hamilton principle for traveling cables. Galarekin method was used to linearize and discretized the governing equations. Burgess and Triantafyllou

[87] used an asymptotic solution to explore the properties details of the out-of-plane modes for horizontal and inclined cables of small sag. Experimentally, Russell and Lardner [161] found clear evidence of the avoided crossing phenomenon while determining the in-plane natural frequencies for uniform inclined cable.

The coupled interaction between transversal, vertical, and torsional motions for uniform cables started with more emphasis on the cable galloping phenomena. Samras et al. [101] started the investigation and emphasized on the importance of including the couple extensional-torsional behavior when studying the cable dynamics. Many simplified theories are presented in the literature, such Nigol and Power [89] model, or using finite element modeling, where a range of different elements types were used, from simple two-nodes to a higher order element to analysis the dynamic response. Among which have been reviewed in Desai et al. [99], where they developed a three-node isoperimetric cable element to perform a geometric nonlinear, static analysis of single cable structure experiencing only translational deformations. And, Desai et al. [90] showed the vertical and torsion coupling, also, Jones [91] studied the coupled longitudinal and vertical motions. Yu et al. [88,93] proposed analysis for the longitudinal, vertical, and torsional coupling. Yu stated that the previous investigations on that resolved to be not satisfactorily, because there is no simple model available that captures the full coupling between the cable motions [93]. Using dynamic stiffness matrix: Starossek [98] studied the vibration behavior of sagged cables. The study is restricted to consider motion within the vertical cable plane only. Desai et al. [94] enhanced the three-node element model to include the torsion and analyzed the galloping of a multi-span transmission line.

Recently, researchers focused more into the nonlinear interaction where it increase in the finite-amplitude dynamic of elastic cable. Rega [116,117] discussed the main features and problems associated with the nonlinear vibration analysis of suspended cables. Wu et al. [162] proposed an explicit formula to show the avoided crossing phenomenon introduced by Triantafyllou [85]. Srinil et al. [163] studied the frequencies and modes of suspended cables considering the coupling between the longitudinal and vertical translation displacements. Thai and Kim [124] solved the nonlinear dynamic problems of cables by employing the catenary cable element for the Newton-Raphson and Newmark direct integration methods. Thai et al. [83] continue using the same method to find the natural frequencies and the geometries of modal shapes. Zhou et al. [81] stated that all the models dealt with inclined cable showed that the natural frequencies did not cross over because of the inclination the modes become hybrid modes, a mix of symmetric and antisymmetric shapes, with an effect on the dynamic tension, and this phenomenon is accompanied by the variation of the curvature along the catenary profile in the static state when the cable is inclined which would not occur when the parabolic assumption is adopted.

As emphasized by Perkins [118] the experimental work done to study the nonlinear motion and/or verify the large amount of numerical method are very limited. For that, introduced a simple two-degrees of freedom analytical results and compare it to an experiments of horizontal untwisted cable, results showed lead to non-planar internal resonance. Also using harmonic time-varying support experimentally Koh and Rong [158] found the three dimensional translation displacements as regards the dynamic tension of non-resonant untwisted cable that is suspended horizontally. For inclined untwisted cables, Rega et al. [164] found the natural frequency and modal shapes numerically and experimentally and showed the out-of-plane and in-plane modes' three-degrees of freedom interactions.

It should be noted that the models mentioned earlier here are limited due ignoring the actual cable geometry, including the twist (by assuming that the cable has a circular cross-section), and boundary conditions used. Many scholars in the literature have been studying the cable helical structures' analytical characterization of the static response to different loading scenarios to describe its behavior. Mostly reacting to only axial forces; the analysis has been performed by modeling the cable as a perfectly flexible element. The analysis can be subdivided on mechanical models' base in describing the wires inside the cable into discrete and semi-homogenization formulations. More into finding the stiffness and cables geometry modeling can be found in the review paper by Spak et al. [133]. Recently, Foti and Martinelli [155] presented a model to find the axial-torsional response of a one layered strand that consider the deformability of the internal contact surfaces, and derived a symmetric stiffness matrix.

Further, as for solving the vibration problem while including the actual geometry of the cable (twist). For horizontal tight cables, Alkharisi and Heyliger [157] calculated the effective mass and stiffness components for coupled cables using constants that are driven from the three-dimensional elasticity model. Then, using that, a typical cable segment's vibration behavior was analyzed with both analytical and finite element models for homogenous and composite cable geometries for three different representative types of cables.

In this paper, the three-dimensional cable geometry is included to study its vibration characteristics using a finite element model. After solving the nonlinear static behavior which considered the self-weight and sag of the cable. Identical properties are used for the cable tested experimentally to measure the frequencies and coupled displacements. Results for the inclined cable are assessed and compared with well-known analytical model and commercial finite element software ABAQUS. New conclusions are drawn from the investigation and comparison and discussed in details.

6.3 Strand Mechanics

The focus of this paper on metallic strands which are made of a single layer of wires that have circular cross-section. The outer wires are helically twisted around a cylindrical core wire. The core wire is assumed to be a straight configuration and the number of outer wires is denoted as n_w. It is common in engineering applications to used the 1/6 cable, characterized by six outer wires (i.e. $n_w = 6$) which are wrapped around a core wire. As the primary purpose of the present paper is to compute the natural frequency and modes shapes of an inclined cable, for that it is necessary to have accurate stiffness and mass matrices that represent the actual cable cross-section details and behavior. In this section, the cable geometry is defined, stiffness matrix derivation using elasticity method approach and mass matrix are represented, and to validate this approach a known one-dimensional analytical approach is used to find the cable stiffness.

6.3.1 Strand Geometry

For simplification, the 1/6 strand wire is considered in this study as shown in Fig. 6.1. In which the cable has a central straight core and 6 outer helical wires. The helical wire is characterized by the pitch (lay) length, P, and it is the reciprocal of twist per unit length. The lay angle denoted by α is measured with respect to the axis of the cable (Z axis). The centerline of the helical wire is a helical curve of radius R_h. And it relates to the outer wire radius, and the core wire radius R_c by

$$R_h = R_c + R_w \qquad (6.1)$$

Costello [20] determined the pitch length of the strand by:

$$P = \frac{2\pi R_h}{\tan\alpha} \qquad (6.2)$$

Fig. 6.1 The six-stranded cable with a single layer (ACSR)

From that the actual lay angle of the cable given the pitch length can be found using this equation

$$\alpha_{actual} = \arctan(\frac{2\pi R_h}{P}) \qquad (6.3)$$

And the maximum lay angle of the cable used in this research can be found using [155]:

$$\alpha_{max} = \arccos\left(\sqrt{\frac{\tan^2(\frac{\pi}{2} - \frac{\pi}{n_w})}{(1+\xi_0^{-1})^2 - 1}}\right), \xi_0 = \frac{2R_w}{2R_c} < 1 \qquad (6.4)$$

A small length of the cable L_e, where the twist is included, is described by single-layer of three-dimensional continuums element. To find the effective stiffness coefficients, the actual cable geometry is used in representing its kinematic response in a three-dimensional elasticity-based model. When the cable domain is cut at this length, the front fact nodes coordinate becomes unknown, to overcome that the transformed lay angle can be computed using

$$\Theta_e = \frac{360}{(\frac{P}{L_e})} \qquad (6.5)$$

Feyrer [7] has more detialds on the cable constructions, and more insight into the geometry modeling cab be found in Lee [3].

In this work, the displacements and strains are assumed to be small, the cable has coupling behavior between axial and torsion. In addition, the lay angle variation is considered.

6.3.2 Elasticity Method and Finite Element Model Base

The differential equation of equilibrium is the governing equation in the Cartesian coordinate system of plan elasticity for shapes that are hexahedron. Which can be expressed in expanded form as

$$\frac{\partial \sigma_{XX}}{\partial X} + \frac{\partial \sigma_{YX}}{\partial Y} + \frac{\partial \sigma_{ZX}}{\partial Z} + f_X = 0$$

$$\frac{\partial \sigma_{XY}}{\partial X} + \frac{\partial \sigma_{YY}}{\partial Y} + \frac{\partial \sigma_{ZY}}{\partial Z} + f_Y = 0$$

$$\frac{\partial \sigma_{XZ}}{\partial X} + \frac{\partial \sigma_{YZ}}{\partial Y} + \frac{\partial \sigma_{ZZ}}{\partial Z} + f_Z = 0 \quad (6.6)$$

Where σ is the stress component and f is the body force in the X, Y, Z axes. The strain relation are then used while small displacement is assumed. Stress-strain relations is expressed by the generalized Hook's law of elastic stiffness tensor denoted as C_{ijkl} as

$$\sigma_{ij} = C_{ijkl}\varepsilon_{kl} \qquad (6.7)$$

As discussed by many researchers ([41], [101],[103]), for any cross-section shape and single or multi-layered cable, the constitutive equations relating the strand tension and torque to the cable deformation may be postulated to be of the generalized linear matrix:

$$\begin{Bmatrix} F_X \\ M_X \end{Bmatrix} = \begin{bmatrix} k_{\varepsilon\varepsilon} & k_{\varepsilon\theta} \\ k_{\theta\varepsilon} & k_{\theta\theta} \end{bmatrix} \begin{Bmatrix} u_{X,X} \\ \theta_{X,X} \end{Bmatrix} \qquad (6.8)$$

Where F_X represent the axial force, M_X the axial twisting moment, $u_{X,X}$ axial strain, $\theta_{X,X}$ twist per unit length. And, $k_{\varepsilon\varepsilon}$ is the axial stiffness, $k_{\varepsilon\theta}$ and $k_{\theta\varepsilon}$ are the coupling stiffnesses, they are equal to zero in case of the untwisted cable, and $k_{\theta\theta}$ is the torsional stiffness coefficients. These are all effective one-dimensional relations, and they depend on both the cable material and construction. Hence then must be a transition between the three-dimensional behavior of the cable and the effective one-dimensional relation.

Experimental results by Samras et la. [101] verified that assumed the constitutive relation are in linear form and shown that within experimental accuracy

$$k_{\varepsilon\theta} \approx k_{\theta\varepsilon} \qquad (6.9)$$

Which is compatible with Maxwell's reciprocal theorem for linear elastic structure. In many of the methods used to derive these measures in the literature, unequal values are typically averaged. In this work, using this method, the coupling coefficients differences were found to be negligible (always less than 4%).

Linear elasticity elements are in the form of hexahedron solids which are used in the finite element analysis to find the mechanical behavior of what so-called six-stranded straight wire. Each node has been given three degrees of freedom in the three directions as displacements (U), (V), and (W). To compute the stiffness terms represented in Eq. (8), two different sets of loading conditions are imposed: 1) at one end, all nodal displacements in all directions are fully clamped. The control volume other end has a unit displacement in the axial direction ($U = 1$), and other displacements are set to zero. From this set $k_{\varepsilon\varepsilon}$ and $k_{\theta\varepsilon}$ are computed from the total forces and moments required to hold this displacement. Then, 2) at one end, all node displacements are fully clamped, and other face nodal displacements in the Y and Z directions, are having an equivalent amount of value to present a unit rotation, and the displacement in X direction is set to zero.

The one-dimensional model mass matrix where the kinetic energy terms are shown can be expressed as

$$[M] = \begin{bmatrix} m_{\varepsilon\varepsilon} & m_{\varepsilon\theta} \\ m_{\theta\varepsilon} & m_{\theta\theta} \end{bmatrix} \qquad (6.10)$$

Where

$$m_{\varepsilon\varepsilon} = \int_V \rho dV \qquad (6.11)$$

$$m_{\theta\theta} = \int_V \rho r^2 dV \qquad (6.12)$$

Here the terms are dependents on the pointwise mass density ρ, r is the distance from the polar origin of the strand to any arbitrary location in the cable cross-section, and V represents the total volume. The off-diagonal terms of the mass matrix are zero.

6.3.3 One-Dimensional Analytical Model

The validity of the three-dimension elastic model presented is measured against an analytical formulation that evaluates the axial-torsional response of isotropic single-layered metical strands which has been presented by Foti and Martinelli [155]. This model fully accounts for the contraction of the helix radius of the external wires due to both the Poisson effect and the local deformation of the internal contact surface. Besides, the expressions for the terms of the stiffness matrix are compact and simple. They were shown to be accurate compared to experimental, analytical, and finite element results from the literature for only single-layered and circular cross-section cables. In this work, Foti and Martinelli's model has been replicated for identical six-stranded cable. Where the model presented in section 3.2 accounts for the Poisson effect and ignores the contact deformation.

Foti and Martinelli's cross-sectional stiffnesses of the strand are evaluated through a classic energetic approach. And, can be represented here as

$$k_{\varepsilon\varepsilon} = EA_c + \frac{n_w EA_w A^2}{\cos(\alpha)} \tag{6.13}$$

$$k_{\varepsilon\theta} = k_{\theta\varepsilon} = \frac{n_w EA_w AB}{\cos(\alpha)} \tag{6.14}$$

$$k_{\theta\theta} = \frac{EI_c}{1+\nu} + \frac{\cos(\alpha)^3 n_w EI_w}{1+\nu} + \cos(\alpha)\sin(\alpha)^2 n_w EI_w + \frac{n_w EA_w B^2}{\cos(\alpha)} \tag{6.15}$$

Where E is the modulus of elasticity, A_w is the outer wire cross-section area, A_c is the core wire cross-section area, I_c is the moment of inertia of the core wire, I_w is the moment of inertia of the outer wire, and ν is the Poisson ratio. The coefficients A and B 's resulting expressions are

$$A = \frac{\cos(\alpha)^2 - \dfrac{\nu \sin(\alpha)^2}{1+\xi_0}}{1 + \dfrac{\nu\xi_0 \sin(\alpha)^2}{1+\xi_0} + \dfrac{2(1-\nu^2)\xi_0{}^2\bar{C}_{n0}\sin(\alpha)^4}{(1+\xi_0)(1+\xi_0(1-\sin(\alpha)^2))}} \qquad (6.16)$$

$$B = \frac{\sin(\alpha)\cos(\alpha)R_h}{1 + \dfrac{\nu\xi_0 \sin(\alpha)^2}{1+\xi_0} + \dfrac{2(1-\nu^2)\xi_0{}^2\bar{C}_{n0}\sin(\alpha)^4}{(1+\xi_0)(1+\xi_0(1-\sin(\alpha)^2))}} \qquad (6.17)$$

Here $\bar{C}_{n0}$ is the value of the non-dimensional normal contact compliance and considered as a parameter of this model.

6.4 Vibration Analysis

For finding the dynamic behavior of inclined twisted cable, many methods are used in this study. First, it involves a computational routine that uses the finite element method. Second, analytical models from the literature are mainly used for horizontal cables. Third, using the standard finite element software ABAQUS [159]. Fourth, using large-scale experiments. These are used to study in detail the natural frequency and corresponding modal shapes and are described below.

6.4.1 Finite Element Model

The sagged twisted cable is represented as a series of one-dimension finite elements which have linear elastic properties. Each nodal point has six degrees of freedom. The stiffness, mass matrices (from the previous section), the translation and rotation at each nodal point are given in terms of the global coordinate system. At this stage the inclination angle of the cable is introduced, and in this study the inclination denoted as ϕ is between 10 and 60 degrees. The equation of motion is derived which is based on small dynamics perturbation about the deformed static equilibrium that is caused by the cable self-weight. Prior the free vibration the parabolic static configuration include initial sag of the cable and the boundary conditions as presented in Fig. 6.2. After the assembly the cable stiffness is updated and the sag at its final shape the standard linear eigenproblem is solved using

$$([K_t] - \omega^2 [M]) \begin{Bmatrix} U_X \\ U_Y \\ U_Z \\ \theta_X \\ \theta_Y \\ \theta_Z \end{Bmatrix} = 0 \qquad (6.18)$$

Where $[K_t]$ and $[M]$ are the $N \times N$ assembled global stiffness and mass matrices of the cable structure. The stiffness matrix is the summation of the elastic stiffness matrix $[K^e]$ and geometric matrix $[K^g]$. The natural frequency is denoted as ω and as f in Hz. The global translations displacements are U_X, U_Y, and U_Z, and rotations displacements are θ_X, θ_Y, and θ_Z in the X, Y, and Z directions. The boundary conditions for the cable system, where one of its ends is higher than the other in the Y direction, is corresponding to pinned-pinned condition.

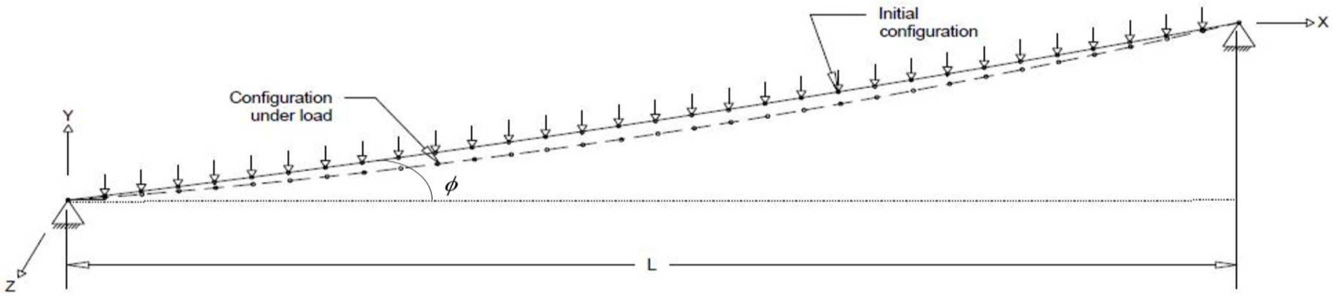

Fig. 6.2 Inclined cable configuration before and after self-weight load given the inclination angle

The local elastic stiffness matrix which its coefficients are derived in section 6.3 is the modified version of the conventional symmetric truss member. Here the stiffness include the axial, torsional, and coupling terms and defined as

$$\left[k^e\right]=\begin{bmatrix} \frac{k_{\varepsilon\varepsilon}}{L_e} & 0 & 0 & \frac{k_{\varepsilon\theta}}{L_e} & 0 & 0 & -\frac{k_{\varepsilon\varepsilon}}{L_e} & 0 & 0 & -\frac{k_{\varepsilon\theta}}{L_e} & 0 & 0 \\ 0 & 0 & 0 & 0 & 0 & 0 & 0 & 0 & 0 & 0 & 0 & 0 \\ 0 & 0 & 0 & 0 & 0 & 0 & 0 & 0 & 0 & 0 & 0 & 0 \\ \frac{k_{\theta\varepsilon}}{L_e} & 0 & 0 & \frac{k_{\theta\theta}}{L_e} & 0 & 0 & -\frac{k_{\theta\varepsilon}}{L_e} & 0 & 0 & -\frac{k_{\theta\theta}}{L_e} & 0 & 0 \\ 0 & 0 & 0 & 0 & 0 & 0 & 0 & 0 & 0 & 0 & 0 & 0 \\ 0 & 0 & 0 & 0 & 0 & 0 & 0 & 0 & 0 & 0 & 0 & 0 \\ -\frac{k_{\varepsilon\varepsilon}}{L_e} & 0 & 0 & -\frac{k_{\varepsilon\theta}}{L_e} & 0 & 0 & \frac{k_{\varepsilon\varepsilon}}{L_e} & 0 & 0 & \frac{k_{\varepsilon\theta}}{L_e} & 0 & 0 \\ 0 & 0 & 0 & 0 & 0 & 0 & 0 & 0 & 0 & 0 & 0 & 0 \\ 0 & 0 & 0 & 0 & 0 & 0 & 0 & 0 & 0 & 0 & 0 & 0 \\ -\frac{k_{\theta\varepsilon}}{L_e} & 0 & 0 & -\frac{k_{\theta\theta}}{L_e} & 0 & 0 & \frac{k_{\theta\varepsilon}}{L_e} & 0 & 0 & \frac{k_{\theta\theta}}{L_e} & 0 & 0 \\ 0 & 0 & 0 & 0 & 0 & 0 & 0 & 0 & 0 & 0 & 0 & 0 \\ 0 & 0 & 0 & 0 & 0 & 0 & 0 & 0 & 0 & 0 & 0 & 0 \end{bmatrix} \quad (6.19)$$

Where L_e is the updated element length after the initial nonlinear state deformation.

In this study, the case of uncoupled cable is also solved. For that, the axial stiffness is simply $k_{\varepsilon\varepsilon} = EA$, the coupling stiffnesses are $k_{\varepsilon\theta} = k_{\theta\varepsilon} = 0$, and the torsional stiffness is $k_{\theta\theta} = GJ$.

The geometric stiffness matrix is related to the forces which are employed by the stressed element associated with the direction changes of the cable element when deformed. This stiffness can be described in the local coordinate system as

$$\left[k^{g}\right] = \frac{F_a}{L_e}\begin{bmatrix} I & O & -I & O \\ O & O & O & O \\ -I & O & I & O \\ O & O & O & O \end{bmatrix} \quad (6.20)$$

Here F_a is the axial force at the start of each incremental step and I is a 3×3 unit matrix while O is a 3×3 null matrix.

The mass matrix is also discretized over the cable domain. The mass terms defined earlier are then used. The local mass matrix is defined as

$$[m] = \frac{L_e}{6}\begin{bmatrix} 2m_{\varepsilon\varepsilon}I & O & m_{\varepsilon\varepsilon}I & O \\ O & 2m_{\theta\theta}I & O & m_{\theta\theta}I \\ m_{\varepsilon\varepsilon}I & O & 2m_{\varepsilon\varepsilon}I & O \\ O & m_{\theta\theta}I & O & 2m_{\theta\theta}I \end{bmatrix} \quad (6.21)$$

All the defined matrices here are mapped to the global coordinate system using a transformation matrix similar to typical structural elements. The inclined cable elements involve cosines in the three local directions. The element is then oriented in the global three-dimensions using these angles. After that, the free vibration problem then solved using Eq. (6.18).

6.4.2 *Analytical Model*

The finite element model accuracy and applicability is tested against the well-known Irvine and Caughey [80] linear vibration theory for horizontal cables ($\phi = 0$). In their work, they calculated the out-of-plane, symmetric in-plane, and anti-symmetric in-plane frequencies using

$$f_o = \frac{1}{2\pi}\sqrt{\frac{H}{m}} \quad (6.22)$$

$$f_s = \sqrt{\frac{\beta_i^2 H}{m}} \quad (6.23)$$

$$f_{an} = \frac{2}{2\pi}\sqrt{\frac{H}{m}} \quad (6.24)$$

Where H is the horizontal component of the cable tension, and β_i value can be calculated from a transcendental equation.

The axial and torsional frequencies for the case of the cable is assumed to be straight and have a solid circular section under axial and torsional vibration and are also compared with the finite element model, and these are found using [130]

$$f_a = \frac{1}{2L}\sqrt{\frac{E}{\rho}} \quad (6.25)$$

$$f_t = \frac{1}{2L}\sqrt{\frac{G}{\rho}} \quad (6.26)$$

6.4.3 *ABAQUS*

The inclined cable in this study is modeled using the commercial finite element program, ABAQUS [159]. The initial configuration is given in the X, Y plane as in Fig. 6.2. To stabilize the cable, an additional node in the Y direction was used and connected using truss elements. The additional elements are given a very small stiffness value. By applying the boundary condition where the translation displacements are fixed, the given initial small sag will increase under the nonlinear static analysis where the self-weight of the cable is considered. The cable will be in equilibrium, having a parabolic shape. The undamped free vibration will then be solved for the cable models where the inclination angle ϕ varied between 10 and 60 degrees. In the ABAQUS model, the twist configurations are not included, and the cable cross-section is assumed to be circular. This software lacks the ability to include the torsional and axial-torsional coupling terms in the cable element.

6.4.4 Experimental Model

The frequency spectrum of inclined cable hanging where its endpoints are different in the Y direction is studied using series of experiments. The focus of these tests is on the out-of-plane, symmetric in-plane, and anti-symmetric in-plane frequencies. The same length in the other approaches is also used to study the behavior. The experimental setup overview is shown in Fig. 6.3. At one end, a MTS's 243.20 hydraulic actuator [127] is used, which can simulate a harmonically time-varying support motion in the Y direction. This actuator has a stroke length of 25.4 cm and is driven by a power control unit, which is MTS 407 controller [128], that is able to generate a repeated driving motion that is controllable by a frequency. The other end is used to fix the lower point of the inclined cable using a c-clamp.

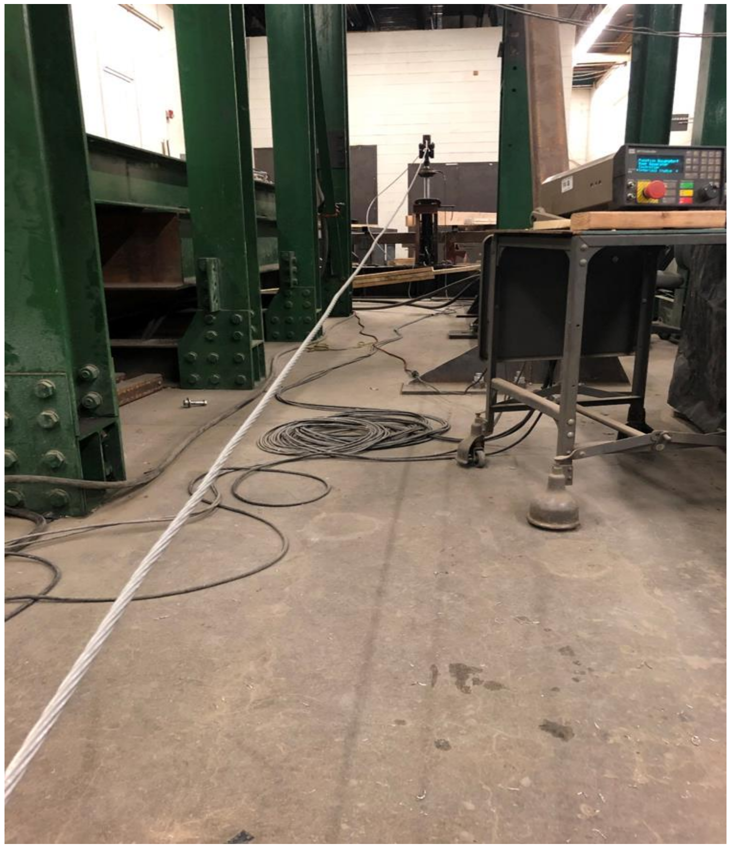

Fig. 6.3 Experimental setup for the twisted inclined cable study with the actuator at the far end

Each test (frequency) is repeated 20 times to minimize the errors. A MetaTracker sensor Fig. 6.4 [129] was used to obtain the dynamic data. This device contains an accelerometer and gyroscope that can give the acceleration time history signal $\ddot{U}_X, \ddot{U}_Y$, and $\ddot{U}_Z$ which are longitudinal, vertical, and transverse motions which are parallel to X, Y, Z axes, respectively. And, give the angular velocity time history signal in the three-axis as well: $\dot{\theta}_X, \dot{\theta}_Y$, and $\dot{\theta}_Z$. Two points on the span were the interest, mid-span and quarter span, for that, two sensors were used for all tests.

Fig. 6.4 Sensor mountain on the inclined cable

The acquisition duration for each reading ranged from 20 to 45 seconds, and the sampling frequency for the measured accelerations is $f_{s-acceleration} = 12.5$ Hz and $f_{s-angular-velocity} = 20$ Hz for the angular velocity. In dynamic experiments, acquisition rate plays an important role, if it is not fast enough the results may not results the correct dynamic response of the system tested [165]. The natural frequency of the inclined cable studied in this paper was obtained by recording the frequency when a response peak was observed. To use the data results, each history signal's frequency was found using the Fast Fourier Transform algorithm function. The translation and rotation displacements are found by integrating, for instance, for the longitudinal direction:

$$U_X = -\frac{\ddot{U}_{X-data}}{\omega^2} \sin(\omega t) \qquad (6.27)$$

$$\theta_X = -\frac{\dot{\theta}_{X-data}}{\omega} \sin(\omega t) \qquad (6.28)$$

Similarity for U_Y, U_Z, θ_Y, and θ_Z for peak displacement motions

6.5 Results and Discussion

With the solution model that considered Poisson's ratio and difference lay angles values, the six-stranded cable's stiffness matrix subjected to axial tension and torsion is studied. In addition to the mass matrix, which are the functions of finding the natural frequency and modal shapes of the inclined sagged cable. The parameters used for the cable, which is an Aluminum Conductor Steel Reinforced cable (ACSR) as follows: weight $m = 0.35\ \mathrm{kg/m}$, a modulus of elasticity of $E = 74.2\ \mathrm{GPa}$, shear modulus $G = 37.1\ \mathrm{GPa}$, $R_c = 2.25\ \mathrm{mm}$, $R_w = 2\ \mathrm{mm}$ for a total cross-section area of $A = 91.3\ \mathrm{mm}^2$, and Poisson ratio $\nu = 0.3$ [166]. The lay angle α is between 0 to 30 degrees. And, the inclination angle ϕ is between 10 to 60 degrees. Throughout the four approaches used here, the cable length is $L = 8.07\ \mathrm{m}$, and the small sag value is $d = 2\ \mathrm{cm}$. The results are presented in this section.

6.5.1 Lay Angle Effect on Stiffness Matrix

The stiffness coefficients obtained using the three-dimensional elasticity finite element model where the Poisson effect is included for straight twisted cable are compared to the one-dimensional analytical model where in addition to the Poisson ratio, the internal contact deformation is included. The lay angle α varied in this work between 0 and 30 degrees for this twisted cable which is the practical range commonly used. These coefficients are important and reflect the mechanical performance of the strand that is subjected to axial loads. The strand can break if the stiffness is too small. However, the large stiffness does not efficiently suppress the oscillation caused by the impact force applied in the strand [33]. In this study, both methods used to calculate the stiffnesses are obtained in which a small axial extensile strain and small axial torsional strain are respectively applied to the strand. The comparison between stiffness matrices obtained using the present model and those of Foti and Martinelli [155] are given in Fig. 6.6-Fig. 6.8. And, non-dimensional values in the figures are defined as

$$\bar{k}_{\varepsilon\varepsilon} = \frac{k_{\varepsilon\varepsilon}}{E\pi R_h^2}$$

$$\bar{k}_{\varepsilon\theta} = \frac{k_{\varepsilon\theta}}{E\pi R_h^3}$$

$$\bar{k}_{\theta\varepsilon} = \frac{k_{\theta\varepsilon}}{E\pi R_h^3}$$

$$\bar{k}_{\theta\theta} = \frac{k_{\theta\theta}}{E\pi R_h^4} \quad (6.29)$$

The actual lay angle for this particular cable is $\alpha_{actual} = 8$ degrees, while the maximum angle it can reach given the pitch length ($P = 190$ mm, see Fig. 6.5) is $\alpha_{max} = 22.5$ degrees.

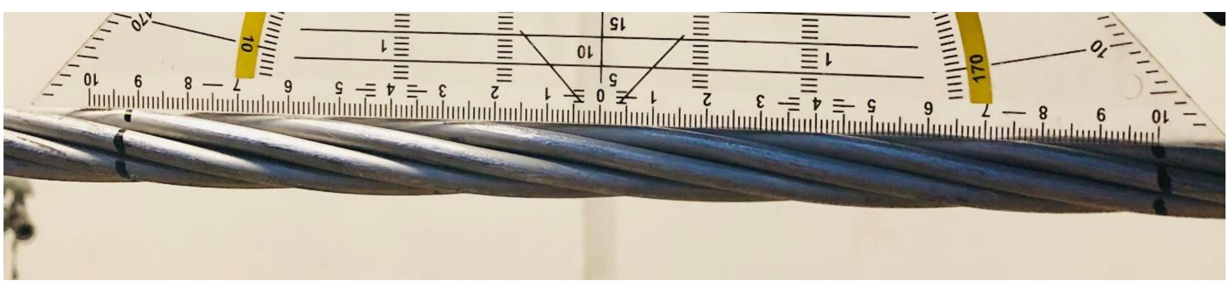

Fig. 6.5 The cable pitch length found to be 190 mm from the outer wire which takes a full turn around the circular core wire

The axial stiffness $\bar{k}_{\varepsilon\varepsilon}$ versus lay angle α for the three-dimensional elasticity finite element model and the one-dimensional analytical model for the considered twisted cable are shown in Fig. 6.6. Both stiffnesses results decrease with lay angle increase. The present finite element results are slightly lower by approximately 1.45% when the lay angle is less than 20 degrees. The results then coincide at this point. And, when the lay angle is larger than 20 degrees, the finite element results become slightly higher than those of Foti and Martinelli model by 2.92%.

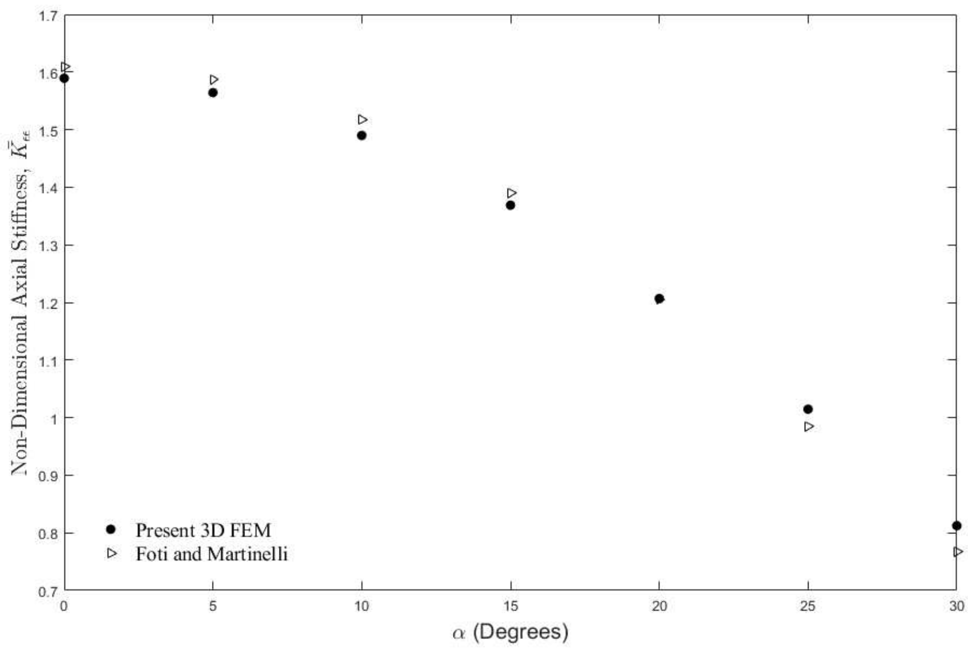

Fig. 6.6 Axial stiffness $\bar{k}_{\varepsilon\varepsilon}$ for cable used (ACSR) versus lay angle α for the present 3D FEM and comparative one-dimensional analytical model of Foti and Martinelli [155]

The non-dimensional coupling coefficients $\bar{k}_{\varepsilon\theta}$ and $\bar{k}_{\theta\varepsilon}$ variation with the lay angles are presented in Fig. 6.7. The present model appeared to give excellent results with the one-dimensional model for lay angles below 15 degrees. It is approximately linearly increasing with about 18-25% rate for every 5 degrees. While the one-dimensional model approaches to stable value at a large lay angle (20 degrees) and which is close to the maximum lay angle, then start to decrease.

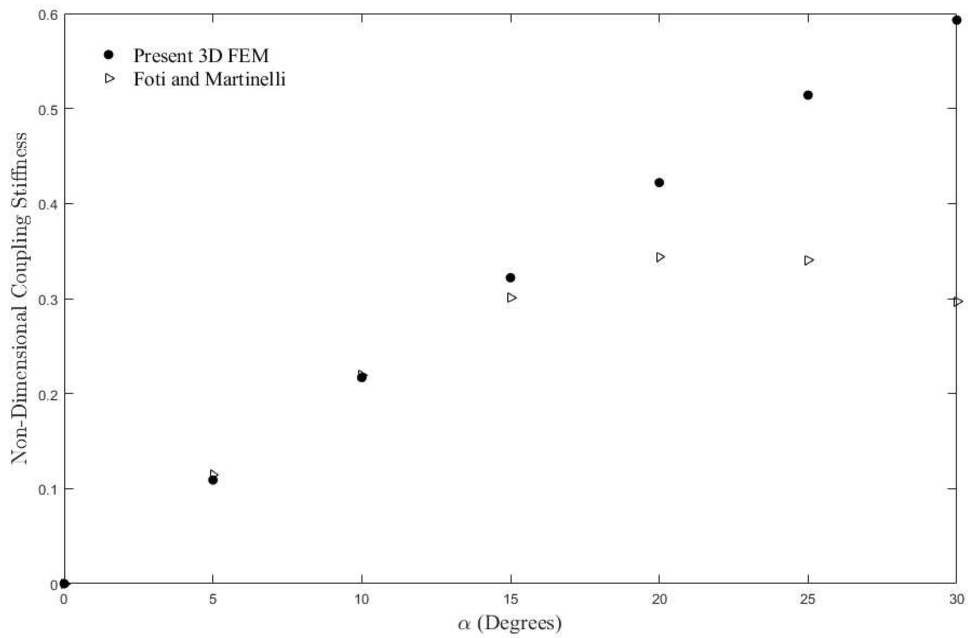

Fig. 6.7 Coupling stiffness $\overline{k}_{\varepsilon\theta}$ and $\overline{k}_{\theta\varepsilon}$ for cable used (ACSR) versus lay angle α for the present 3D FEM and comparative one-dimensional analytical model of Foti and Martinelli [155]

Figure 6.8 shows the non-dimensional torsional coefficients $\overline{k}_{\theta\theta}$ versus lay angle. The stiffnesses results increase with lay angle increase. The present three-dimensional finite element model is behaving similarly to the axial stiffness results. It is lower by about 8.4-15% than the one-dimensional analytical model for angles below 20 degrees. While it is higher by 9.4-23.5% for angles after 20 degrees. The increasing rate in Foti and Martinelli model decreases after this point (20 degrees) from 23% to be 15%.

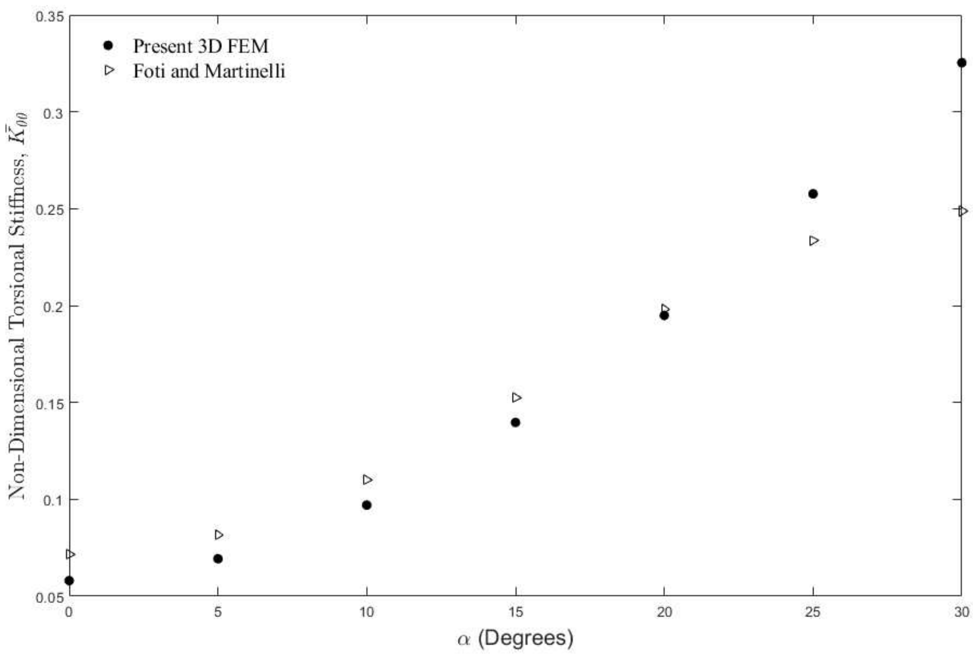

Fig. 6.8 Torsional stiffness $\bar{k}_{\theta\theta}$ for cable used (ACSR) versus lay angle α for the present 3D FEM and comparative one-dimensional analytical model of Foti and Martinelli [155]

The results showed that the three-dimensional elasticity finite element model is accurate in predicting the stiffness coefficients. The model gives excellent results for the actual lay angle ($\alpha_{actual} = 8$ degrees) and generally good results near the maximum angle ($\alpha_{max} = 22.5$ degrees) of the cable used. The significant difference between the two models is observed at large lay angles. This difference is attributed to the fact that the internal contact deformation can lead to a smaller cross-section and further weaken the stiffness terms of the strand.

The vibration analysis was done for the same cable, where only the actual lay angle is used. In addition, Meng et al. [33] stated that even though the deformation effect on the stiffness matrix depends on the lay angle, it can precisely evaluate a small lay angle strand while ignoring the contact deformation.

6.5.2 *Inclination Angle Effect on Natural Frequency*

The finite element model used the derived effective stiffness and mass matrices to find the natural frequency of the inclined sagged cable that is in equilibrium state after the nonlinear static analysis done using the initial parabolic configuration (Eq. (6.18)). This model used the actual cross-section of the cable (twist) and is compared with the results obtained experimentally for the same cable material and geometry. In addition to the frequency spectrum found using the limited analytical solution as well as using ABAQUS.

The actual lay angles α_{actual} for cable is used (8 degrees) to describe the coupled cable in the finite element model, where 16 elements were utilized. To test the validity of the model, the inclination angle was first set to zero (horizontal cable) and the twisted of the cable was ignored (assumed circular cross-section) so the cable is uncoupled, and results are compared to the well-known Irvine and Caughey [80] model and straight circular section analytical solutions.

The frequencies results are shown in Table 6.1. The comparison showed that all the out-of-plane, symmetric in-plane, anti-symmetric in-plane, axial, and torsional frequencies have less 0.45% error. Which indicate that the present finite element model is very accurate and effective in finding the frequencies.

Table 6.1 The natural frequencies using finite element model and analytical models for uncoupled cable

	Frequency $f(\text{Hz})$		
	Irvine and Caughey	Circular Section	Present Finite Element Model
Out-of-Plane	2.514	-	2.515
In-plane symmetric	4.232	-	4.242
In-plane anti-symmetric	5.0350	-	5.020
Axial	-	267.520	267.902
Torsional	-	189.165	189.543

The cable is then inclined, and the results from the present finite element model are then compared with those obtained experimentally from 20 tests (see Fig. 6.9), where the data were analyzed using box plot and from that the median values are used, and from the ABAQUS model, for cable with an inclination angle is $\phi = 10$ degrees. First, the finite element model results found for uncoupled and then coupled inclined cable case (where twisted and the Poisson ratio is considered). The comparison presented in Table 6.2 shows that for uncoupled case the results are within 1.22% error of the ABAQUS model where the twist was also not considered. However, the present finite element model has more advantages where it was able to find the axial and torsional frequencies. The frequencies for $\phi = 10$ degrees decrease by about 4% from when the cable is horizontal (from Table 6.1).

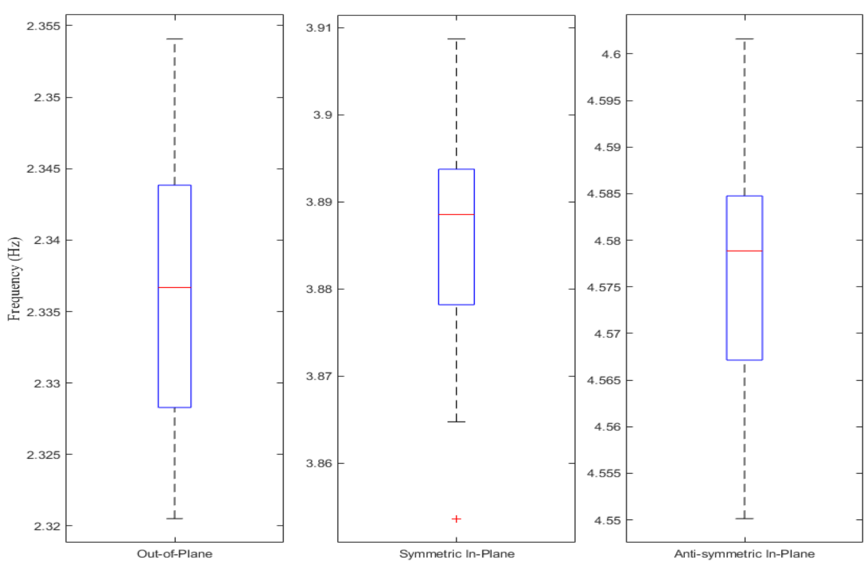

Fig. 6.9 Frequencies obtained experimentally for cable with 10 degrees inclination angle

Then the coupled finite element results are compared with the experimental results for the identical cable properties. It showed that the finite element frequencies results are higher by approximately 2.68%. And when axial and torsional frequencies are tested against the uncoupled case (using the finite element model), it showed that they are lower by 21.21% and 7.20%, respectively, due to using the actual cross-section confirmation and Poisson ratio.

Table 6.2 The natural frequencies using finite element model, experimental model, and ABAQUS model for cable with 10 degrees inclination angle

	Frequency f (Hz)			
	ABAQUS	Present Finite Element Model (uncoupled)	Experimental (median)	Present Finite Element Model (coupled)
Out-of-Plane	2.453	2.454	2.336	2.379
In-plane symmetric	4.176	4.169	3.888	3.969
In-plane anti-symmetric	4.881	4.820	4.5789	4.706
Axial	-	263.731	-	211.067
Torsional	-	186.593	-	175.891

Further, the effect of inclination angle ϕ was also studied using the present finite element (for twisted cable) and ABAQUS models. The out-of-plane, symmetric in-plane, anti-symmetric in-plane, axial, and torsional frequencies variation were found for cables between 10 to 60 degrees inclination angle. The results are shown in Table 6.3. Both models give frequencies that decrease with the inclination angle increase, which showed that it dependents on the inclination angle and the cordwise static cable tension. The out-of-plane frequency gradually decreases with an approximate rate of 6.44% for each inclination angle; the difference in magnitude is 59.88% less between 10 and the maximum angle tested (60 degrees). Similar decreasing rate is for the symmetric and anti-symmetric in-plane frequencies. The axial and torsional frequencies have a decreasing rate of about 4.75% for each angle used. The ABAQUS gave the same percentages for the out-of-plane, symmetric, and anti-symmetric in-plane frequencies; however, the model is not able to retrieve the axial and torsional frequencies.

Table 6.3 The natural frequencies using the present finite element model (FE), and ABAQUS model for cable with inclination angle between 10 and 60

	Frequency f (Hz)											
ϕ (degrees)	10		20		30		40		50		60	
	FE	ABAQUS	FE	ABAQUS	FE	ABAQUS	FE	ABAQUS	FE	ABAQUS	FE	ABAQUS
Out-of-Plane	2.379	2.453	2.225	2.304	1.988	2.066	1.689	1.755	1.336	1.389	0.954	0.993
In-plane symmetric	3.969	4.176	3.772	3.927	3.421	3.522	2.931	2.989	2.342	2.3656	1.675	1.692
In-plane anti-symmetric	4.706	4.881	4.418	4.585	3.975	4.112	3.388	3.493	2.679	2.7651	1.923	1.978
Axial	211.067	-	201.025	-	184.102	-	159.749	-	128.061	-	91.756	-
Torsional	175.891	-	167.623	-	154.122	-	135.805	-	113.295	-	87.230	-

6.5.3 Modal Shapes of the Inclined Cable

To study the interaction between the modes, the out-of-plane, symmetric in-plane, anti-symmetric in plane, axial, and torsional modals shapes were investigated using the finite element model and experiments data for sagged twisted inclined cable (coupled with lay angle 8 degrees, and have 10 degrees inclination angle). In addition, sagged untwisted horizontal cable (uncoupled and inclination angle is zero) is also solved using the finite element model and presented to have a base and observe the differences. The translational and rotation displacements that are denoted as U_X, U_Y, U_Z , θ_X, θ_Y, and θ_Z show the coupled motion for each type. Each modal plot for both approaches is normalized to the primary peak translation or rotation displacement. The inclined cable's ($\phi = 10$) experimental results in the mid and quarter span of the cable are shown as the median of 20 tests done for each modal type. To analyze the data, a box plot was used to visualize the range, distribution, and central tendency of the distribution of the data, in order to show variability and concentration of the displacement values within a distribution (the median is indicated by a line across the box).

Figure 6.10 shows the out-of-plane frequency amplitudes in the three directions. Comparing the finite element model results for the horizontal and inclined cable shows that when $\phi = 0$ the rotation displacements are equal to zero because the cable is assumed to be untwisted. Moreover, the horizontal and inclined results showed that the coupled longitudinal and vertical translation displacements have small magnitude and are different in shape. The inclined experimental results from Fig. 6.11 (median) are following the general inclined finite element model modes trends. The maximum rotation displacement is in the X direction where the experimental result at quarter-span is higher by 50.78%, and it is largest at the lower end support.

The vertical and transversal rotation displacements results at mid-span are lower than the experimental results by approximately 25%, however, they are small in magnitude comparing with the longitudinal rotation. It should be noted that all the inclined cable coupled translation and rotation displacements are not symmetric about the mid-span.

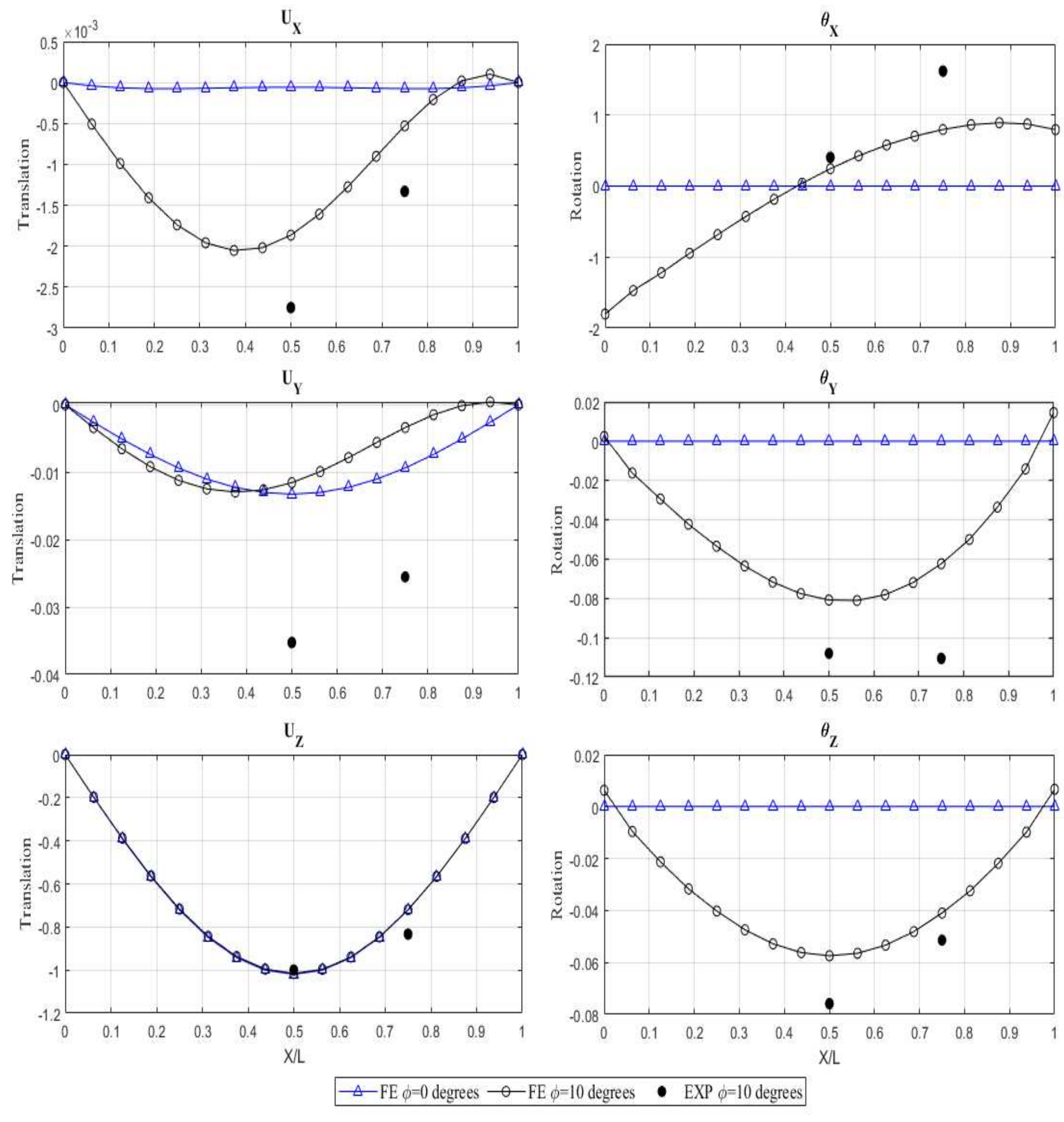

Fig. 6.10 The out-of-plane modal shapes displacements for horizontal cable (inclination angle zero), inclined cable (inclination angle 10) using the present finite element model (FE) and experimental results (EXP) for inclined cable (inclination angle 10)

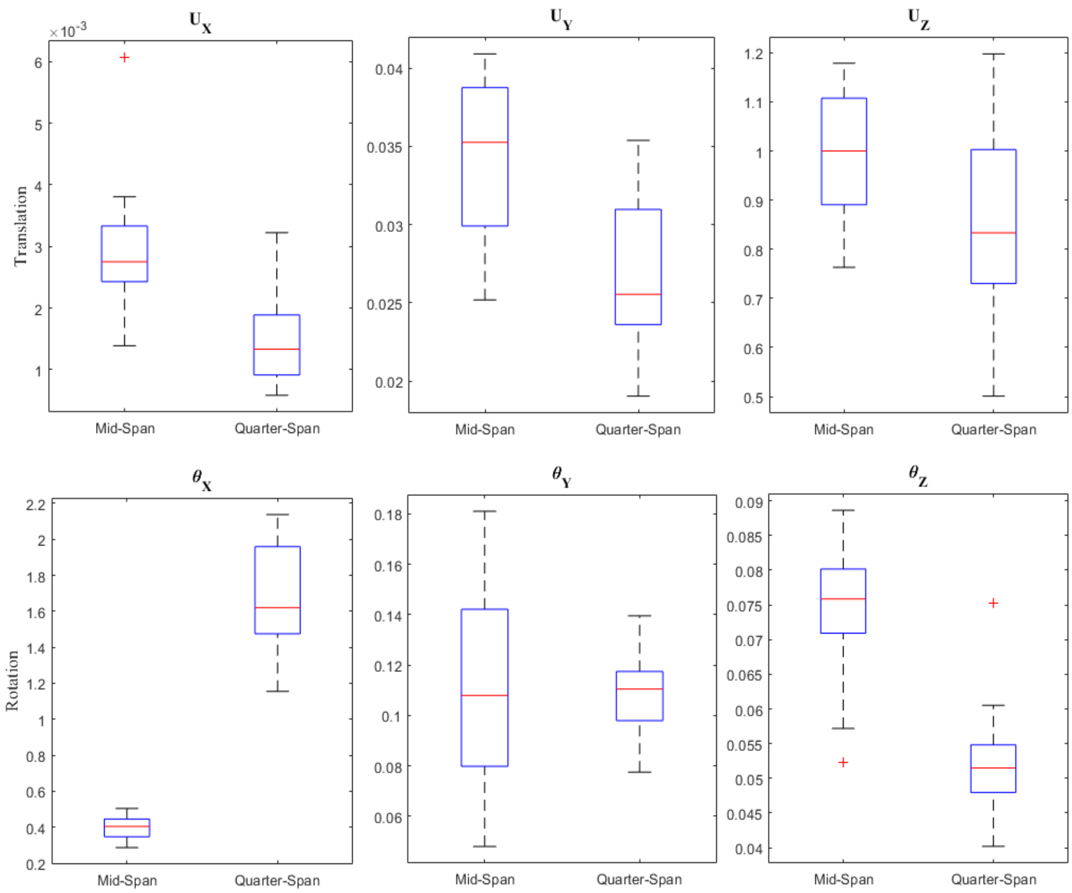

Fig. 6.11 The out-of-plane translation and rotation displacements data distribution at mid and quarter span of the cable found experimentally for the inclined cable (results are normalized to the median value of the primary motion)

The modal interactions of the symmetric in-plane frequency are showing in Fig. 6.12. The longitudinal and vertical translation displacements features of the horizontal cable are in accordance with the linear vibration theory presented by Irvine and Caughey [80]. However, the inclined cables results using the finite element model for these modes and the transversal translation have a symmetrical shape about the cable's mid-span. The longitudinal rotation displacement is maximum at the support, with 2.26 unit per a unit vertical translation, and the experimental results at quarter-span are higher by 61.43% and are shown as the median values of Fig. 6.13. And, the vertical and transversal rotation displacements are lower in magnitude at the inclined cable's higher endpoint by 80.34% and 96.54% than the rotation in the X direction, respectively.

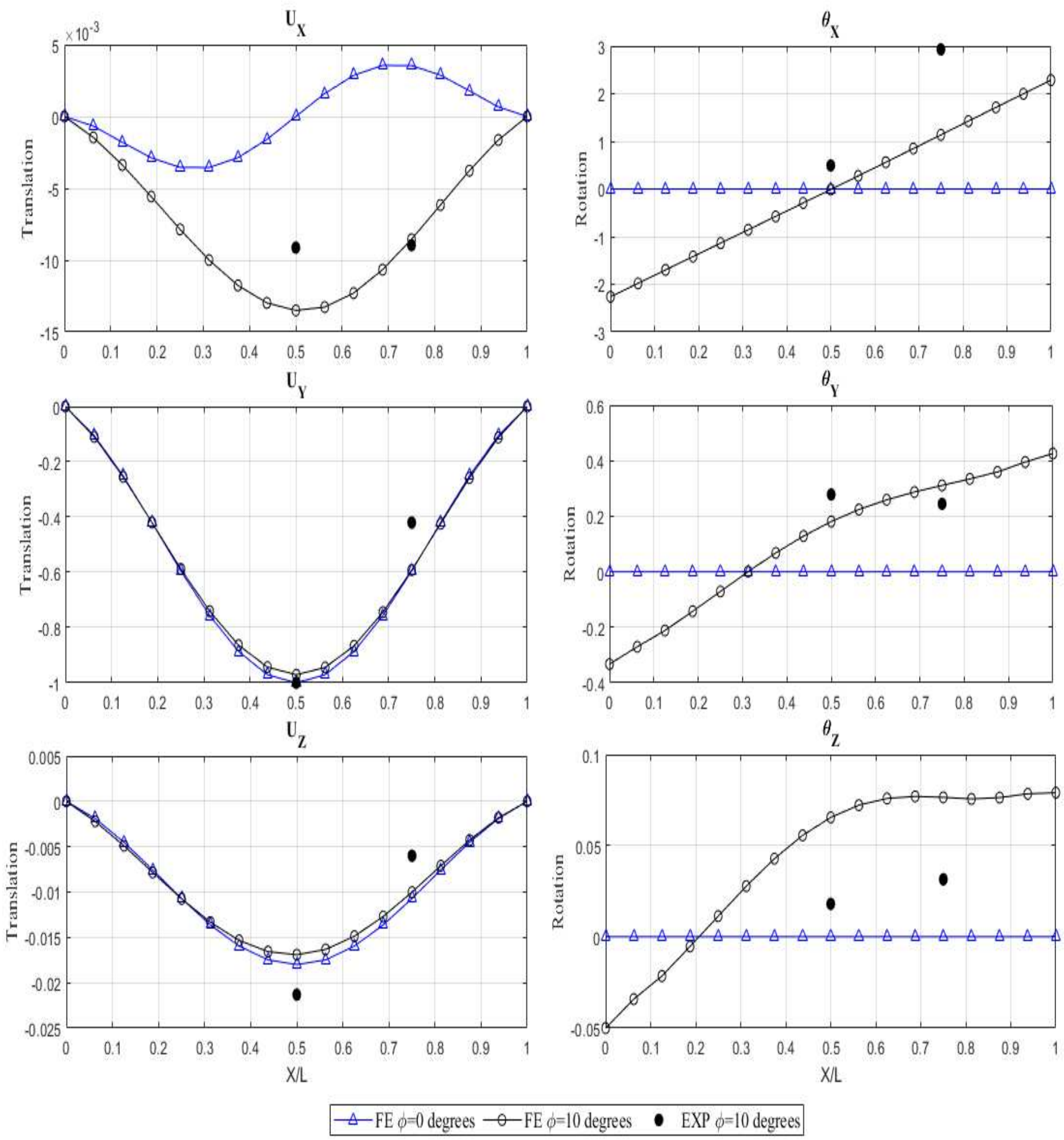

Fig. 6.12 The symmetric in-plane modal shapes displacements for horizontal cable (inclination angle zero), inclined cable (inclination angle 10) using the present finite element model (FE) and experimental results (EXP) for inclined cable (inclination angle 10)

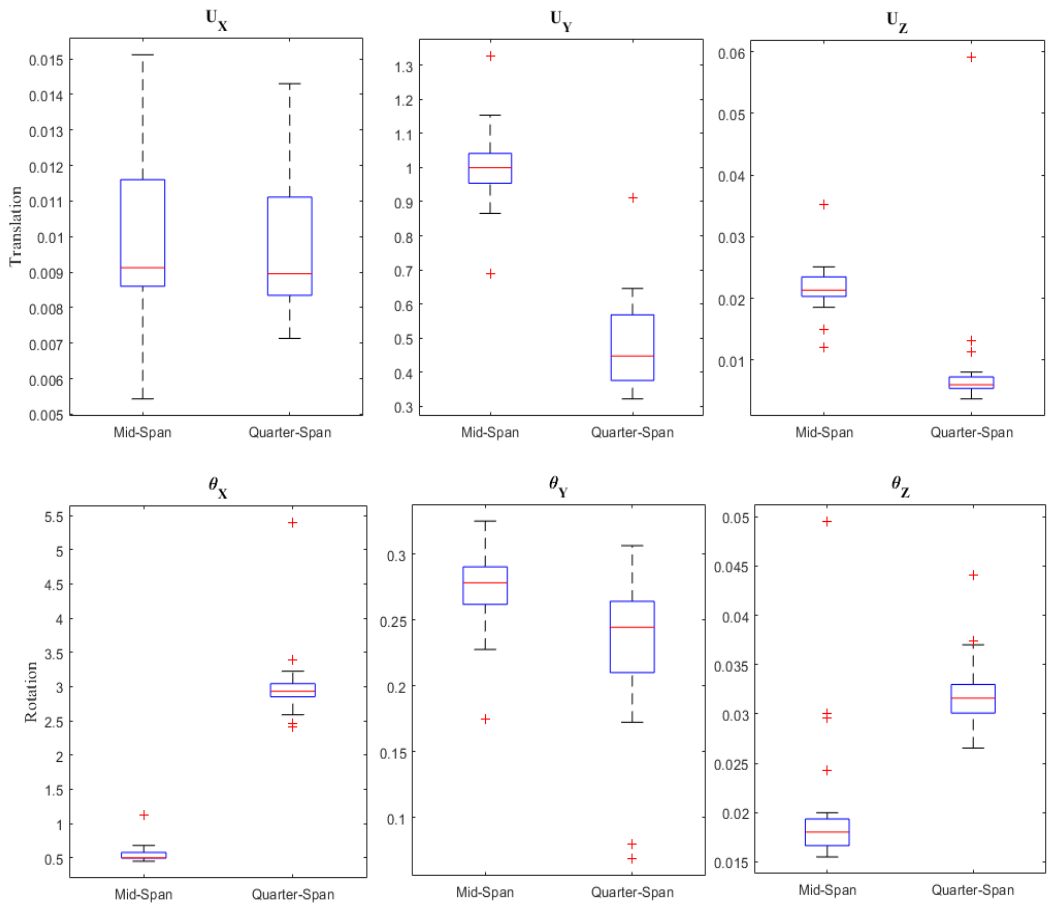

Figure 6.13 The symmetric in-plane translation and rotation displacements data distribution at mid and quarter span of the cable found experimentally for the inclined cable (results are normalized to the median value of the primary motion)

The coupled displacement with the primary anti-symmetric in-plane is observed and shown in Fig. 6.14. The finite element model results showed that the inclined cable translation displacements differ in shape in the longitudinal direction with similar magnitude, while it is largest by 60% in the transversal direction where the cable has 10 degrees inclination angle. The experimental results obtained for that are inbound with the finite element model for inclined cable, see Fig. 6.15. In addition, the mode shapes in all directions are not symmetrical about the mid-span of the inclined cable. The coupled rotation displacement is large in the X direction, and it is higher than the experimental results by 61.72% at quarter-span. Moreover, the vertical and transversal rotation displacements has a anti-symmetrical shape with smaller magnitude comparing with the large rotation found.

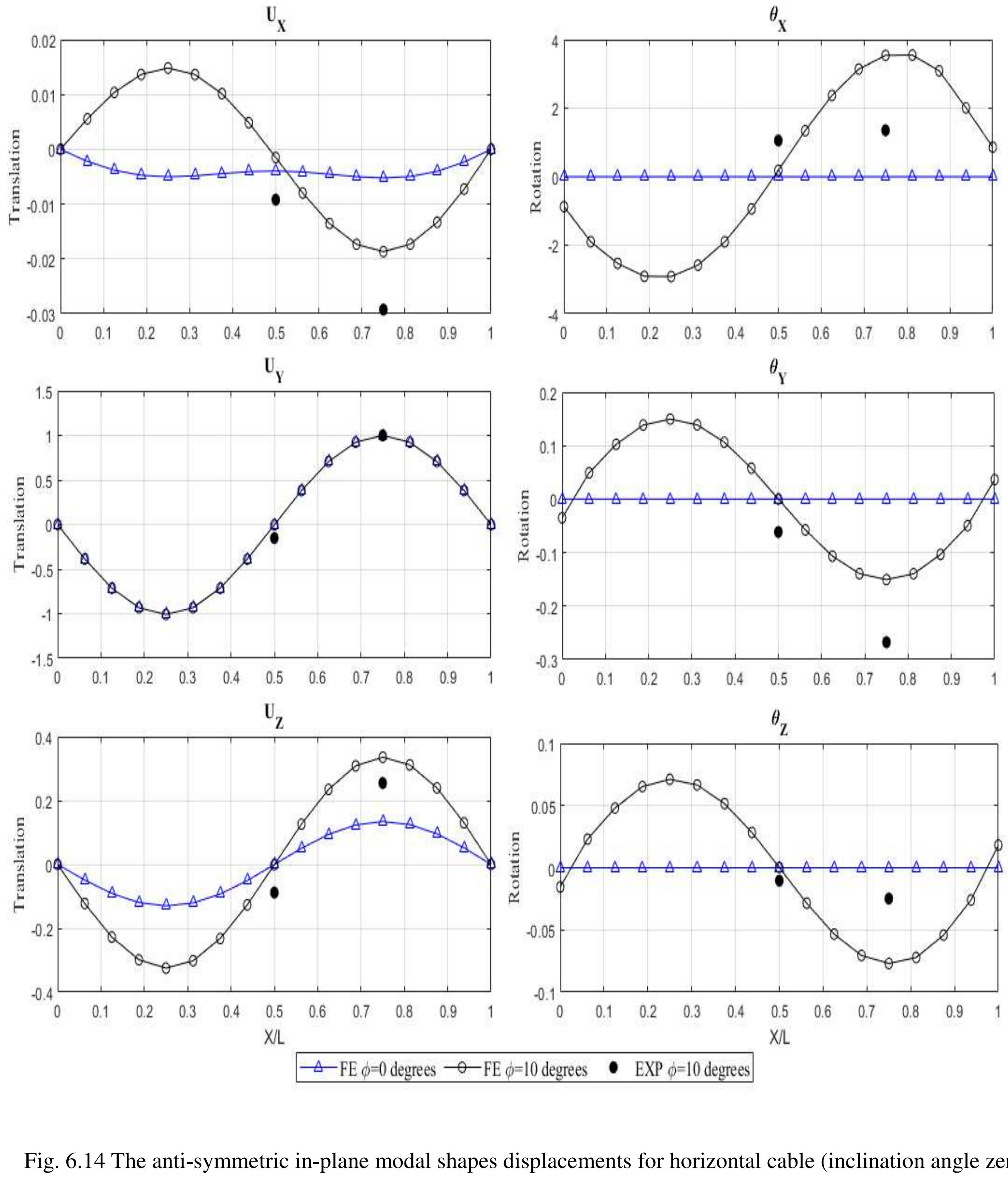

Fig. 6.14 The anti-symmetric in-plane modal shapes displacements for horizontal cable (inclination angle zero), inclined cable (inclination angle 10) using the present finite element model (FE) and experimental results (EXP) for inclined cable (inclination angle 10)

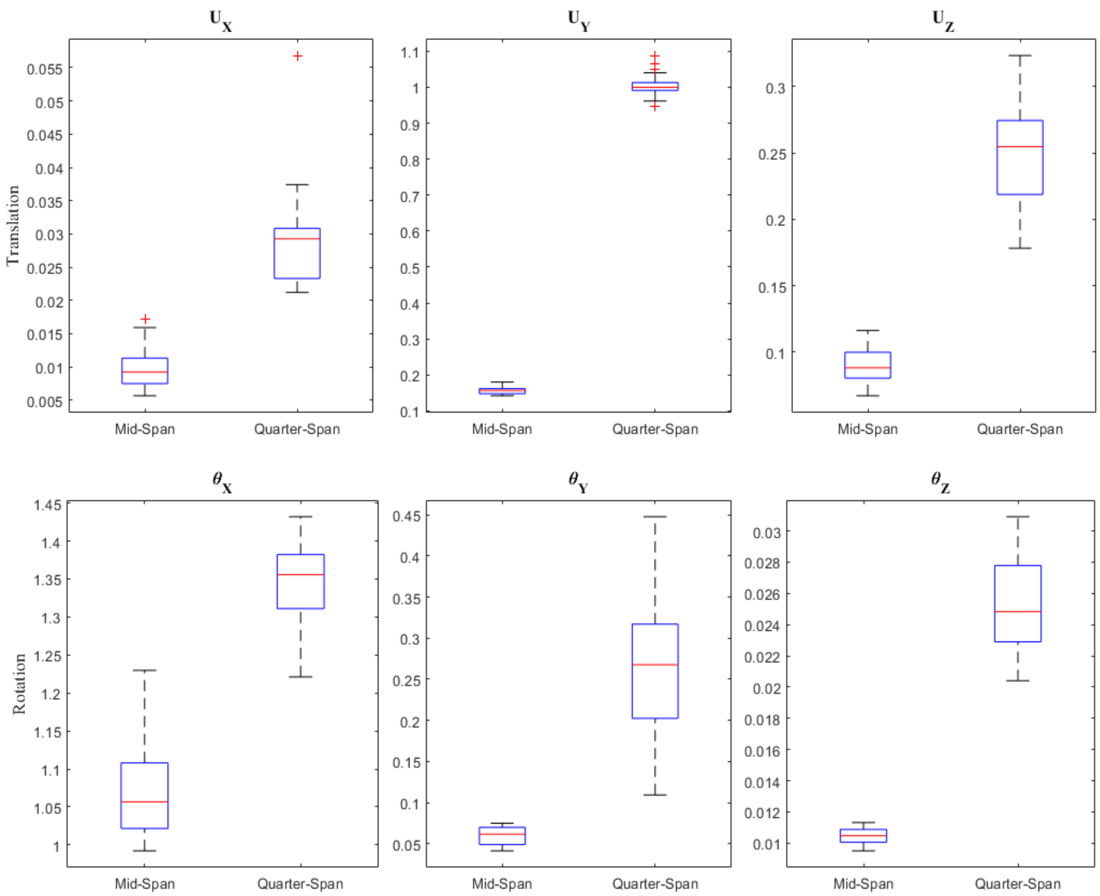

Fig. 6.15 The anti-symmetric in-plane translation and rotation displacements data distribution at mid and quarter span of the cable found experimentally for the inclined cable (results are normalized to the median value of the primary motion)

The axial frequency modal shape is presented in Fig. 6.16. The modes here are computed using the finite element model and normalized to the longitudinal translation. It is observed that the rotation displacements for the uncoupled horizontal cable are all equal to zero. However, for both uncoupled and coupled cable, the interactions captured in the translations displacement are small in magnitude, and are having different shapes. For inclined cable the rotation displacements are unsymmetrical and the largest magnitude is in the longitudinal direction where it is maximum in the lower endpoint of the cable (156 unit per a unit longitudinal translation) and it is higher by

28.6% of the displacement at mid-span. The vertical and transversal rotation displacements at mid-span is lower by 83.31% and 97.21% than the longitudinal rotation displacement, respectively.

The modal shape for the torsional frequency is shown in Fig. 6.17, and the primary motion have the maximum displacement value at the support and it is symmetric about the mid-span of the cables. The coupled translation displacements in all direction are very small in magnitude, the largest value is in the longitudinal direction which is 0.00014 unit per a unit longitudinal rotation displacement at the quarter-span of the inclined cable, therefore it becomes unimportant. The corresponding translation displacements for the horizontal cable are equal to zero. The coupled rotation displacements shapes for the inclined cable differ than those of the horizontal cable and are not symmetric about the mid-span, and it takes the primary motion shape. However, they the maximum displacement, which occur at the supports, are also smaller in magnitude comparing with the longitudinal rotation displacement by 81% for the vertical and 96.4% transversal rotation displacements.

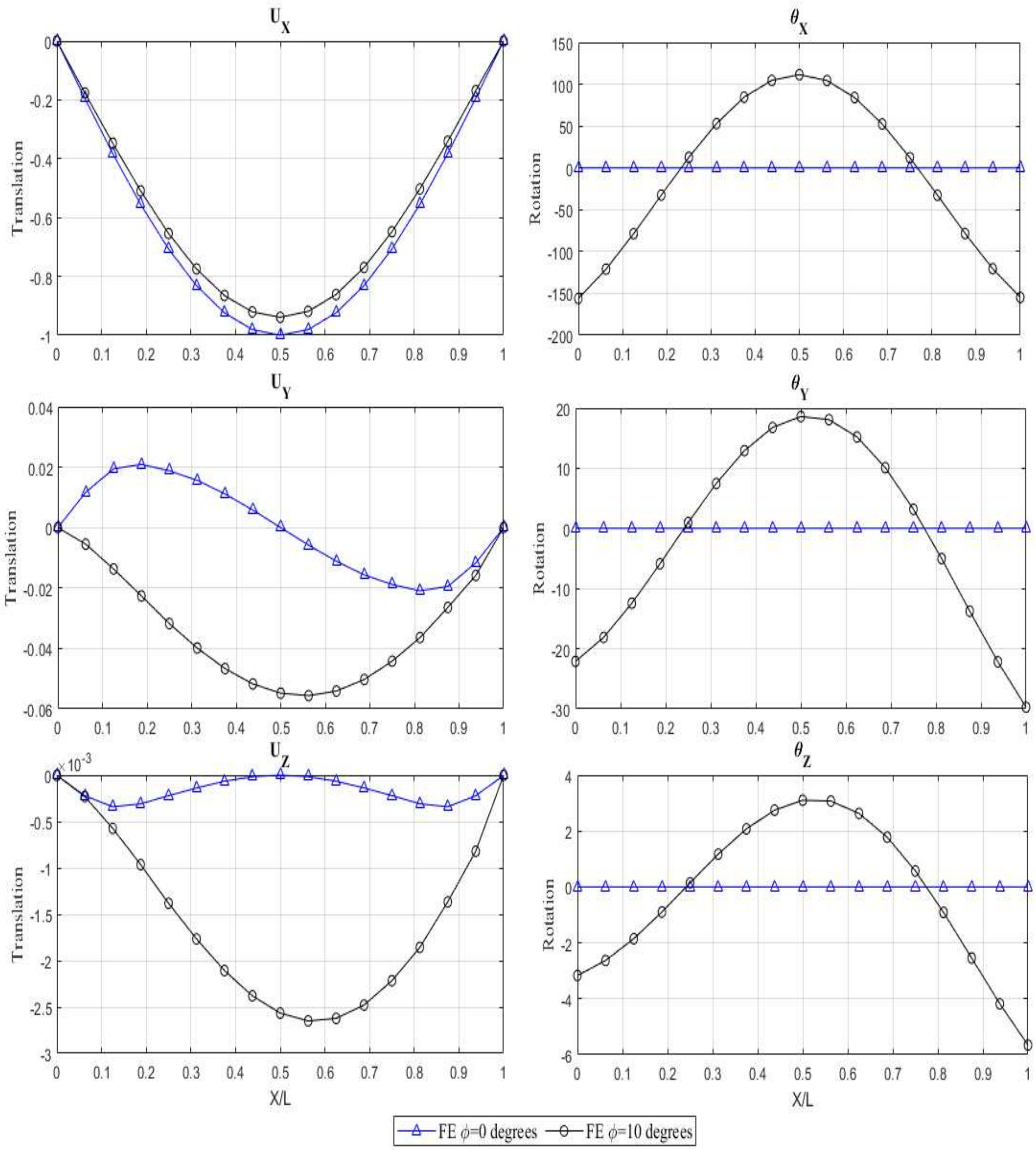

Fig. 6.16 The axial modal shapes displacements for horizontal cable (inclination angle zero), inclined cable (inclination angle 10) using the present finite element model (FE)

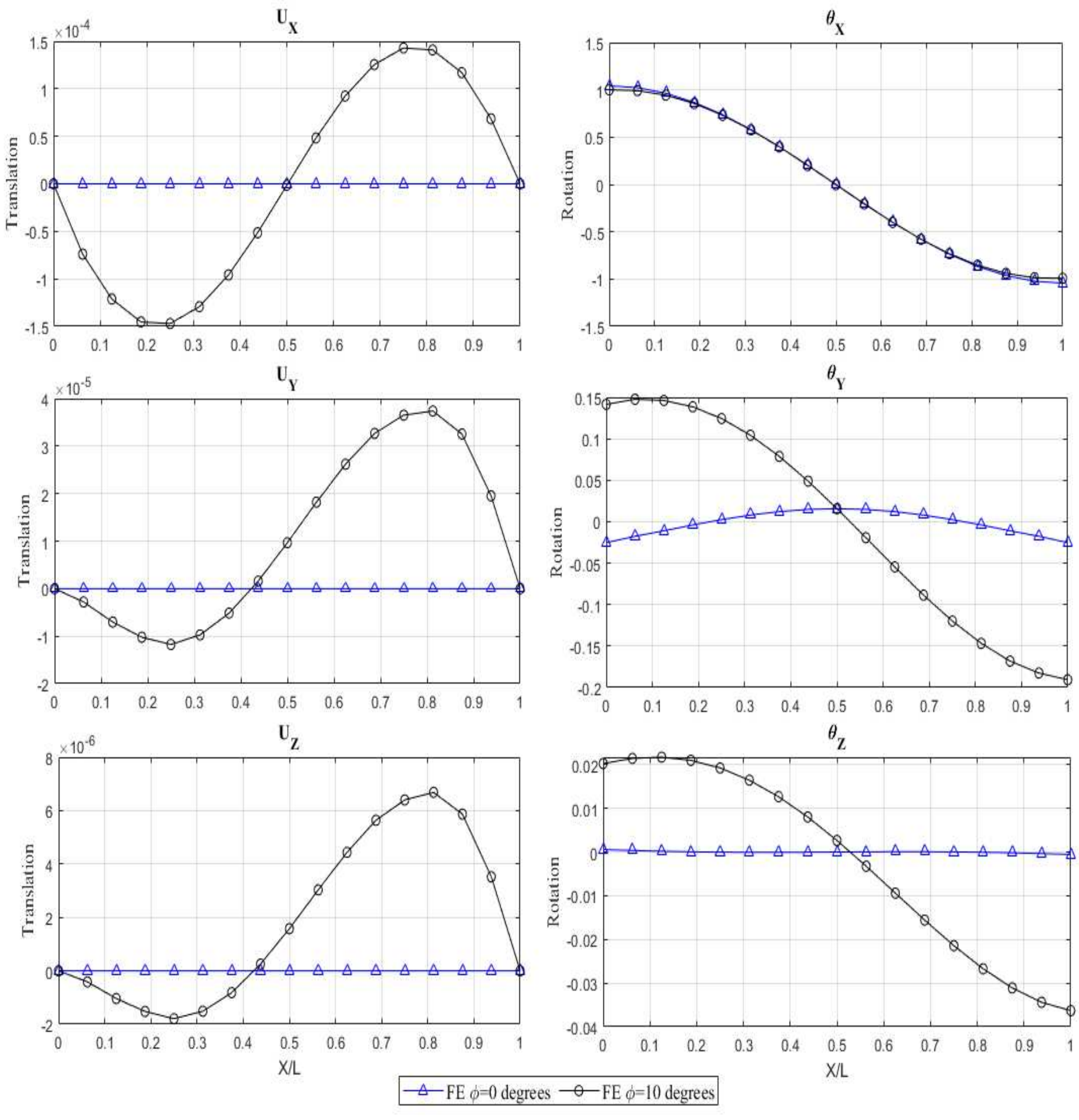

Fig. 6.17 The torsional modal shapes displacements for horizontal cable (inclination angle zero), inclined cable (inclination angle 10) using the present finite element model (FE)

6.6 Conclusion

In order to precisely model the complex vibration behavior of an inclined cable, the single-layered helical six-strand cable actual geometry configuration, where lay angle varied between 0 to 30 degrees, modeled using three-dimensional elasticity model, the method are comparing to an analytical model where axial and torsional coupling is considered. The derived symmetric stiffness and mass matrix were discretized over the cable domain using finite element analysis where the self-weight of the cable is taking into account. The model frequencies and mode shapes, which have simultaneous translation and rotation displacements, were validated using a comparison with large experimental data. In addition to a well-know analytical model and ABAQUS model for different range of inclination angles. The main conclusions drawn are as follows:

1. Using the three-dimensional elastic-based finite element model, the stiffness coefficients for the six-stranded cable studied (with lay angle 8 degrees) give excellent results compared to one-dimensional analytical results. It showed that for small lay angles, the internal contact deformation can be ignored. The axial and torsional stiffness finite element results were lower than the analytical model by approximately 1.5% and 14% for lay angles below 20 degrees and then higher by 3% and 23%, respectively. The coupling stiffness coefficients results coincided with lay angles below 15 degrees.
2. The natural frequency of cable that has an inclination angle of 10 degrees with the lay angle of 8 degrees was found using the present finite element model. The results are higher by 2.68% when compared with frequencies values obtained experimentally. The model has more advantages than other available analytical models and commercial finite element programs. It can include the actual cable configuration, and also gives the axial and torsional frequencies. The inclination angle variation between 10 and 60 degrees was studied using the finite element model and ABAQUS, and results showed that due to the variation in the dynamic tension the out-of-plane, symmetric in-plane, anti-symmetric in-

plane, axial, and torsional frequencies decrease with a 4-7% rate for each ten inclination angle.

3. The corresponding modal shapes and the displacements interaction for the out-of-plane, symmetric in-plane, and anti-symmetric in-plane were found using the present finite element model and the experimental work for twisted inclined sagged cable ($\phi = 10$). The comparison presented confirmed that the finite element model can give good predictions of the displacements for each type. For all mode types the highest coupled rotation motion is in the longitudinal direction and they are different by approximately 60% of the results obtained experimentally. It was observed that the rotation displacements in other two axes are smaller in magnitude. The translation displacements are small in magnitude comparting to the primary translation motions, the transversal translation displacement in the anti-symmetric motion is being the exception where it is about 30% of the vertical motion magnitude.
4. The modal interactions were also found for the axial and torsional in addition to the out-of-plane and in-plane frequencies for a cable where axial and torsion coupling was neglected with inclination angle is set to zero. The results were compared to the model where the coupling and inclination angel is 10 is considered. It showed that the inclined cable mode shapes have translation and rotation displacements in the three-directions. The rotation displacements in the out-of-plane and in-plane modes are zeros for the horizontal cable. The inclined cable modes found to be unsymmetrical about the mid-span and differ from the shapes when inclination angle is zero. The coupled rotation displacements were signification at the supports endpoints in the primary axial modal shape. In the torsional

modal shape, the rotation displacements were found smaller in magnitude by 81% and 96.4%.

This present finite element model holds promise in solving more complex analysis of strands and ropes behavior. Future work can consider the application of the derived formulation in more complex problems.

CHAPTER 7: CONCLUSION

This dissertation investigated the use of the finite element method and experiment apparatus to model the dynamic response of untwisted and twisted cables. The general concluding remarks and recommendations for future work are presented here for this research.

7.1 Concluding Remarks

In this work, the effective stiffness and mass matrix were found using a three-dimensional elasticity method for twisted cables for lay angles 5 to 30 degrees. These are then used to describe the nature of the dynamic motion and resonances considering the free vibration analysis for cables under axial loads that are supported at the same level and inclined cables (inclination angle between 10 to 60 degrees), using a finite element model where the sag, self-weight, and six degrees of freedom are considered. Sag variation (small to relatively large values) effects were also examined for uncoupled cables. The finite element model was validated with large experimental tests, commercial finite element software ABAQUS, and available analytically solutions. The study showed that the proposed finite element model gives an excellent prediction of the dynamic response for untwisted and twisted cables, which results in enhancing a safe design and reliable system. Very detailed conclusions are included in chapters 3-6. However, in here, the main dissertation conclusions drawn are as follows:

1. An extensive review of the publications shows that cables' general dynamic behavior has been known for a long time; recently, an increasing interest in using cables in a wide variety of engineering applications required more understanding of the vibration of the cable. However, very little attention has been paid to studying the coupled translations and rotations interaction between various coordinates, either numerically or experimentally.

2. In order to accurately study the dynamic behavior of the cable, stiffness coefficients using a three-dimensional finite element elasticity-based method are introduced. The model provided the same general trend using replicated 8 one-dimensional analytical solutions from literature for the six-stranded cables examined. It gives a consistent determination method of the stiffness coefficients for twisted cables examined. The axial stiffness coefficients for lay angles between 5 to 30 degrees using the elasticity-based approach are slightly lower (4%) than those on the one-dimensional models for the studied cables' actual lay angle. The coupling and the torsional stiffness are generally within the bounds of the simple one-dimensional models. In addition, the model showed that for cable with a small lay angle, the internal contact can be ignored.
3. The natural frequency spectrum, including out-of-plane, symmetric in-plane, anti-symmetric in-plane, axial and torsional frequencies, for twisted and untwisted cables studied using the finite element model are within excellent agreement with the experimental results (the difference is less than 0.5% for horizontal cable and 2% for inclined cable), also analytical and ABAQUS models were used to validate the accuracy of the present model. The present finite element model has more advantages than the other approaches. It can include the actual configuration (twist and sag), the coupling and torsional stiffnesses, and the self-weight of the cable. In addition, the non-dimensional parameter λ^2 effect was captured using the present model. The influence of sag, lay angle, and inclination angle variation on the frequency spectrum was also studied.
4. The vibrational modal shapes of the cables were found using the finite element model, where the interaction between various axes was captured. For the five dynamic motions studied, the coupled six translation and rotation displacements were found. For instant, in

the out-of-plane mode, there are longitudinal and vertical translation components and longitudinal, vertical, and transverse rotation components coupled with the primarily transverse translation motion. The influence of sag variation, lay angle, and inclination angle were investigated. It was found that the sag value has a strong effect on the translation motions for the low-frequency spectrum, as well as on the axial frequency. The torsional frequency rotational modal shapes were also affected by the sag. The lay angle almost completely affects the translation mode shapes for the low frequencies (rotation mode shape for in-plane is strongly influenced). And, the lay angle has minimum impact on the axial frequency's translation mode shapes, where it has the reverse behavior for the torsional frequency. The inclination angle effect on the cable was found to be significant comparing with the results of horizontal cable. In general, the results of the coupled interactions were confronted with results obtained experimentally, and the comparison showed that the finite element model can give a good prediction of the dynamic cable behavior.

5. In order to study the cable vibration mitigation, the horizontal cables internal damping ratios were also found from the out-of-plane and in-plane motion. In addition, the effect of using viscous damper on the support on the cable vibration were tested. The results showed that the peak in-plane translation motion decreases by approximately 27% when the damper is used.

7.2 Future Work

The presented finite element model holds much promise in solving more complex problems of strands and ropes. It can be extended to study the dynamic behavior of multi-layered strands and ropes and other cables with complex cross-sections such as trapezoidal wires. In addition, the sag (sag to span ratio more than 1:8) and inclination angle effect on twisted cables modal shape can also be studied. Other work may consider applying the finite element model to more complex problems, including post-elastic, bending effects, and fatigue analysis of strands and ropes.

The model presented in this dissertation can also be extended to include the effect of damping and its effect on the coupling between the various coordinate vibrations. The Rayleigh method can be used to find the system damping matrix; then, the quadratic eigenproblem can be then solved. The effect created by damping related terms on the frequency spectrum and mode shapes can then be investigated. In addition, as it is known the vibration mitigation is a must on such a structure. Therefore, more experimental work using viscous dampers near or on the supports is required to understand their effectiveness on the coupled displacements.

REFERENCES

[1] J. Scalzi, W.M. Division, Mechanical properties of structural cables, J. Struct. Div. Trid.Trb.Org. (1971). https://trid.trb.org/view/99694 (accessed August 28, 2019).

[2] Y.J. Chiang, Characterizing simple-stranded wire cables under axial loading, Finite Elem. Anal. Des. 24 (1996) 49–66. https://doi.org/10.1016/S0168-874X(97)80001-E.

[3] W.K. Lee, An insight into wire rope geometry, Int. J. Solids Struct. 28 (1991) 471–490. https://doi.org/10.1016/0020-7683(91)90060-S.

[4] X. Huang, Mechanics of cables with interwire friction, University of Calgary, 1992. https://doi.org/http://dx.doi.org/10.11575/PRISM/19424.

[5] M. Raoof, I. Kraincanic, Simple derivation of the stiffness matrix for axial/torsional coupling of spiral strands, Comput. Struct. 55 (1995) 589–600. https://doi.org/10.1016/0045-7949(94)00502-T.

[6] D.G. Pavlou, Essentials of the Finite Element Method: For Mechanical and Structural Engineers, Elsevier Inc., 2015. https://doi.org/10.1016/C2014-0-03143-7.

[7] K. Feyrer, Wire ropes: Tension, endurance, reliability, 2015. https://doi.org/10.1007/978-3-642-54996-0.

[8] F.H. Hruska, Tangential forces in wire ropes, 27 (1952) 459–463.

[9] F.H. Hruska, Radial forces in wire ropes, 27 (1952) 459–463.

[10] R. Knapp, Nonlinear analysis of a helically armored cable with nonuniform mechanical properties in tension and torsion, Ocean 75 Conf. (1975) 155–164. https://doi.org/10.1109/OCEANS.1975.1154154.

[11] K.G. McConnell, W.P. Zemke, A model to predict the coupled axial torsion properties of ACSR electrical conductors, Exp. Mech. 22 (1982) 237–244. https://doi.org/10.1007/BF02326388.

[12] A.E.H. Love, A treatise on the mathematical theory of elasticity., (1906) xviii, 551 p. http://hdl.handle.net/10111/UIUCBB:loveau0001tremat.

[13] S. Machida, A.J. Durelli, Response of a Strand to Axial and Torsional Displacements, J. Mech. Eng. Sci. 15 (1973) 241–251. https://doi.org/10.1243/JMES_JOUR_1973_015_045_02.

[14] R.H. Knapp, Derivation of a new stiffness matrix for helically armoured cables considering tension and torsion, Int. J. Numer. Methods Eng. 14 (1979) 515–529. https://doi.org/10.1002/nme.1620140405.

[15] G.A. Costello, J.W. Philips, Effective Modulus of Twisted Wire Cables, J. Eng. Mech. Div. 102 (1976) 171–181.

[16] N.C. Huang, Finite Extension of an Elastic Strand With a Central Core, J. Appl. Mech. 45 (1978) 852–858. http://dx.doi.org/10.1115/1.3424431.

[17] S.R. Ghoreishi, T. Messager, P. Cartraud, P. Davies, Validity and limitations of linear analytical models for steel wire strands under axial loading, using a 3D FE model, Int. J. Mech. Sci. 49 (2007) 1251–1261. https://doi.org/10.1016/j.ijmecsci.2007.03.014.

[18] S.A. Velinsky, General nonlinear theory for complex wire rope, Int. J. Mech. Sci. 27 (1985) 497–507. https://doi.org/10.1016/0020-7403(85)90040-2.

[19] J.W. Phillips, G.A. Costello, Analysis of Wire Ropes With Internal-Wire-Rope Cores, J. Appl. Mech. 52 (1985) 510–516. http://dx.doi.org/10.1115/1.3169092.

[20] George A. Costello, Theory of Wire Ropes, 2nd ed., Springer-Verlag New York, 1997. https://doi.org/10.1007/978-1-4612-1970-5.

[21] S. Ghoreishi, Modélisation analytique et caractérisation expérimentale du comportement de câbles synthétiques, (2005). https://www.theses.fr/2005NANT2048 (accessed January 29, 2020).

[22] K. Kumar, J. Cochran J. E., Closed-Form Analysis for Elastic Deformations of Multilayered Strands, J. Appl. Mech. 54 (1987) 898–903. http://dx.doi.org/10.1115/1.3173136.

[23] W.S. Utting, N. Jones, The response of wire rope strands to axial tensile loads-Part I. Experimental results and theoretical predictions, Int. J. Mech. Sci. 29 (1987) 605–619. https://doi.org/10.1016/0020-7403(87)90033-6.

[24] W.S. Utting, N. Jones, The response of wire rope strands to axial tensile loads—Part II. Comparison of experimental results and theoretical predictions, Int. J. Mech. Sci. 29 (1987) 621–636. https://doi.org/10.1016/0020-7403(87)90034-8.

[25] R.A. Le Clair, G.A. Costello, Axial, Bending and Torsional Loading of a Strand With Friction, J. Offshore Mech. Arct. Eng. 110 (1988) 38–42. https://doi.org/10.1115/1.3257121.

[26] C. Jolicoeur, A. Cardou, A Numerical Comparison of Current Mathematical Models of Twisted Wire Cables Under Axisymmetric Loads, J. Energy Resour. Technol. 113 (1991) 241–249. http://dx.doi.org/10.1115/1.2905907.

[27] M.R. Labrosse, Contribution à l'étude du rôle du frottement sur le comportement et la durée de vie des câbles monocouches, (1998).

[28] K. Kumar, J. Botsis, Contact Stresses in Multilayered Strands Under Tension and Torsion, J. Appl. Mech. 68 (2001) 432. https://doi.org/10.1115/1.1355777.

[29] H. Ramsey, A theory of thin rods with application to helical constituent wires in cables, Int. J. Mech. Sci. 30 (1988) 559–570. https://doi.org/10.1016/0020-7403(88)90099-9.

[30] H. Ramsey, Analysis of interwire friction in multilayered cables under uniform extension

and twisting, Int. J. Mech. Sci. 32 (1990) 709–716. https://doi.org/10.1016/0020-7403(90)90011-7.

[31] S. Sathikh, M.B.K. Moorthy, M. Krishnan, A symmetric linear elastic model for helical wire strands under axisymmetric loads, J. Strain Anal. Eng. Des. 31 (1996) 389–399. https://doi.org/10.1243/03093247V315389.

[32] I. Argatov, Response of a wire rope strand to axial and torsional loads: Asymptotic modeling of the effect of interwire contact deformations, Int. J. Solids Struct. 48 (2011) 1413–1423. https://doi.org/10.1016/j.ijsolstr.2011.01.021.

[33] F. Meng, Y. Chen, M. Du, X. Gong, Study on effect of inter-wire contact on mechanical performance of wire rope strand based on semi-analytical method, Int. J. Mech. Sci. 115–116 (2016) 416–427. https://doi.org/10.1016/j.ijmecsci.2016.07.012.

[34] Y. Chen, F. Meng, X. Gong, Full contact analysis of wire rope strand subjected to varying loads based on semi-analytical method, Int. J. Solids Struct. 117 (2017) 51–66. https://doi.org/10.1016/J.IJSOLSTR.2017.04.004.

[35] N. Karathanasopoulos, G. Kress, Mechanical response of a helical body to axial, torsional and radial strain, Int. J. Mech. Sci. 94–95 (2015) 260–265. https://doi.org/10.1016/j.ijmecsci.2015.02.022.

[36] N. Karathanasopoulos, J.F. Ganghoffer, K.O. Papailiou, Analytical closed-form expressions for the structural response of helical constructions to thermal loads, Int. J. Mech. Sci. 117 (2016) 258–264. https://doi.org/10.1016/j.ijmecsci.2016.08.010.

[37] F. Foti, L. Martinelli, Mechanical modeling of metallic strands subjected to tension, torsion and bending, Int. J. Solids Struct. 91 (2016) 1–17. https://doi.org/10.1016/j.ijsolstr.2016.04.034.

[38] R.E. Hobbs, M. Raoof, Interwire slippage and fatigue prediction in stranded cables for TLP tethers, (1982) 77–99.

[39] M. Raoof, Interwire contact forces and the static, hysteretic and fatigue properties of multi-layer structural strandsitle, Imperial Collage of Science and Technology, London, UK., 1983.

[40] M. Raoof, R.E. Hobbs, Analysis of Multilayered Structural Strands, J. Eng. Mech. 114 (1988) 1166–1182. http://gateway.webofknowledge.com/gateway/Gateway.cgi?GWVersion=2&SrcApp=PARTNER_APP&SrcAuth=LinksAMR&KeyUT=WOS:A1988P108400004&DestLinkType=FullRecord&DestApp=ALL_WOS&UsrCustomerID=1ba7043ffcc86c417c072aa74d649202.

[41] M. Raoof, Methods for analysing large spiral strands, J. Strain Anal. Eng. Des. 26 (1991) 165–174. https://doi.org/10.1243/03093247V263165.

[42] M. Raoof, I. Kraincanic, Simple derivation of the stiffness matrix for axial/torsional coupling of spiral strands, Comput. Struct. 55 (1995) 589–600.

https://doi.org/10.1016/0045-7949(94)00502-T.

[43] R. Mohammed, K. Ivana, Analysis of Large Diameter Steel Ropes, J. Eng. Mech. 121 (1995) 667–675. https://doi.org/10.1061/(ASCE)0733-9399(1995)121:6(667).

[44] F. Blouin, A. Cardou, A study of helically reinforced cylinders under axially symmetric loads and application to strand mathematical modelling, Int. J. Solids Struct. 25 (1989) 189–200. https://doi.org/10.1016/0020-7683(89)90006-1.

[45] L. Xiang, H.Y. Wang, Y. Chen, Y.J. Guan, Y.L. Wang, L.H. Dai, Modeling of multi-strand wire ropes subjected to axial tension and torsion loads, Int. J. Solids Struct. 58 (2015) 233–246. https://doi.org/10.1016/j.ijsolstr.2015.01.007.

[46] C. Jolicoeur, Comparative study of two semicontinuous models for wire strand analysis, (1997).

[47] J. Claude, C. Alain, Semicontinuous Mathematical Model for Bending of Multilayered Wire Strands, J. Eng. Mech. 122 (1996) 643–650. https://doi.org/10.1061/(ASCE)0733-9399(1996)122:7(643).

[48] J.A. Crossley, A.J.M. Spencer, A.H. England, Analytical solutions for bending and flexure of helically reinforced cylinders, Int. J. Solids Struct. 40 (2003) 777–806. https://doi.org/10.1016/S0020-7683(02)00625-X.

[49] J.A. Crossley, A.H. England, A.J.M. Spencer, Bending and flexure of cylindrically monoclinic elastic cylinders, Int. J. Solids Struct. 40 (2003) 6999–7013. https://doi.org/10.1016/S0020-7683(03)00351-2.

[50] E. Stanova, G. Fedorko, M. Fabian, S. Kmet, Computer modelling of wire strands and ropes Part I: Theory and computer implementation, Adv. Eng. Softw. 42 (2011) 305–315. https://doi.org/10.1016/j.advengsoft.2011.02.008.

[51] D. Elata, R. Eshkenazy, M.P. Weiss, The mechanical behavior of a wire rope with an independent wire rope core, Int. J. Solids Struct. 41 (2004) 1157–1172. https://doi.org/10.1016/j.ijsolstr.2003.11.021.

[52] H. Usabiaga, J.M. Pagalday, Analytical procedure for modelling recursively and wire by wire stranded ropes subjected to traction and torsion loads, Int. J. Solids Struct. 45 (2008) 5503–5520. https://doi.org/10.1016/j.ijsolstr.2008.04.009.

[53] C.M. Leech, J.W.S. Hearle, M.S. Overington, S.J. Banfield, Modelling Tension and Torque Properties of Fibre Ropes and splices, Third Int. Offshore Polar Eng. Conf. Singapore, 6-11 June 1993 Model. (1993) 6–11.

[54] J.F. Beltran, J. Rungamornrat, E.B. Williamson, Computational Model For the Analysis of Damaged Ropes, (n.d.).

[55] J.F. Beltran, Computational modeling of synthetic-fiber ropes, The University of Texas at Austin, 2006. https://search.proquest.com/docview/304980548?accountid=10223.

[56] J.F. Beltran, E.B. Williamson, Investigation of the Damage-Dependent Response of Mooring Ropes, J. Eng. Mech. 135 (2009) 1237–1247. https://doi.org/10.1061/(ASCE)0733-9399(2009)135:11(1237).

[57] S.R. Ghoreishi, P. Cartraud, P. Davies, T. Messager, Analytical modeling of synthetic fiber ropes subjected to axial loads. Part I: A new continuum model for multilayered fibrous structures, Int. J. Solids Struct. 44 (2007) 2924–2942. https://doi.org/10.1016/j.ijsolstr.2006.08.033.

[58] S.R. Ghoreishi, P. Davies, P. Cartraud, T. Messager, Analytical modeling of synthetic fiber ropes. Part II: A linear elastic model for 1 + 6 fibrous structures, Int. J. Solids Struct. 44 (2007) 2943–2960. https://doi.org/10.1016/j.ijsolstr.2006.08.032.

[59] A.D. Carlson, R.G. Kasper, M.A. Tucchio, N.U.S.C.N.E.W.L.C.N.E.W.L. LAB., A Structural Analysis of a Multiconductor Cable, Defense Technical Information Center, 1973. https://books.google.com/books?id=Kzc1OAAACAAJ.

[60] M.A. Cutchins, J. Cochran, J. E., S. Guest, N.G. Fitz-Coy, M.L. Tinker, An investigation of the damping phenomena in wire rope isolators, 5 (1987) 197–204.

[61] Y.J. Chiang, Characterizing simple-stranded wire cables under axial loading, Finite Elem. Anal. Des. 24 (1996) 49–66. https://doi.org/10.1016/S0168-874X(97)80001-E.

[62] A. Nawrocki, M. Labrosse, A finite element model for simple straight wire rope strands, Comput. Struct. 77 (2000) 345–359. https://doi.org/10.1016/S0045-7949(00)00026-2.

[63] A. Nawrocki, CONTRIBUTION A LA MODELISATION DES CABLES MONOTORONS PAR ELEMENTS FINIS, 1997. https://books.google.com/books?id=IpzdOgAACAAJ.

[64] W.G. Jiang, M.S. Yao, J.M. Walton, A concise finite element model for simple straight wire rope strand, Int. J. Mech. Sci. 41 (1999) 143–161. https://doi.org/10.1016/S0020-7403(98)00039-3.

[65] W.G. Jiang, J.L. Henshall, J.M. Walton, Concise finite element model for three-layered straight wire rope strand, Int. J. Mech. Sci. 42 (2000) 63–86. https://doi.org/10.1016/S0020-7403(98)00111-8.

[66] M. Labrosse, A. Nawrocki, T. Conway, Frictional dissipation in axially loaded simple straight strands, J. Eng. Mech. 126 (2000) 641–646. https://doi.org/10.1061/(ASCE)0733-9399(2000)126:6(641).

[67] K. Wehking, S. Zieglen, Calculation of a standard rope with FEM. Wire, 54 (2004) 69–100.

[68] T. Messager, P. Cartraud, Homogenization of helical beam-like structures: application to single-walled carbon nanotubes, Comput. Mech. 41 (2008) 335–346. https://doi.org/10.1007/s00466-007-0189-3.

[69] W.G. Jiang, M.K. Warby, J.L. Henshall, Statically indeterminate contacts in axially

loaded wire strand, Eur. J. Mech. A/Solids. 27 (2008) 69–78. https://doi.org/10.1016/j.euromechsol.2007.02.003.

[70] W.G. Jiang, A concise finite element model for pure bending analysis of simple wire strand, Int. J. Mech. Sci. 54 (2012) 69–73. https://doi.org/10.1016/j.ijmecsci.2011.09.008.

[71] A. Cardou, C. Jolicoeur, Mechanical Models of Helical Strands, Appl. Mech. Rev. 50 (1997) 1–14. http://dx.doi.org/10.1115/1.3101684.

[72] D. Liu, S. Zheng, Y. He, Effect of friction on the mechanical behavior of wire rope with hierarchical helical structures, Math. Mech. Solids. 24 (2019) 2154–2180. https://doi.org/10.1177/1081286518816519.

[73] M.K. Alkharisi, P.R. Heyliger, Axial–Torsional Vibrational Modes of Braided and Trapezoidal Wires, J. Vib. Acoust. 141 (2018) 024501. https://doi.org/10.1115/1.4041398.

[74] H.M. Irvine, Cable structures, Dover Publications, 1992.

[75] S. Rohrs, On the oscillations of a suspended cable, (1851).

[76] E.J. Routh, E.J. Routh, The Advanced Part of a Treatise on the Dynamics of a System of Rigid Bodies, in: Adv. Part a Treatise Dyn. a Syst. Rigid Bodies, 2015: pp. iii–iv. https://doi.org/10.1017/cbo9781139237284.001.

[77] A.G. Pugsley, ON THE NATURAL FREQUENCIES OF SUSPENSION CHAINS, 1949. https://academic.oup.com/qjmam/article-abstract/2/4/412/1930282 (accessed February 12, 2020).

[78] D.S. Saxon, A.S. Cahn, MODES OF VIBRATION OF A SUSPENDED CHAIN, 1953. https://academic.oup.com/qjmam/article-abstract/6/3/273/1878823 (accessed February 12, 2020).

[79] U. Starossek, Cable dynamics-a review, Struct. Eng. Int. 4 (1994) 171–176.

[80] H.M. Irvine, T.K. Caughey, The linear theory of free vibrations of a suspended cable, Proc. R. Soc. London. A. Math. Phys. Sci. 341 (1974) 299–315. https://doi.org/10.1098/rspa.1974.0189.

[81] X. Zhou, S. Yan, F. Chu, In-Plane Free Vibrations of an Inclined Taut Cable, J. Vib. Acoust. 133 (2011) 031001. https://doi.org/10.1115/1.4003397.

[82] H.M. Irvine, J.H. Griffin, On the dynamic response of a suspended cable, Earthq. Eng. Struct. Dyn. 4 (1976) 389–402. https://doi.org/10.1002/eqe.4290040406.

[83] S. Thai, N.-I. Kim, J. Lee, Free Vibration Analysis of Cable Structures Using Isogeometric Approach, Int. J. Comput. Methods. 14 (2017) 1750033.

[84] H. M. Irvine, Free Vibrations of Inclined Cables, 1978.

[85] M.S. TRIANTAFYLLOU, THE DYNAMICS OF TAUT INCLINED CABLES, Q. J. Mech. Appl. Math. 37 (1984) 421–440. https://doi.org/10.1093/qjmam/37.3.421.

[86] M.S. Triantafyllou, L. Grinfogel, Natural Frequencies and Modes of Inclined Cables, J. Struct. Eng. 112 (1986) 139–148. https://doi.org/10.1061/(asce)0733-9445(1986)112:1(139).

[87] J.J. Burgess, M.S. Triantafyllou, The elastic frequencies of cables, J. Sound Vib. 120 (1988) 153–165. https://doi.org/10.1016/0022-460X(88)90340-9.

[88] P. Yu, Y.M. Desai, A.H. Shah, N. Popplewell, Three-Degree-of-Freedom Model for Galloping. Part I: Formulation, J. Eng. Mech. 119 (1993) 2404–2425. https://doi.org/10.1061/(ASCE)0733-9399(1993)119:12(2404).

[89] O. Nigol, G.C.-I.T. on Power, U. 1974, Conductor galloping and control based on torsional mechanism, (1974).

[90] Y.M. Desai, A.H. Shah, N. Popplewell, Galloping Analysis for Two-Degree-of-Freedom Oscillator, J. Eng. Mech. 116 (1990) 2583–2602. https://doi.org/10.1061/(ASCE)0733-9399(1990)116:12(2583).

[91] K.F. Jones, Coupled Vertical and Horizontal Galloping, J. Eng. Mech. 118 (1992) 92–107. https://doi.org/10.1061/(ASCE)0733-9399(1992)118:1(92).

[92] P. Yu, Y.M. Desai, A.H. Shah, N. Popplewell, Three-Degree-of-Freedom Model for Galloping. Part I: Formulation, J. Eng. Mech. 119 (1993) 2404–2425. https://doi.org/10.1061/(asce)0733-9399(1993)119:12(2404).

[93] P. Yu, Y.M. Desai, N. Popplewell, A.H. Shah, Three-Degree-of-Freedom Model for Galloping. Part II: Solutions, J. Eng. Mech. 119 (1993) 2426–2448. https://doi.org/10.1061/(ASCE)0733-9399(1993)119:12(2426).

[94] Y.M. Desai, P. Yu, N. Popplewell, A.H. Shah, Finite element modelling of transmission line galloping, Comput. Struct. 57 (1995) 407–420. https://doi.org/10.1016/0045-7949(94)00630-L.

[95] A.G. Davenport, G.N. Steels, Dynamic behavior of massive guy cables, J. Struct. Div. 91 (1965) 43–70.

[96] A.S. Veletsos, G.R. Darbre, Dynamic stiffness of parabolic cables, Earthq. Eng. Struct. Dyn. 11 (1983) 367–401.

[97] U. Starossek, Boundary induced vibration and dynamic stiffness of a sagging cable, 1990.

[98] U. Starossek, Dynamic stiffness matrix of sagging cable, J. Eng. Mech. 117 (1991) 2815–2828.

[99] Y.M. Desai, N. Popplewell, A.H. Shah, D.N. Buragohain, Geometric nonlinear static analysis of cable supported structures, Comput. Struct. 29 (1988) 1001–1009. https://doi.org/10.1016/0045-7949(88)90326-4.

[100] M. Raoof, Y.P. Huang, K.D. Pithia, RESPONSE OF AXIALLY PRELOADED SPIRAL STRANDS TO IMPACT LOADING, 1994.

[101] R.K. Samras, R.A. Skop, D.A. Milburn, An analysis of coupled extensional-torsional oscillations in wire rope, J. Eng. Ind. 96 (1974) 1130–1135.

[102] J. Wang, G. Cao, M. Lin, S. Liu, 13 . Coupled vibration of hoisting cable in cable-guided hoisting system with different swivels, (2015) 102–110.

[103] R.A. Skop, R.K. Samras, Effects of coupled extensional-torsional oscillations in wire rope during ocean salvage and construction operations, J. Manuf. Sci. Eng. Trans. ASME. 97 (1975) 485–492. https://doi.org/10.1115/1.3438609.

[104] W. Jiang, T.L. Wang, W.K. Jones, Forced vibration of coupled extensional-torsional systems, J. Eng. Mech. 117 (1991) 1171–1190. https://doi.org/10.1061/(ASCE)0733-9399(1991)117:5(1171).

[105] W. JIANG, W. JONES, K. WU, T. WANG, Non-linear and linear, static and dynamic analyses of helical springs, in: American Institute of Aeronautics and Astronautics (AIAA), 1989. https://doi.org/10.2514/6.1989-1200.

[106] M. Raoof, I. Kraincanic, Critical examination of various approaches used for analysing helical cables, J. Strain Anal. Eng. Des. 29 (1994) 43–55. https://doi.org/10.1243/03093247V291043.

[107] J.W. Phillips, G.A. Cosfello, Axial impact of twisted wire cables, J. Appl. Mech. Trans. ASME. 44 (1977) 127–131. https://doi.org/10.1115/1.3423977.

[108] C.M. Leech, M.S. Overington, Dynamics of Wire Rope Subjected to Shock Axial Loads, in: Offshore Technol. Conf., Offshore Technology Conference, 1982. https://doi.org/10.4043/4308-MS.

[109] A.S.K. Kwan, A new approach to geometric nonlinearity of cable structures, Comput. Struct. (1998). https://doi.org/10.1016/S0045-7949(98)00052-2.

[110] J. Mitsugi, Static analysis of cable networks and their supporting structures, Comput. Struct. (1994). https://doi.org/10.1016/0045-7949(94)90035-3.

[111] G.D. Stefanou, E. Moossavi, S. Bishop, P. Koliopoulos, Conjugate gradients method for calculating the response of large cable nets to static loads, Comput. Struct. (1993). https://doi.org/10.1016/0045-7949(93)90031-8.

[112] O. Vilnay, P. Rogers, Statical and dynamical response of cable nets, Int. J. Solids Struct. (1990). https://doi.org/10.1016/0020-7683(90)90042-T.

[113] T.J.R. Hughes, J.A. Cottrell, Y. Bazilevs, Isogeometric analysis: CAD, finite elements, NURBS, exact geometry and mesh refinement, Comput. Methods Appl. Mech. Eng. (2005). https://doi.org/10.1016/j.cma.2004.10.008.

[114] S.M. Hashemi, A. Roach, A DYNAMIC FINITE ELEMENT FOR VIBRATION ANALYSIS OF CABLES AND WIRE ROPES, 2006.

[115] W.M. Henghold, J. Russell, J. Morgan, Free Vibrations of Cable in Three Dimensions,

(1977).

[116] G. Rega, Nonlinear vibrations of suspended cables—Part I: Modeling and analysis, Appl. Mech. Rev. 57 (2004) 443. https://doi.org/10.1115/1.1777224.

[117] G. Rega, Nonlinear vibrations of suspended cables - Part II: Deterministic phenomena, Appl. Mech. Rev. 57 (2004) 479–514. https://doi.org/10.1115/1.1777225.

[118] N.C. Perkins, Modal interactions in the non-linear response of elastic cables under parametric/external excitation, Int. J. Non. Linear. Mech. (1992). https://doi.org/10.1016/0020-7462(92)90083-J.

[119] N. Srinil, G. Rega, Two-to-one resonant multi-modal dynamics of horizontal/inclined cables. Part II: Internal resonance activation, reduced-order models and nonlinear normal modes, Nonlinear Dyn. 48 (2007) 253–274. https://doi.org/10.1007/s11071-006-9087-z.

[120] L. Wang, Y. Zhao, Nonlinear interactions and chaotic dynamics of suspended cables with three-to-one internal resonances, Int. J. Solids Struct. (2006). https://doi.org/10.1016/j.ijsolstr.2006.04.006.

[121] W. Lacarbonara, A. Pacitti, Nonlinear modeling of cables with flexural stiffness, Math. Probl. Eng. (2008). https://doi.org/10.1155/2008/370767.

[122] W. Lacarbonara, Nonlinear structural mechanics: Theory, dynamical phenomena and modeling, 2013. https://doi.org/10.1007/978-1-4419-1276-3.

[123] A. Arena, A. Pacitti, W. Lacarbonara, Nonlinear response of elastic cables with flexural-torsional stiffness, Int. J. Solids Struct. (2016). https://doi.org/10.1016/j.ijsolstr.2015.09.019.

[124] H.T. Thai, S.E. Kim, Nonlinear static and dynamic analysis of cable structures, Finite Elem. Anal. Des. (2011). https://doi.org/10.1016/j.finel.2010.10.005.

[125] M. Lepidi, V. Gattulli, Static and dynamic response of elastic suspended cables with thermal effects, Int. J. Solids Struct. 49 (2012) 1103–1116. https://doi.org/10.1016/J.IJSOLSTR.2012.01.008.

[126] R. Karoumi, Some modeling aspects in the nonlinear finite element analysis of cable supported bridges, Comput. Struct. 71 (1999) 397–412. https://doi.org/10.1016/S0045-7949(98)00244-2.

[127] MTS Hydraulic Actuators & Servo-Valves, (n.d.). https://test.mts.com/en/products/test-system-components/actuators-servo-valves (accessed February 21, 2021).

[128] Model 407 Controller, n.d. https://www.mts.com/cs/groups/public/documents/library/dev_002063.pdf (accessed February 21, 2021).

[129] MetaTracker – MbientLab, (n.d.). https://mbientlab.com/metatracker/ (accessed February 21, 2021).

[130] S.S. Rao, Vibration of Continuous Systems, John Wiley & Sons, Inc., Hoboken, NJ, USA, 2006. https://doi.org/10.1002/9780470117866.

[131] E.A. Johnson, R.E. Christenson, B.F. Spencer, Semiactive damping of cables with sag, Comput. Civ. Infrastruct. Eng. 18 (2003) 132–146. https://doi.org/10.1111/1467-8667.00305.

[132] A.-T. Yu, VIBRATION DAPING OF STRANDED CABLE: VIBRATION DAMPING OF STRANDED CABLE, 1949.

[133] K. Spak, G. Agnes, D. Inman, Cable Modeling and Internal Damping Developments, Appl. Mech. Rev. 65 (2013) 10801–10818. http://dx.doi.org/10.1115/1.4023489.

[134] R. Claren, G. Diana, Mathematical Analysis of Transmission Line Vibration, IEEE Trans. Power Appar. Syst. PAS-88 (1969) 1741–1771. https://doi.org/10.1109/TPAS.1969.292291.

[135] R. Claren, G. Diana, Dynamic Strain Distribution on Loaded Stranded Cables, IEEE Trans. Power Appar. Syst. PAS-88 (1969) 1678–1690. https://doi.org/10.1109/TPAS.1969.292376.

[136] A.K. Maji, Y.Z. Qiu, Experimental and numerical investigation of axially preloaded carbon fiber cable vibration, J. Aerosp. Eng. 27 (2014). https://doi.org/10.1061/(ASCE)AS.1943-5525.0000346.

[137] M. Otrin, M. Boltežar, Damped lateral vibrations of straight and curved cables with no axial pre-load, J. Sound Vib. 300 (2007) 676–694. https://doi.org/10.1016/j.jsv.2006.08.032.

[138] A.R. Hard, R.D. Holben, Application of the Vibration Decay Test to Transmission Line Conductors, IEEE Trans. Power Appar. Syst. PAS-86 (1967) 189–199. https://doi.org/10.1109/TPAS.1967.291835.

[139] X. Huang, O. Vinogradov, Interwire Slip And Its Influence On The Dynamic Properties Of Tension Cables, (1992).

[140] H. Yamaguchi, R. Adhikari, Energy-based evaluation of modal damping in structural cables with and without damping treatment, J. Sound Vib. 181 (1995) 71–83. https://doi.org/10.1006/jsvi.1995.0126.

[141] C.Y. Wei, S.N. Kukureka, Evaluation of damping and elastic properties of composites and composite structures by the resonance technique, J. Mater. Sci. 35 (2000) 3785–3792. https://doi.org/10.1023/A:1004817011240.

[142] C. Wei, S.K.-M. evaluation, undefined 2004, Temperature dependence of dynamic modulus and damping in composites and optical telecommunication cables tested by the vibration resonance, Am. Soc. Nondestruct. (n.d.).

[143] H. Yamaguchi, M. Alauddin, N. Poovarodom, Dynamic characteristics and vibration control of a cable system with substructural interactions, Eng. Struct. 23 (2001) 1348–

1358. https://doi.org/10.1016/S0141-0296(01)00019-0.

[144] N. Barbieri, O.H. De Souza Júnior, R. Barbieri, Dynamical analysis of transmission line cables. Part 2 - Damping estimation, Mech. Syst. Signal Process. 18 (2004) 671–681. https://doi.org/10.1016/S0888-3270(02)00218-2.

[145] N. Barbieri, P.R. Novak, R. Barbieri, Experimental identification of damping, Int. J. Solids Struct. 41 (2004) 3585–3594. https://doi.org/10.1016/j.ijsolstr.2004.02.006.

[146] F. Casciati, L. Faravelli, C. Fuggini, Cable vibration mitigation by added SMA wires, Acta Mech. 195 (2008) 141–155. https://doi.org/10.1007/s00707-007-0541-x.

[147] L. Faravelli, C. Fuggini, F. Ubertini, Experimental study on hybrid control of multimodal cable vibrations, Meccanica. 46 (2011) 1073–1084. https://doi.org/10.1007/s11012-010-9364-2.

[148] A. Maji, Y. Qiu B A Professor, Experimental Study of Cable Vibration Damping, (2011). https://doi.org/10.1007/978-1-4614-0216-9_46.

[149] N. Barbieri, M.K. Tenório Calado, M.J. Mannala, K.F. De Lima, G. De Sant'Anna Vitor Barbieri, Dynamical analysis of various transmission line cables, in: Procedia Eng., Elsevier Ltd, 2017: pp. 516–521. https://doi.org/10.1016/j.proeng.2017.09.143.

[150] I.F. Lazar, S.A. Neild, D.J. Wagg, Vibration suppression of cables using tuned inerter dampers, Eng. Struct. 122 (2016) 62–71. https://doi.org/10.1016/j.engstruct.2016.04.017.

[151] Stock - Airpot Air Dashpots - Airpot, (n.d.). https://www.airpot.com/product-category/product-lines/dashpots-shock-absorbers/airpot-precision-dashpots/stock/ (accessed March 22, 2021).

[152] J.A. Main, N.P. Jones, Free Vibrations of Taut Cable with Attached Damper. I: Linear Viscous Damper, J. Eng. Mech. 128 (2002) 1062–1071. https://doi.org/10.1061/(asce)0733-9399(2002)128:10(1062).

[153] W. Thomson, Theory of vibration with applications, 2018. https://content.taylorfrancis.com/books/download?dac=C2009-0-22514-4&isbn=9781351408509&format=googlePreviewPdf (accessed January 16, 2020).

[154] S. Sathikh, M.B.K. Moorthy, M. Krishnan, A symmetric linear elastic model for helical wire strands under axisymmetric loads, J. Strain Anal. Eng. Des. 31 (1996) 389–399. https://doi.org/10.1243/03093247V315389.

[155] F. Foti, L. Martinelli, Modeling the axial-torsional response of metallic strands accounting for the deformability of the internal contact surfaces: Derivation of the symmetric stiffness matrix, Int. J. Solids Struct. 171 (2019) 30–46. https://doi.org/10.1016/j.ijsolstr.2019.05.008.

[156] W. Jiang, T.L. Wang, W.K. Jones, Forced Vibration of Coupled Extensional-Torsional Systems, J. Eng. Mech. 117 (1991) 1171–1190. https://doi.org/10.1061/(ASCE)0733-9399(1991)117:5(1171).

[157] M.K. Alkharisi, P.R. Heyliger, Axial–Torsional Vibrational Modes of Braided and Trapezoidal Wires, J. Vib. Acoust. (2018). https://doi.org/10.1115/1.4041398.

[158] C.G. Koh, Y. Rong, Dynamic analysis of large displacement cable motion with experimental verification, J. Sound Vib. 272 (2004) 187–206. https://doi.org/10.1016/S0022-460X(03)00326-2.

[159] M. Smith, ABAQUS/Standard User's Manual, Version 6.9, Undefined. (2009).

[160] N.C. Perkins, C.D. Mote, Three-dimensional vibration of travelling elastic cables, J. Sound Vib. 114 (1987) 325–340. https://doi.org/10.1016/S0022-460X(87)80157-8.

[161] J.C. Russell, T.J. Lardner, Experimental Determination of Frequencies and Tension for Elastic Cables, J. Eng. Mech. 124 (1998) 1067–1072. https://doi.org/10.1061/(asce)0733-9399(1998)124:10(1067).

[162] Q. Wu, K. Takahashi, S. Nakamura, Formulae for frequencies and modes of in-plane vibrations of small-sag inclined cables, J. Sound Vib. 279 (2005) 1155–1169. https://doi.org/10.1016/j.jsv.2004.01.004.

[163] N. Srinil, G. Rega, S. Chucheepsakul, Two-to-one resonant multi-modal dynamics of horizontal/inclined cables. Part I: Theoretical formulation and model validation, Nonlinear Dyn. 48 (2007) 231–252. https://doi.org/10.1007/s11071-006-9086-0.

[164] R. Rega, G. and Srinil, N. and Alaggio, Experimental and numerical studies of inclined cables: free and parametrically-forced vibrations - Strathprints, (2008). https://strathprints.strath.ac.uk/18551/ (accessed March 28, 2021).

[165] C.G. Koh, Y. Zhang, S.T. Quek, Low-Tension Cable Dynamics: Numerical and Experimental Studies, J. Eng. Mech. 125 (1999) 347–354. https://doi.org/10.1061/(asce)0733-9399(1999)125:3(347).

[166] A.B. Peabody, G. McClure, Modeling the EPRI-Wisconsin power and light broken wire tests, IEEE Trans. Power Deliv. 25 (2010) 1826–1833. https://doi.org/10.1109/TPWRD.2010.2041559.